



UNIwersYTET
ŁÓDZKI



WYDZIAŁ
CHEMII
Uniwersytet Łódzki

UNIVERSITY OF LODZ

Faculty of Chemistry
Department of Organic and Applied Chemistry
Tamka Street, 12, 91-403 Łódź

Doctoral Dissertation

Functionalization and π -Extension of the Planar Blatter Radical

Mahshid Teymouri

mahshid.teymouri@edu.uni.lodz.pl

Supervisor: prof. Piotr Kaszyński

Łódź, 2024

Table of Contents

Abstract	6
1. Introduction	7
1.1. Nanographenes	7
1.1.1. Polycyclic aromatic hydrocarbons (PAHs)	8
1.1.2. Polycyclic heteroaromatic molecules (PHAs)	9
1.2. Stable organic radicals	11
1.3. Stability of radicals.....	13
1.3.1. Steric protection with bulky substituents.....	13
1.3.2. Tuning the delocalization of spin density	14
1.3.3. Extension of π -conjugates	14
1.3.4. The incorporation of polar substituents	17
1.3.5. Heteroatom-based radicals	18
1.4. Benzo[<i>e</i>][1,2,4]triazinyl radicals: properties and applications.....	20
1.4.1. Benzo[<i>e</i>][1,2,4]triazinyl radicals: structure	20
1.4.2. Benzo[<i>e</i>][1,2,4]triazinyl radicals: synthesis	22
1.5. Planar benzo[<i>e</i>][1,2,4]triazinyl radicals: structure	25
1.5.1. Planar benzo[<i>e</i>][1,2,4]triazinyl radicals: synthesis.....	26
1.5.2. Planar benzo[<i>e</i>][1,2,4]triazinyl radicals: functionalization and π -expansion.....	28
1.6. Preparation of aromatic thiols.....	32
1.6.1. Preparation of thiols <i>via</i> xanthates from aromatic diazonium salts	35
1.6.2. Preparation of thiols from disulfides and polysulfides	35
1.6.3. Preparation of thiols through thiocyanates	36
1.6.4. Reduction of thiocyanates to thiols.....	37
1.7. References	40
2. Objectives and scope of work	47
3. Discussion of the results of own research	50

3.1. Ring expansion of the planar Blatter radical.....	50
3.1.1. Post-radical-generation ring-extended planar Blatter radicals.....	50
3.1.1.1. Synthesis of ring-fused [1,2,4]triazines.....	52
3.1.1.1.1. Synthesis of 3-phenylnaphtho[2,1- <i>e</i>][1,2,4]triazine.....	53
3.1.1.1.2. Synthesis of 3,5-diphenyl[1,2,4]triazino[5,6- <i>c</i>]quinoline.....	54
3.1.1.1.3. Synthesis of ring-fused [1,2,4]triazines through diketones.....	55
3.1.1.1.4. Electronic absorption spectroscopy of fused [1,2,4]triazines (UV-vis).....	56
3.1.1.2. Synthesis of radicals by azaphilic ArLi addition to fused [1,2,4]triazines.....	63
3.1.1.2.1. Characterisation of the electronic structure of the radicals.....	65
3.1.1.2.1.1. Electronic absorption spectroscopy (UV-vis).....	65
3.1.1.2.1.2. Electrochemistry (cyclic voltammetry measurements).....	70
3.1.1.2.1.3. Electron paramagnetic resonance spectroscopy (EPR).....	73
3.1.1.3. Synthesis of ring-fused π -extended Blatter radicals by photocyclization.....	77
3.1.1.4. Synthesis of ring expanded Blatter radicals at the N(1) position.....	78
3.1.2 Synthesis of ring expanded planar Blatter radicals through cyclization.....	79
3.1.2.1. Synthesis of naphtho[2,1- <i>e</i>]triazine derivatives.....	80
3.1.2.1.1. Synthesis of 10-bromo-3-phenylnaphtho[2,1- <i>e</i>][1,2,4]triazine.....	80
3.1.2.1.1.1. Synthesis of 8-bromo-1-naphthol.....	81
3.1.2.1.1.2. Synthesis of 8-bromo-2-nitro-naphthol.....	83
3.1.2.1.2. Synthesis of naphtho[2,1- <i>e</i>][1,2,4]triazine <i>via</i> Suzuki-Miyaura coupling....	84
3.1.2.2. Synthesis of radicals through intramolecular photocyclization.....	85
3.1.2.2.1. Characterisation of the electronic structure of the radicals.....	86
3.1.2.2.1.1. Electron paramagnetic resonance spectroscopy (EPR).....	86
3.2. Functionalization of <i>S-peri</i> -annulated benzo[<i>e</i>][1,2,4]triazinyl radicals.....	88
3.2.1. Synthesis of 8-phenylsulfanyl-3-phenylbenzo[1,2,4]triazines.....	90
3.2.1.1. Synthesis of <i>ortho</i> -iodothiophenols.....	91
3.2.1.1.1. Synthesis of <i>ortho</i> -iodothiophenols through thiocyanate.....	91

3.2.1.1.2. Synthesis of <i>ortho</i> -iodothiophenols through disulfide	93
3.2.2. Synthesis of 2-phenyl-3 <i>H</i> -[1,2,4]triazino[5,6,1- <i>kl</i>]phenothiazin-3-yls	94
3.2.2.1. Characterisation of the electronic structure of the radicals.....	95
3.2.2.1.1. Electronic absorption spectroscopy (UV-vis)	95
3.2.2.1.2. Electrochemistry (cyclic voltammetry measurements).....	101
3.2.2.1.3. Electron paramagnetic resonance spectroscopy (EPR).....	105
3.3. Summary and conclusions.....	109
3.4. References	111
4. Experimental part	114
4.1. General information	114
4.2. Post-radical-generation ring-extended planar Blatter radicals	115
4.2.1. Synthesis of ring-fused [1,2,4]triazines	115
4.2.1.1. Preparation of 3-phenylnaphtho[2,1- <i>e</i>][1,2,4]triazine	115
4.2.1.2. Synthesis of 3,5-diphenyl[1,2,4]triazino[5,6- <i>c</i>]quinoline.....	118
4.2.1.3. Synthesis of ring-fused [1,2,4]triazines through the diketones.....	122
4.2.2. General procedure for synthesis of radicals	124
4.3. Synthesis of ring expanded planar Blatter radicals through cyclization	126
4.3.1. Synthesis of 10-bromo-3-phenyl-naphtho[2,1- <i>e</i>][1,2,4]triazine.....	126
4.3.2. General procedure for the Suzuki-Miyaura coupling.....	131
4.3.3. General procedure for synthesis of radicals	132
4.4. Functionalization of <i>S-peri</i> -annulated benzo[<i>e</i>][1,2,4]triazinyl.....	133
4.4.1. Synthesis of <i>ortho</i> -iodothiophenols.....	133
4.4.1.1. General procedure for synthesis of thiocyanates through method A.....	133
4.4.1.2. General procedure for synthesis of thiocyanates through method B	136
4.4.1.3. General procedure for synthesis of aryl iodides <i>via</i> Sandmeyer reaction.....	138
4.4.1.4. General procedure for synthesis of aryl iodides by pyridiniumiodochloride	141
4.4.1.5. General procedure for synthesis of mercaptans	143

4.4.1.6. General procedure for synthesis of disulfides.....	145
4.4.2.Synthesis of phenylsulfanyl-3-phenylbenzo[1,2,4]triazines	146
4.4.3. Synthesis of 2-phenyl-3 <i>H</i> -[1,2,4]triazino[5,6,1- <i>kl</i>]phenothiazin-3-yls	149
4.5. References	152

Abstract

Stable organic radicals have attracted tremendous attention as structural elements for the development of modern functional materials due to their outstanding performance in a variety of fields. Particularly attractive in this context are π -delocalized radicals based on the benzo[*e*][1,2,4]triazin-4-yl known as the Blatter radicals, which stand out for their exceptional stability, spin delocalization, low excitation energies and interesting electrochemical and photophysical properties. Planar Blatter radicals can be obtained through planarization of the N(1) aryl substituent, which offers greater spin delocalization, change in packing of the solid state, and a new platform for the design of functional materials. The methods for increasing the stability of radicals and preparation of Blatter radicals and planar Blatter radicals and synthesis of their extended and substituted derivatives in previous works are described in the Introduction (Section 2). The main goal of this Doctoral Thesis, is to conduct research on synthetic methods that will allow for the systematic and detailed characterization of a new type of paramagnetic nanographenes which is docked to the [1,2,4]triazinyl fragment for fundamental studies in the context of electronic and magnetic applications.

In the first part of the Thesis, synthesis of derivatives of π -expanded planar Blatter radicals as a new class of paramagnetic nanographenes, through two different methodologies and understand their structure-property relationships are presented (Section 3.1). To assess the effect of π expansion on the electronic properties, the radicals were characterized using spectroscopic (UV–vis and electron paramagnetic resonance (EPR)) and electrochemical methods and the results are described (Section 3.1).

In the second part of this Thesis (Section 3.2), preparative routes to five new functionalized derivatives of *S-peri*-annulated benzo[*e*][1,2,4]triazinyl, containing CO₂Me, CN, CF₃ and NO₂ groups at the C(10) or C(9) positions through TMS₃SiH-assisted cyclization of aryl iodides are discussed. The goal of this effort was to gain a better knowledge of the parameters that govern the crystal packing of benzo[*e*][1,2,4]triazinyl derivatives and their impact on magnetic interactions. Spectroscopic, structural, electrochemical, chemical properties and the investigation of the impact of chemical structure and morphology on these properties, are provided (Section 3.2).

1.Introduction

1.1. Nanographenes

Nanographenes or extended polycyclic aromatic hydrocarbons, are defined as systems that contain a contiguous π -conjugated framework with at least 20 sp^2 -hybridized atoms which typically corresponds to systems containing at least five fused rings in their structures.¹ Nanographenes have gotten increased interest since the first experimental demonstration of graphene in 2004.¹ Systematic research and knowledge gathered over the last century offer guidance on adjusting electrical properties and a variety of synthetic techniques leading to expanded π systems.¹ Two-dimensional extension of the π -conjugated framework, which is the defining feature of nanographene structures, can provide faster reduction of the HOMO–LUMO gap than that observed in structurally similar linear molecules.

Recently, nanographenes have received significant attention,² notably in the field of molecular electronics³ and photovoltaics.⁴ Some synthetic methods^{5,6} and structure-property relationship studies in the context of modern technologies have been developed. *Peri*-annulated nanographenes come in a variety of families, such as phenalenoids, pyrenoids, peryleneoids and coronenoids.¹

Available technology does not provide easy access to structurally uniform material. Therefore, the use of a graphene as a semiconductor is limited by its problematic production and handling. In molecular electronics, heteroatom doping modifies the material's electronic structure in order to introduce or improve desired properties like the bandgap opening, charge polarization, and electrochemical activity. Important aspects of the electronic structure, including the band gap, optical absorption spectra, photoluminescence, and redox behavior, can be controlled by modifying the topology and heteroatom content of the π -conjugated system.¹

In this Thesis, we planned to develop a new class of paramagnetic nanographenes, which are docked to the [1,2,4]triazinyl fragment to increase delocalization of the unpaired electron in the π system of a variety of polycyclic aromatic compounds, and provide maximum spin delocalization, and understand their structure-property relationships.

1.1.1. Polycyclic aromatic hydrocarbons (PAHs)

The term "polycyclic aromatic hydrocarbons" (PAHs) refers to a vast class of different chemical compounds with two or more fused aromatic rings. These compounds range from simple two-ring compounds, like naphthalene and its derivatives, to more complicated ring structures with up to 10 rings.

The term "big" PAHs refers to compounds having more than six fused aromatic rings as opposed to "small" PAHs, which typically have up to six fused aromatic rings.⁹ Alternant and nonalternant compounds are two categories for polycyclic aromatic hydrocarbons (PAHs). Nonalternant PAHs contain both six-member benzene and five-member carbon rings, whereas alternant PHs are made entirely of fused six-member benzene rings. Rings can have different qualities depending on their configuration. PAHs are low volatility solids which might be colorless, white, or pale yellow-green in appearance. The majority of them can be photooxidized and broken down into simpler compounds, and they are comparatively insoluble in water.⁹

π -Conjugated hydrocarbons are a significant group of hydrocarbons that can be broadly divided into two groups: alternant and nonalternant (Figure 1.1).⁷ The two sets of alternative carbon atoms in nonalternant hydrocarbons, such azulene, are all directly connected to one another, whereas the two sets of conjugated carbon atoms in alternant hydrocarbons such propenyl cation, radical, and anion, 1,3-butadiene, benzene, naphthalene are all distinct and not all directly connected.

Based on the number of carbon atoms, alternant hydrocarbons are further divided into two groups: even alternant hydrocarbons and odd alternant hydrocarbons. Even alternant hydrocarbons have an equal number of bonding and antibonding orbitals, an even number of total molecular orbitals, and an even number of conjugated carbon atoms. These hydrocarbons include 1,3-butadiene, benzene, naphthalene, and anthracene. An odd alternant hydrocarbon (OAH) has an odd number of conjugated carbon atoms and an odd number of total molecular orbitals, which includes a nonbonding molecular orbital (NBMO) and an equal number of bonding and antibonding orbitals. In order to obtain overall π -conjugation, these molecules exist as cations, radicals, or anion. Examples of this class include the radical, cation, or anion propenyl and benzyl.⁸

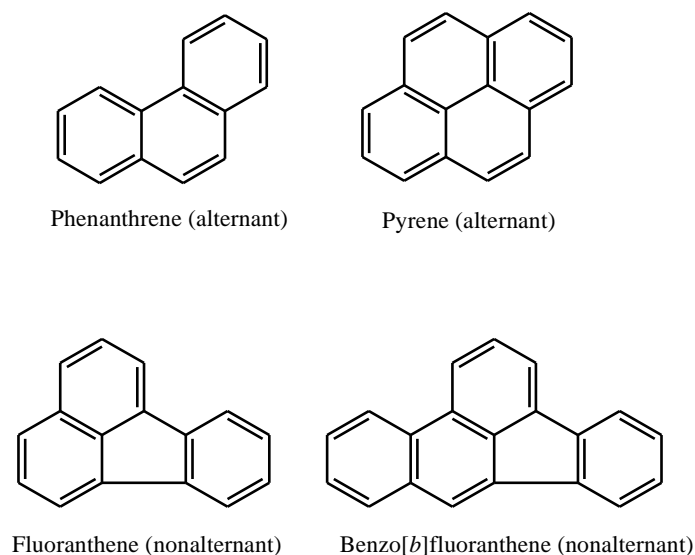


Figure 1.1. Examples of alternant and nonalternant PAHs.

In general, conjugation stabilizes the energy levels of occupied orbitals due to delocalization of charge through resonance and hybridization energy. π -Delocalization is perhaps the most reasonable strategy for radical stabilization due to spreading the spin density throughout the π system and energy level stabilization of occupied orbitals. One of the approaches to tune the delocalization of spin density is extension of a π -conjugated system in the structure of a radical.^{37,38} In this Thesis, we planned to develop a new class of paramagnetic nanographenes, which are docked to the [1,2,4]triazinyl fragment to increasing delocalization of the unpaired electron and spreading the spin density throughout the π system.

1.1.2. Polycyclic heteroaromatic molecules (PHAs)

The PHAs, which serve as the building blocks for nanographenes, have received a lot of interest. A remarkable number of new PHA structures were reported throughout the period of the past two decades, particularly by the groups Partridge and Buu-Hoi. The synthesis of highly functionalized, solution-processable derivatives was made possible by significant advancements in synthetic methods, which completely removed the harsh reaction conditions present in the early work on PHAs. Modern PHA chemistry has made a great use of transition metal-catalyzed coupling processes, which are undoubtedly the most significant recent addition to the synthetic tools.¹

In this sense, fused heterocyclic systems are viewed as doped nanographenes that combine structural uniformity with tunable electronic structure. The π -conjugated framework, which is the distinguishing characteristic of the nanographene structures, can be extended in two dimensions, which can lead to a faster reduction of the HOMO-LUMO gap than seen in linear molecules extending in one dimension.¹⁰ It is possible to modulate crucial aspects of the electronic structure, such as the band gap, optical absorption spectra, photoluminescence, and redox behavior, by changing the topology and heteroatom content of the π -conjugated system.¹

Polycyclic heteroaromatics are particularly interesting as self-assembling materials due to their anisotropic molecular morphologies, structural stiffness, and extended π -surfaces. Notably, the incorporation of heteroatoms in PHAs results in intrinsic dipole moments and edge functionalities, which can be employed as additional means of molecular organization control. Thus, PHA molecules provide an exceptional self-assembling combination of tunable electronic structure, which is widely desired in materials science. By judicious selection of ring fusion, heteroatom doping, and substitution, PHAs can be tuned into both p- and n-type semiconductors and, as a result, they are widely used in organic field-effect transistors and organic light emitting diodes.¹

Due to the accessibility of synthetic methods and the stability, nitrogen has generally been the main "dopant" element in large PHA. A lot of work is presently being put into development of large heteroaromatics containing *e.g.* phosphorus or chalcogens. This expanding inventory of useable heteroatoms gives a new variable in the creation of functional PHA molecules.¹

In this Thesis we plan to develop a new class of paramagnetic nanographenes containing the [1,2,4]triazinyl fragment docked to a π system with a variety of polycyclic aromatic compounds to provide maximum spin delocalization.

1.2. Stable organic radicals

Stable organic radicals are molecular species containing an unpaired electron and refer to a class of radicals that are persistent and so unreactive to air, moisture, and other conditions that they can be stored and handled under ambient conditions. A variety of stable radical species have been identified throughout the history. The first stable organic radical is the triphenylmethyl radical, discovered by Gomberg in 1900, which opened the door to the stable organic radical study (Figure 1.2).¹¹

The remarkable stability of this radical is due to the twisted phenyl rings about $\sim 30^\circ$ out of plane,¹² which causes steric shielding of the central carbon where most of the spin density is held. This shielding effect prevents direct dimerization between the central carbon atoms of two triphenylmethyl radicals, which was the reason why Gomberg was unsuccessful¹³ in synthesizing the triphenylethylene. However, this radical species is in equilibrium with a dimer formed by connecting the central carbon atom to the para position of another triphenylmethyl radical (Figure 1.2).¹¹ Following this discovery, the radical chemistry was gradually developed.

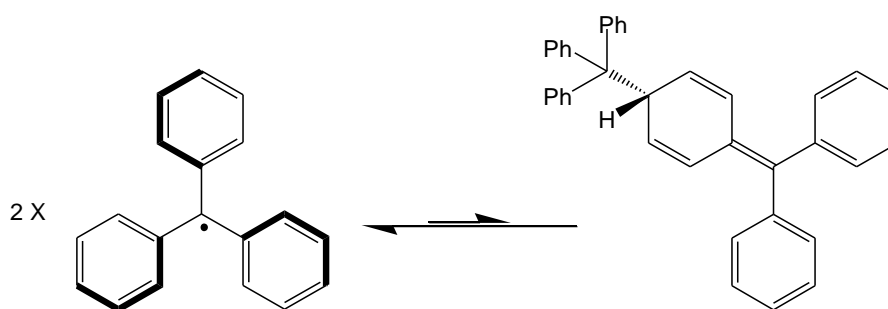


Figure 1.2. Triphenylmethyl radical and its dimer.

Organic radicals have unique magnetic, optical, and redox properties due to their open-shell structure. Stable radicals are unique group of functional materials, which have gained considerable attention in a variety of domains, such as quantum teleportation,¹⁴ conductive polymers,¹⁵ biochemistry sensors,^{16,17} organic magnets,^{18,19} accelerating chemical reactions,²⁰ and others.

Furthermore, organic radicals often serve as key intermediates in a number of organic reactions, including radical polymerization and organic photocatalysis.^{21–26} Examples of some persistent/stable organic radicals are shown in Figure 1.3.

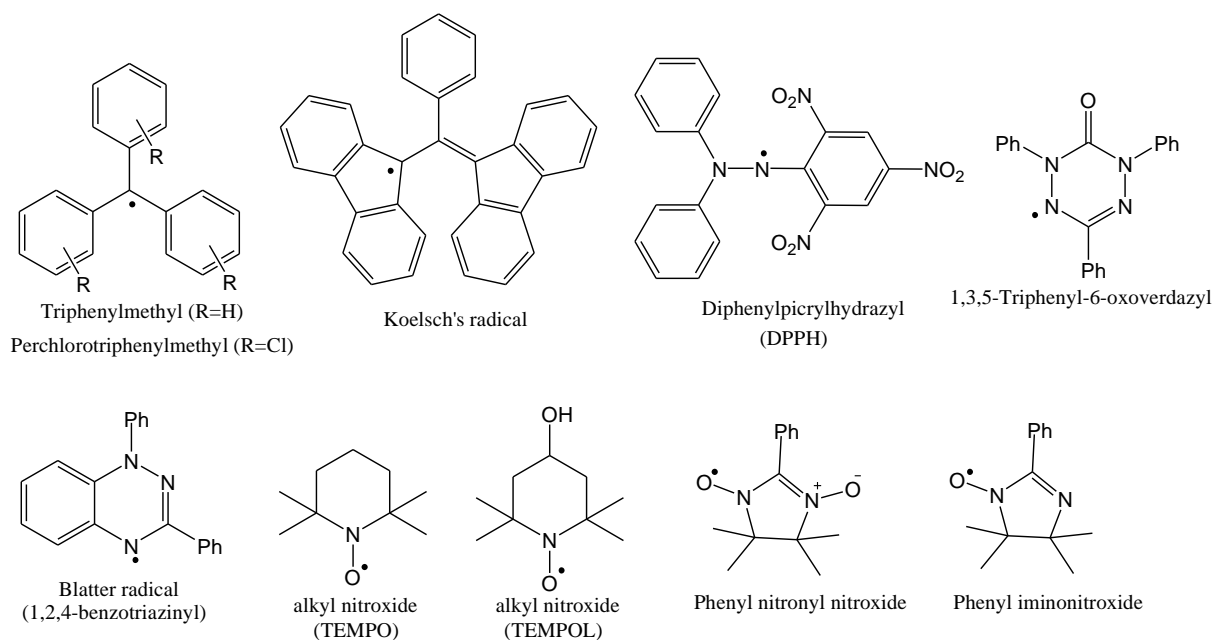


Figure 1.3. Some examples of persistent or stable organic radicals.

In this Doctoral Thesis, synthesis and systematic and detailed characterization of a class of stable π -delocalized organic radicals for fundamental studies in the area of electronic and magnetic applications, are presented, and the influence of the chemical structure and morphology of the radicals on their electronic and magnetic properties is discussed.

1.3. Stability of radicals

Organic radicals are typically unstable compounds possessing high reactivity. They are challenging to isolate and purify and they undergo reactions, such as dimerization, recombination, and electron transfer. Stability of the radicals affects their activities and is crucial for radical-based functional materials.²⁷ Steric and delocalization effects usually play critical roles in tuning the stability of organic radicals.^{28,29}

Numerous strategies relying on covalent modifications have been explored to increase the radicals' stability.^{30,31} One of these methods, is steric protection, which can provide kinetic and thermodynamic stability to organic radicals. Another method is modulating the delocalization of spin density, which is typically stated as an electronic effect that stabilizes the radicals thermodynamically and can be implemented through three main approaches: modulation of π -conjugates, incorporation of polar substituents, and modification of heteroatoms in the radical structure.³⁰

1.3.1. Steric protection with bulky substituents

Steric protection is one of the best and most popular method for stabilizing organic radicals, which can prevent radicals from interacting with other molecules by introducing large protecting groups, such as halogen atoms or alkyls and decreasing their intermolecular side reactions. Steric protection can effectively prevent the dimerization of free radicals. In fact, organic radicals can be significantly stabilized and even isolated through steric protection. Stable radicals with steric protection have been utilized in the field of energy storage and OLEDs.³²⁻³⁴

There are different examples of stable radicals, which are stabilized by steric protection, such as 2,2,6,6-tetramethylpiperidinyloxy, known as TEMPO, and triphenylmethyl radical, which is the first synthesized organic radical (Figure 1.3).

Delocalization of the unpaired electron stabilizes the radical, but dimerization occurs in solution. Triphenylmethyl radical is stabilized by steric protection through its three surrounding phenyl groups, twisted by about 30° in a propeller conformation to prevent the contact of the spin center with other molecules.³⁵ In the triphenylmethyl radical, the steric protection can be improved even more by substituting heavier elements, such chlorine, for the ortho hydrogen atoms on the phenyl groups (Figure 1.3).³⁶ In the perchlorinated triphenylmethyl radical, the

twist angle increased to about 50° due to the strong steric hindrance, which makes it extremely stable. Considerable efforts have been devoted to the development of stable triphenylmethyl radicals by introducing structural modifications at the *ortho*-positions, which are shown in Figure 1.4.³⁶

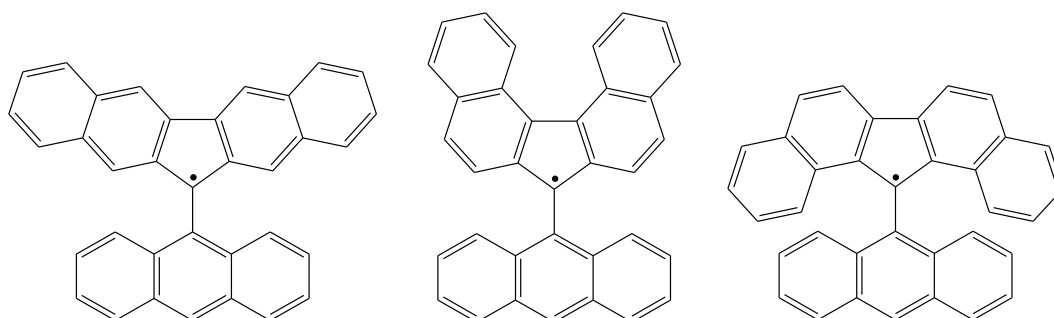


Figure 1.4. Derivatives of triphenyl methyl radicals.

1.3.2. Tuning the delocalization of spin density

The delocalization of spin density becomes a conventional approach to stabilize the radicals. Delocalization of the unpaired electron can be performed using three main approaches: extension of π -conjugation, introduction of polar substituents, and utilization of heteroatom-based radicals.³⁰

1.3.3. Extension of π -conjugates

In general, for both closed-shell and open-shell molecules, conjugation stabilizes the energy levels of occupied orbitals due to factors such as delocalization of charge through resonance and hybridization energy. In conjugated open-shell molecules, when the unpaired electron is well delocalized, the band gap (the relative position of the highest occupied and lowest unoccupied bands) decreases. This leads to higher stability of the radical and increase of the oxidation potential, while the ability to donate electrons becomes weaker. π -Delocalization is perhaps the most reasonable strategy for radical stabilization and is due to spreading the spin density throughout the π system. The phenalenyl radical is an example of an organic radical stabilized by extension of π -conjugation (Figure 1.5,a). This compound is an open-shell derivative with a fused polycyclic planar structure. This tricyclic radical was first prepared and characterized by Reid and Calvin in the 1950s.^{37,38}

The SOMO of the phenalenyl radical distributes the spin density among six peripheral carbon atoms. Notably, no spin density is placed in the central carbon since the remaining π orbitals would form a 12 π electron antiaromatic system. The anion and cation species of the phenalenyl are very thermodynamically stable as well. As a result, the phenalenyl radical shows strong amphoteric redox ability.³⁹

The radical anion of the perylenediimide (PDI) (Figure 1.5,b) consists of a perylene core conjugated with two imide groups at each side. The radical anion produced by reducing the neutral molecule is extremely stable, due to spreading most of the negative charge throughout the π system augmented by the imide group.³⁹

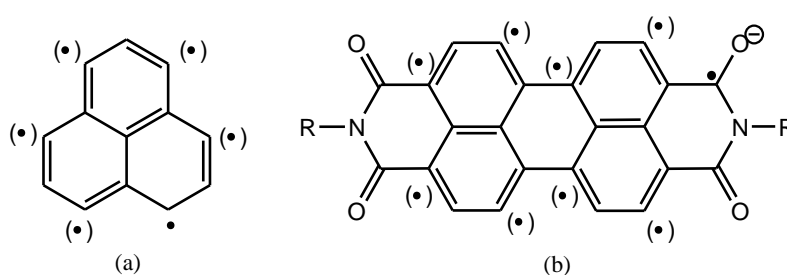


Figure 1.5. Delocalization in the (a) phenalenyl radical and (b) PDI radical anion.

Another example of organic radical stabilized by extension of π -conjugation is the phenoxy radical (Figure 1.6). As the oxygen radical has a low SOMO, phenoxy radicals are not easily oxidized. Two *tert*-butyl groups are normally introduced to the 2,6-positions, to make them sterically hindered from self-coupling reaction. The perylene diimides (PDI) and the naphthalene diimides (NDI) could stabilize radicals against oxidation by delocalization of the unpaired electron in the "electron-deficient" large π -system. Würthner and Kim have introduced 2,6-*di-tert*-butyl-phenoxy radical moieties to PDI or NDI, leading to stable mono- and diradicals with a half-life time of 10–54 h (Figure 1.6).^{40,41}

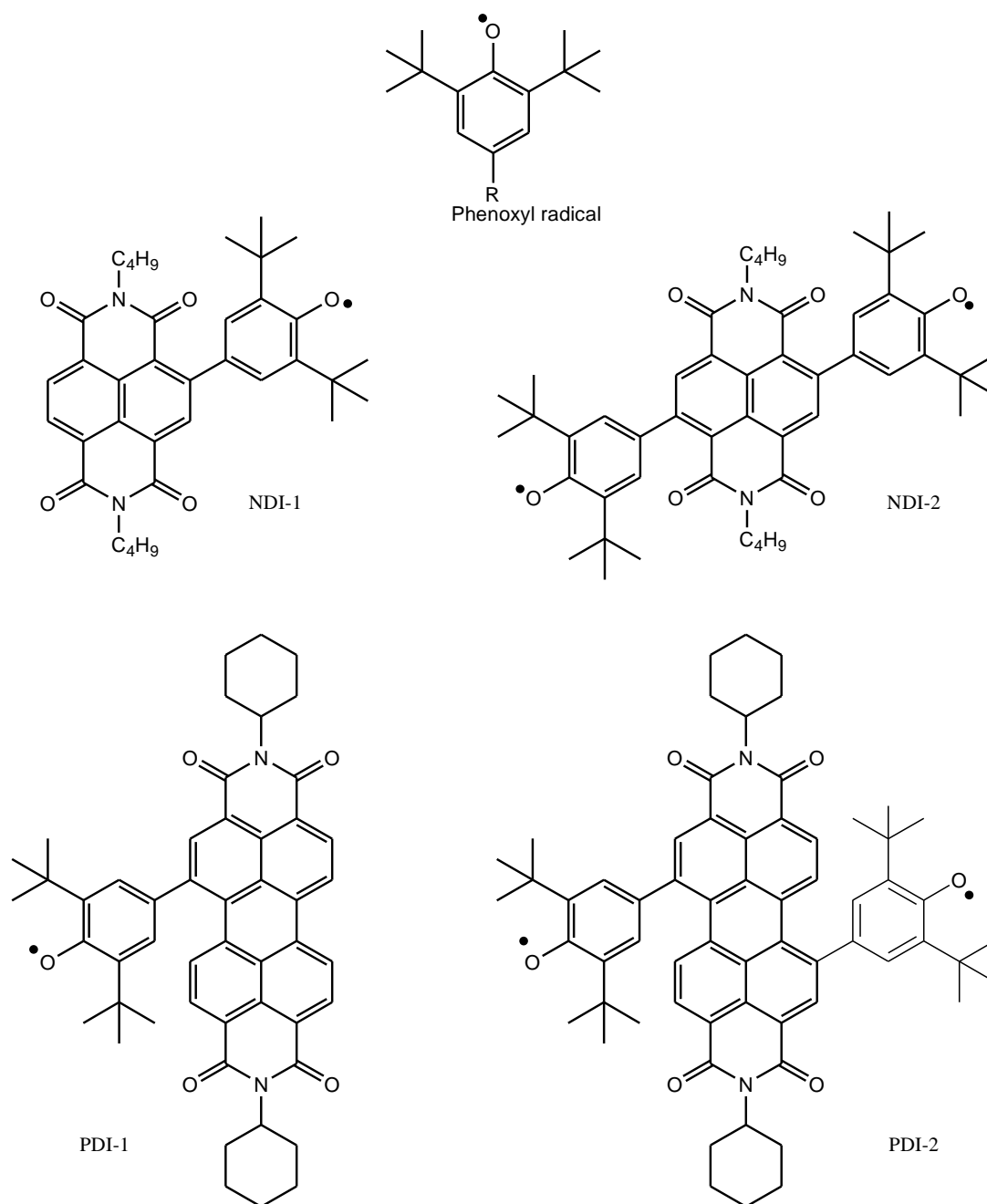


Figure 1.6. Chemical structures of phenoxy radical derivatives.

In general, conjugation stabilizes the energy levels of occupied orbitals due to factors such as delocalization of spin density and hybridization energy. π -Delocalization is perhaps the most reasonable strategy for radical stabilization through spreading the spin density throughout the π system, which can stabilize the energy level of occupied orbitals and also prevents the radical from reacting with air and other surroundings. One of the approaches to tune the delocalization of spin density is extension of the π -conjugated system in radical's structure.^{37,38}

In the first part of this Thesis, synthesis of derivatives of π -expanded planar Blatter radicals is presented. Different polycyclic aromatic compounds are synthesized which are docked to the [1,2,4]triazinyl spin source to delocalize the electron spin in the extended π system and to provide maximum spin delocalization. Simultaneous ring fusion at the *e* and *f* edges of the [1,2,4]triazinyl and planarization of the structure leads to extension of the π -system, spin delocalization and greater control the electronic properties of [1,2,4]triazinyl-based radicals. The structure-property relationships of different derivatives of the [1,2,4]triazinyl are investigated.

1.3.4. The incorporation of polar substituents

Polar substituents, including electron-donating and electron-withdrawing groups, can modify the charge distribution in organic radicals through conjugative and inductive effects, which has a significant impact on their stability. The proper incorporation of electron-donating groups as well as electron-withdrawing groups would modulate the stability of neutral radicals. The transfer of electrons between radicals and molecular oxygen is generally inhibited by electron-withdrawing groups. However, some electron-rich substituents, such as cyclic alkyl-amino carbenes (CAACs) and N-heterocyclic carbenes (NHCs), can also lead to stabilization of organic radicals.⁴²

The addition of substituents with opposite charges will stabilize radical ions.^{43,44} For example perylene-3,4,9,10-tetracarboxylic acid bisimide (PBI) radical anion, reported by Wurthner *et al.*, is stabilized by the placing of a positively charged imidazolium substituent. It can be isolated and even fully characterized by X-ray diffraction under ambient conditions (Figure 1.7).⁴⁵

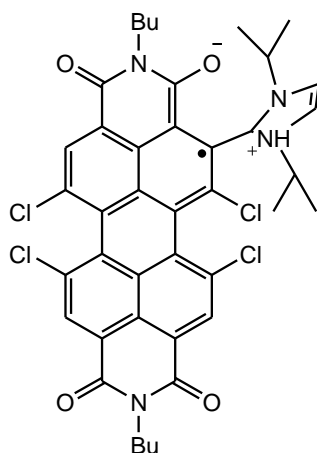


Figure 1.7. Imidazolium cation stabilized PBI radical anion.

1.3.5. Heteroatom-based radicals

The most important method for stabilizing the radicals is placing most of the spin density on heteroatoms. Most of stable radicals are heteroatom-based radicals, particularly those with N, O, or S center. This effect can be explained by the electronegativity of heteroatoms. In radical anions these heteroatoms can tolerate a large amount of the negative charge due to their electronegativity, but radical cations are stabilized by heteroatoms due to participation of their lone pairs. These heteroatoms add electrons to the system from their electron-rich lone pairs which leads to π^* radicals with higher energy of the SOMO and consequently, higher stability. Additionally, radicals situated on heteroatoms do not have such a strong tendency to form dimers due to the weak bonding between two electronegative atoms.^{29,30} Rigid and fused hydrazyl radicals (*e.g.* Blatter and verdazyl radicals), galvinoxyl radical and nitroxyl radicals (TEMPO and TEMPOL), are the examples of this type of stable radicals (Figure 1.8).

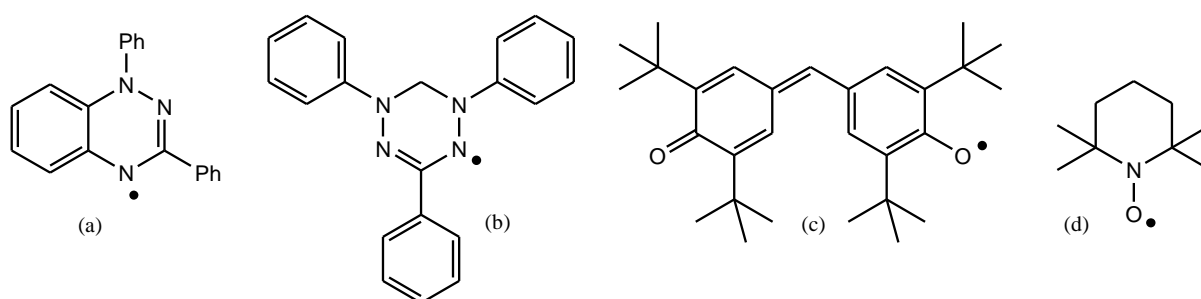


Figure 1.8. Examples of typical heteroatom-based radicals. (a) Blatter radical, (b) verdazyl, (c) galvinoxyl, and (d) nitroxyl.

In hydrazyl radicals, such as Blatter and verdazyl radicals, the unpaired electron is formally centered on a nitrogen atom within a rigid, nitrogen-rich heterocycle, which leads to high delocalization of the SOMO. Therefore, their structures are sensitive to substituent variations. This is a highly valuable property, since simple structural modifications can have significant effects on the overall behavior of the radical.⁴⁶ Blatter radical is stabilized through dipolar resonance forms (Figure 1.9). In Blatter radical the corresponding resonance structure is stabilized by delocalization of the negative charge over two electronegative nitrogen atoms. This probably plays a significant role in the extraordinary stability of Blatter radicals.

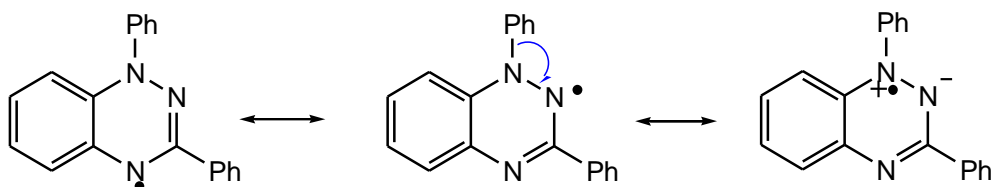


Figure 1.9. Stabilizing dipolar resonance forms of Blatter radical.

The nitrogen-centered verdazyl radical ([Figure 1.8,b](#)), which is air and moisture stable in both solution and solid states, was first reported by Kuhn and Trischmann.⁴⁷ Delocalization of the unpaired electron across all nitrogen atoms in the cyclic hydrazyl structure has a greater significance on the stability of the verdazyl radical comparing to the resonance. Coppinger reported the first stable phenoxyl radical (latter known as galvinoxyl), ([Figure 1.8,c](#)) that showed good stability in air for a few months. Its stability was achieved by the delocalization of oxygen-centered electron *via* the benzene ring.⁴⁸

Nitroxide radicals (aminoxyl radicals, *e.g.* [Figure 1.8,d](#)), which are a well-known family of stable radicals, were first isolated by a Russian chemist in 1959. They possess a high stability, compared to other types of organic radicals, due to delocalization of the unpaired electron in the N–O fragment.⁴⁹ 2,2,6,6-Tetramethylpiperidin-1-oxyl (TEMPO) is the most known and widely used radical belonging to this class of radicals.⁵⁰ It contains four methyl groups at the α position of the nitroxyl moiety, which provide both steric protection and prevent degradation at the α carbon. The unpaired electron in the structure of TEMPO has the π^* orbital character localized on the NO moiety resulting in a three-electron interaction exemplified in the two resonance structures ([Figure 1.10](#)).

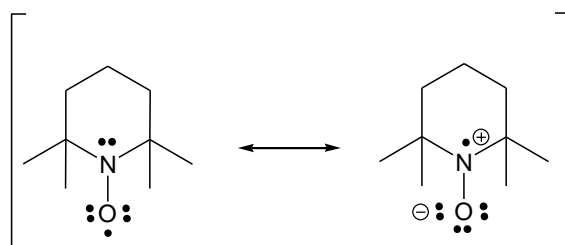


Figure 1.10. Resonance stabilization of (2,2,6,6-tetramethylpiperidin-1-yl)oxyl (TEMPO).

In this Thesis, we focused on synthetic access and systematic and detailed characterization of new derivatives of the Blatter radical, as heteroatom-based radicals with high stability. The spectroscopic, structural, electrochemical, and chemical properties of these radicals are measured to investigate how the chemical structure affects their properties.

1.4. Benzo[*e*][1,2,4]triazinyl radicals: properties and applications

Benzo[*e*][1,2,4]-triazin-4-yl is known as the Blatter radical (Figure 1.11), first described by H. Blatter in 1968, and is the most interesting radical among stable π -delocalized and heteroatom-based radicals.^{46,51,52} It is characterized by exceptional stability,⁵³ spin delocalization,⁵⁴ low excitation energies⁵⁵ and favorable electrochemical and photophysical properties, such as redox behavior with a narrow electrochemical window (~ 1.2 V)⁵⁶ and a broad absorption in the visible range.⁵⁷ Hence, Blatter radicals have recently been applied in controlled polymerization,⁵⁸ organic batteries,⁵⁹ surface chemistry,⁶⁰ photoconductive liquid crystals^{61–64} and also for studies of high-spin molecular systems.^{65–67}

1.4.1. Benzo[*e*][1,2,4]triazinyl radicals: structure

The basic structure of Blatter radicals has three functional aromatic sites (Figure 1.11). Each of them provides different opportunities to alter their properties. Because of the steric interaction between the aryl substituent of N(1) and the benzo[1,2,4]triazinyl core, the unpaired electron is only partially delocalized to the aryl group at the N(1) position. The torsion angle between them can be varied with the change of substituents. Modification of the substituents at the N(1) position will significantly affect the molecular packing in the solid state, leading to a change in magnetic properties.^{68,69}

The C(7) position in the benzo[1,2,4]triazinyl is more reactive than the other positions, which can be used to obtain quinones by oxidation. In order to prevent this oxidation, C(7) position was substituted with the trifluoromethyl group by Koutentis making the radical highly stable.^{58, 70-75} Furthermore, the spin can be more delocalized into the additional aromatic rings when C(6) and C(7) are fused with aromatic groups.⁷⁶⁻⁸⁰

At the C(3) position, the unpaired electron of the [1,2,4]triazinyl cannot delocalized to this position. However, introduction of various substituents at the C(3) position can modify properties of the radicals.⁸¹⁻⁸⁵

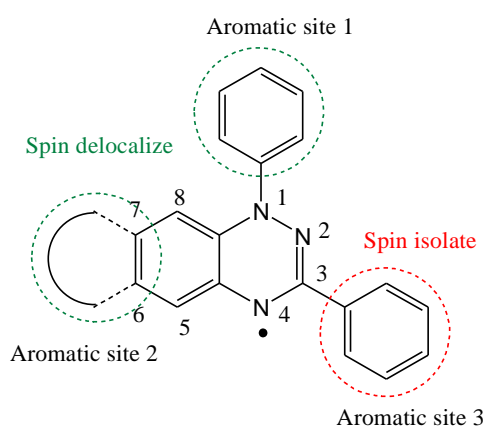


Figure 1.11. The structure of Blatter radicals.

1.4.2. Benzo[*e*][1,2,4]triazinyl radicals: synthesis

The first synthetic access to 1,4-dihydrobenzo[*e*][1,2,4]triazin-4-yl was reported in 1968⁵² and new synthetic pathways have been developed since then. The synthetic methods are categorized in different ways based on various precursors for preparing the Blatter radical (Figure 1.12).

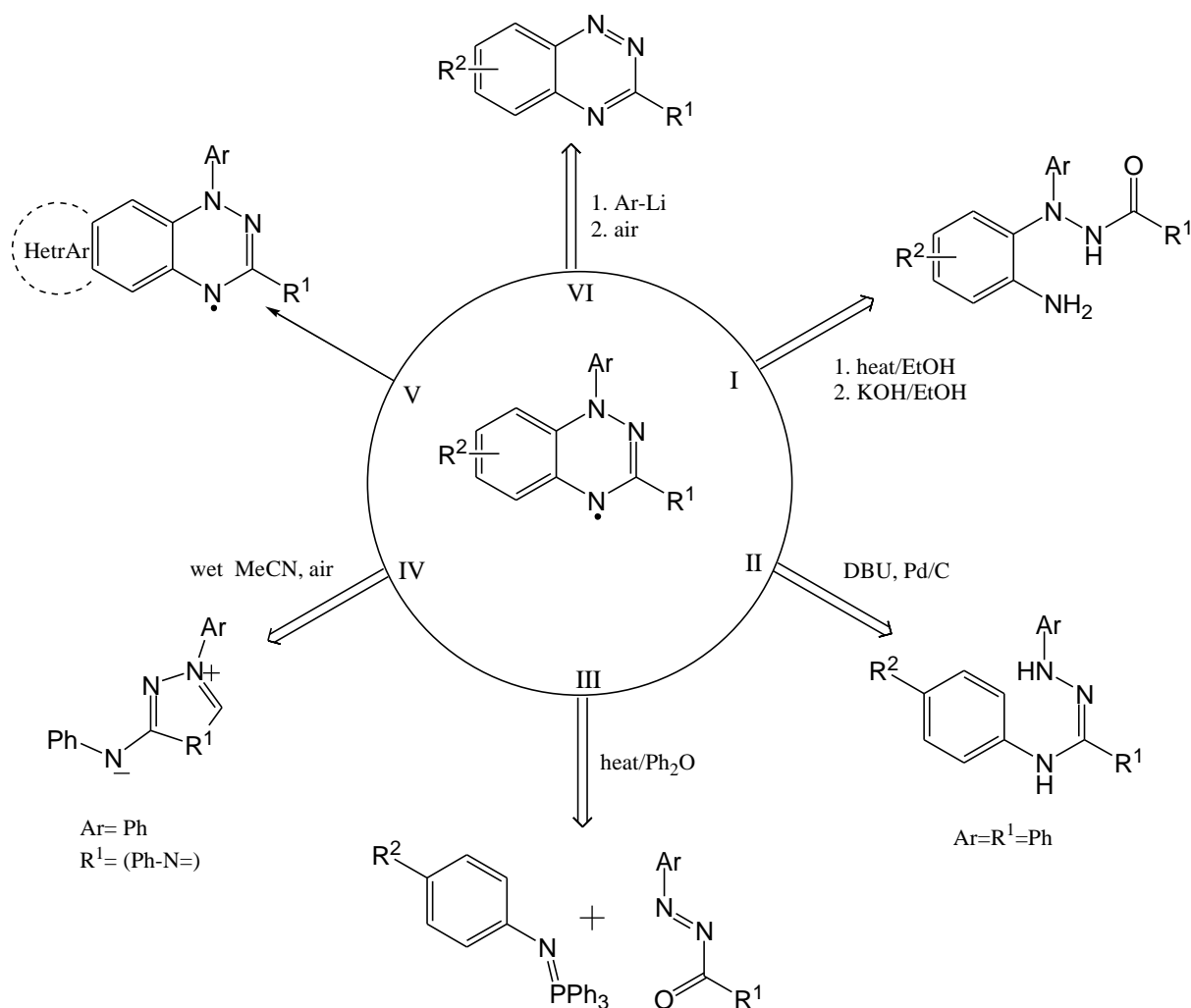


Figure 1.12. Strategies for the synthesis of Blatter radical derivatives (methods I–IV and VI).

The reductive cyclocondensation of the appropriate arylhydrazide (method I) is one of the methods for synthesis of Blatter radicals,⁵⁶ and another method is oxidative 6- π electrocyclization of amidrazones in the presence of catalytic amounts of Pd/C and DBU (Blatter method improvement,⁵² method II), which is the classical route to Blatter radicals.⁷² Both of these methods have some limitations related to the stability of the substrates, low yields and unavailability of some attractive arylhydrazines.

Another synthetic method, which was developed recently, uses the aza-Wittig reaction. In this method the reaction of *N*-aryliminophosphates with acyl diazenes at high temperatures leads directly to Blatter radicals with moderate to good yields (method III).⁸⁶

In method IV, spontaneous hydrolysis of a stable triazolium carbene in acetonitrile that contains a small amount of water has been seen to produce 3-amino-1,4-dihydrobenzo[*e*][1,2,4]triazin-4-yl.⁸⁷

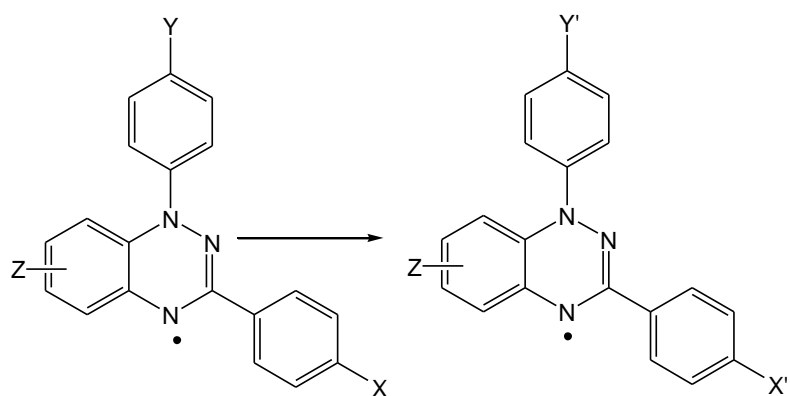
Koutentis has established effective techniques for post-cyclization ring modifications and ring annulations that greatly increase the structural variety of transformation in the Blatter radical. (method V).^{73,74,88}

Lately, a novel method for the synthesis of Blatter radical derivatives was developed in the lab of Prof. Kaszynski, using stable and easily available benzo[*e*][1,2,4]triazine derivatives. This method involves the azaphilic addition of organolithium to benzo[*e*][1,2,4]triazines, which leads to a stable triazinyl anion that slowly oxidises to the radical upon exposure to air (method VI).⁸⁹

Due to the extraordinary stability of Blatter radicals, a number of classical transformations of functional groups can be carried out, while the unpaired spin is present. The transformations include palladium-catalyzed carbon-carbon coupling reactions (e.g. Suzuki-Miyaura, Negishi and Sonogashira, [Figure 1.13](#)).⁵⁷

Other functional group transformations, such as ester hydrolysis, Heck coupling, and nitro group reduction to aniline derivatives, are also carried out without visible decomposition of the radical. ([Figure 1.13](#)).⁵⁷

In my research, as the most convenient method for the synthesis of derivatives of the Blatter radical, I used the azaphilic addition of aryllithium reagents to appropriate benzo[*e*][1,2,4]triazines followed by oxidation of the resulting anion. ([Figure 1.12, method VI](#)).



X, Y = OBn, OBz, NO₂, I, CO₂Me
 Z = H, 7-CF₃, 6-CF₃, 7-I, 6-Br

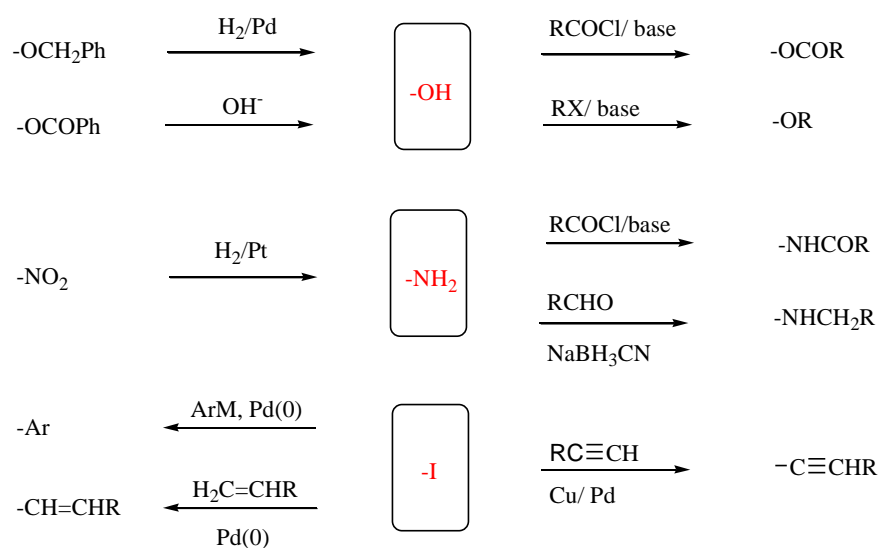


Figure 1.13. Transformation of functional group in benzo[e][1,2,4]triazin-4-yl radical derivatives.⁵⁷

1.5. Planar benzo[*e*][1,2,4]triazinyl radicals: structure

The general feature of all benzo[*e*][1,2,4]triazin-4-yl derivatives is the presence of an aryl substituent at the N(1) position, which due to steric interactions between the C(8)-H and C(*ortho*)-H forms a large dihedral angle θ with the heterocycle (Figure 1.14), typically in a range of 38° – 82° for 1-Ph θ .⁸³ High torsion angle between the π planes limits spin delocalization from N(1)⁵⁴ and affects molecular packing in the solid state, which can affect magnetic properties of the solids.

The connection of the C(8) and C(*ortho*) positions with a chalcogen, such as sulfur or oxygen in structures of planar analogues appears to be the most successful method for addressing these difficulties and planarizing the structure (Figure 1.14),⁶⁹ which enables further research in the field of planar Blatter radicals. Planarizing the structure of the Blatter radical leads to more spin delocalization. This is a conventional approach to stabilize radicals through lowering energy levels of the occupied orbitals and on preventing the radical from reacting with air and moisture.

Kaszynski *et al.* demonstrated the concept of the planar Blatter's radical with the synthesis of several functionalized derivatives by connecting the C(8) and C(*ortho*) positions with oxygen and sulfur atom.⁶⁹ O-annulation results in a much smaller dihedral angle of 3.04° , thus approaching the completely planar geometry. However, owing to the long S-C bond, planar radical with an annulated sulfur atom exhibits moderate dihedral angle of 20.54° .

Since the N(1) position carries the positive spin density, the ability to manipulate with the N(1) substituent plays the crucial role in controlling spin delocalization and, as a consequence, electrochemical properties and intermolecular spin exchange interactions.⁸⁹ A coplanar π substituent at the N(1) would provide maximum spin delocalization, change in packing of the solid state, and enable a novel design framework for functional materials.⁶⁹

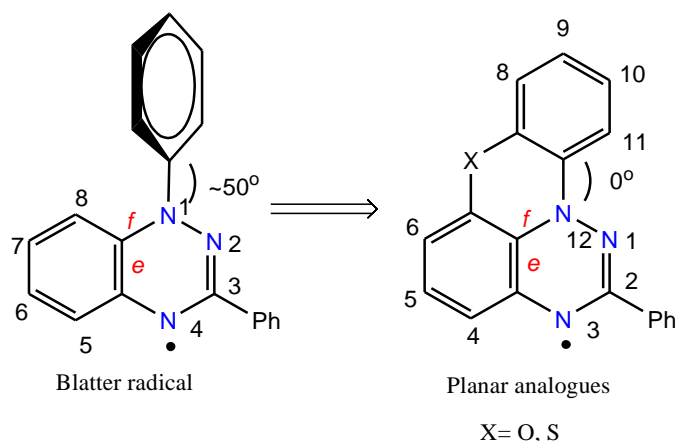


Figure 1.14. Blatter radical and its planar analogues ($X = O, S$).

1.5.1. Planar benzo[*e*][1,2,4]triazinyl radicals: synthesis

There are different strategies for the preparation of planarized Blatter radical, which have greatly broadened the variety of planar radicals in recent advances in the chemistry of the benzo[*e*][1,2,4]triazinyl.

The two parent radicals, containing the phenoxazine ring and based on phenothiazine, were obtained in low yields (20–25%) *via* the intramolecular azaphilic addition of aryllithium reagents generated from the corresponding aryl bromides (Method A, [Figure 1.15](#)).⁶⁹

Pschorr cyclization (Method B) was used in order to increase the yield of *O*-*peri*-annulated analogue and to access its functional derivatives through an azaphilic addition of aryl to the [1,2,4]triazine.⁹⁵ However, these approaches are much less useful for the synthesis of larger planar systems.

For synthesis the π expanded systems of ring-fused planar Blatter radical, Mallory photocyclization of C(8)-substituted benzo[*e*][1,2,4]triazines (Method C, [Figure 1.18](#)) was performed, which is widely used in preparation of closed-shell polycyclic aromatic systems.⁹¹

Unfortunately, methods B and C are not appropriate for synthesizing of sulfur-containing radicals. Strongly oxidative conditions are incompatible with the divalent sulfur in Method B, while in Method C the heavy atom effect causes a rapid decay of the S_1 state. Low yields of method A makes it ineffective.

Due to these issues, a new effective approach for the synthesis of *O*-*peri*-annulated and *S*-fused planar Blatter radicals were developed through a Bu_3SnH - and TMS_3SiH assisted radical chain cyclization of aryl iodides on the [1,2,4]triazine N-atom (Method D, Figure 1.15).⁹²

Like the Pschorr-type cyclization (Method B), it tolerates functional groups, such as COOMe and COMe, and enables the formation of the desired products with noticeably higher yields. Most importantly, it permits the preparation of functionalized derivatives of the [1,2,4]triazino[5,6,1-*kl*]phenothiazinyl, which was previously impossible to prepare through other methods.⁹²

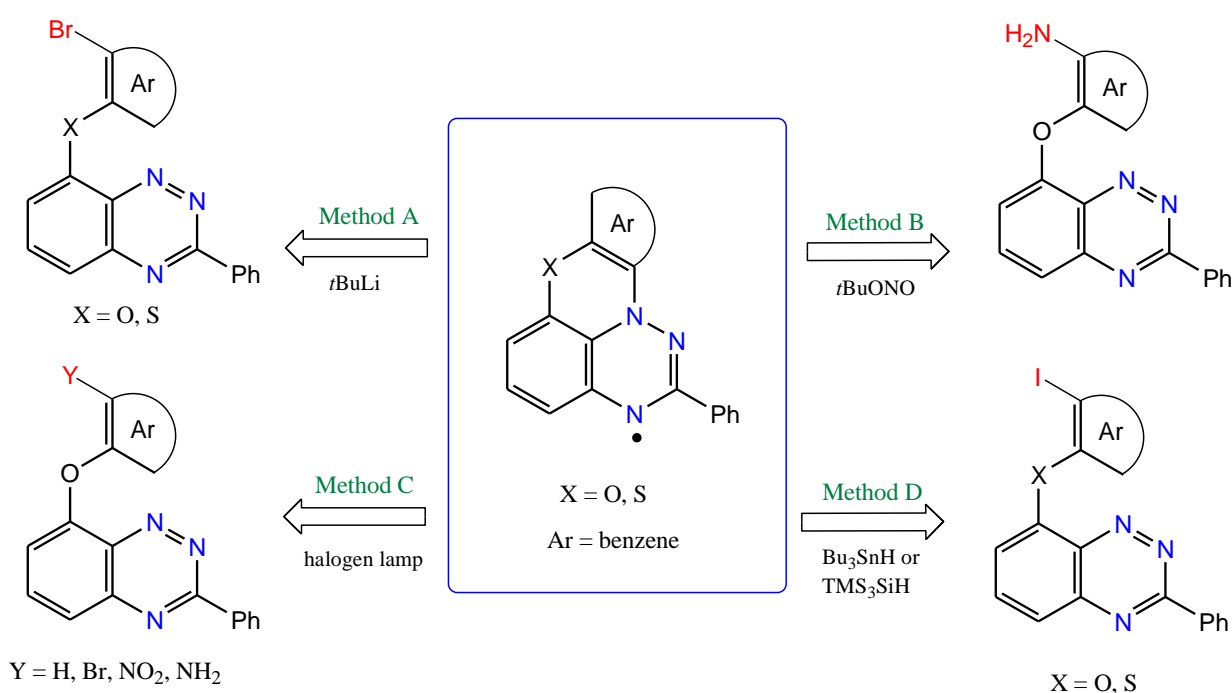


Figure 1.15. Four methods for the preparation of *S*-*peri*-annulated and *O*-*peri*-annulated Blatter radicals.^{69,91,92,95}

1.5.2. Planar benzo[*e*][1,2,4]triazinyl radicals: functionalization and π -expansion

The newest developments in the area of planar Blatter radicals and their derivatives^{90,91} offer not only planarity and greater spin delocalization, but also tunability of properties by judicious choice of substituents and the π -system extension. For these reasons, differently functionalized and π -expanded planar Blatter radicals have been synthesized and their structure property relationship have been studied.

A series of C(10) functionalized sulfur- and oxygen-fused planar Blatter radicals (Figure 1.16) have been obtained in the Kaszyński's group by using different synthetic methods such as Pschorr-type cyclization,⁹⁰ Bu₃SnH- and TMS₃SiH-assisted cyclization of aryl iodides,⁹² Pd-catalyzed C–C cross-coupling functionalization reactions of the C(10)-iodo derivative⁹³ and functional group transformations.⁹⁰

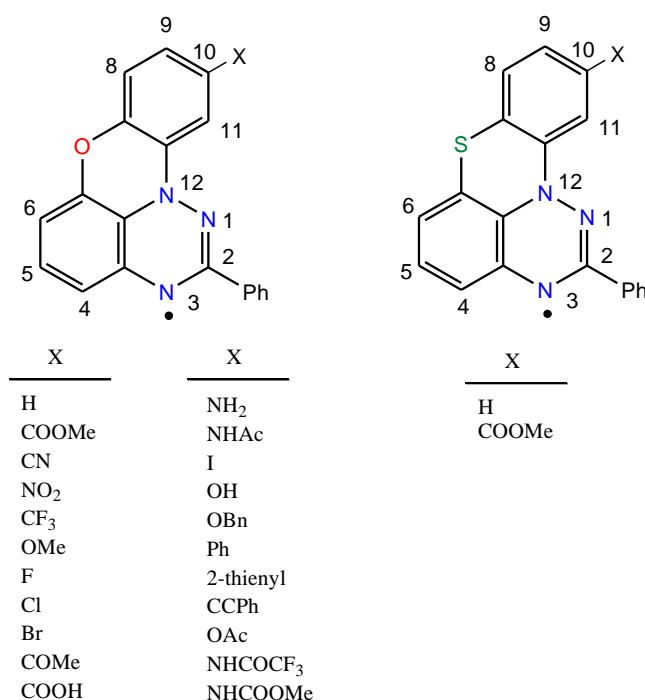


Figure 1.16. The structure of the O-fused and S-fused planar Blatter radical and their C(10) functionalized derivatives.

Ring expansion of the planar Blatter radical (Figure 1.17) up to a total 27 sp^2 -hybridized atoms and 29 π -delocalized electrons in the fused system is reported through photocyclization of 8-aryloxy benzo[*e*][1,2,4]triazines. The effect of substituent and π expansion on the electronic structure was investigated with spectroscopic (UV-vis, electron paramagnetic resonance) and electrochemical methods.^{91,94}

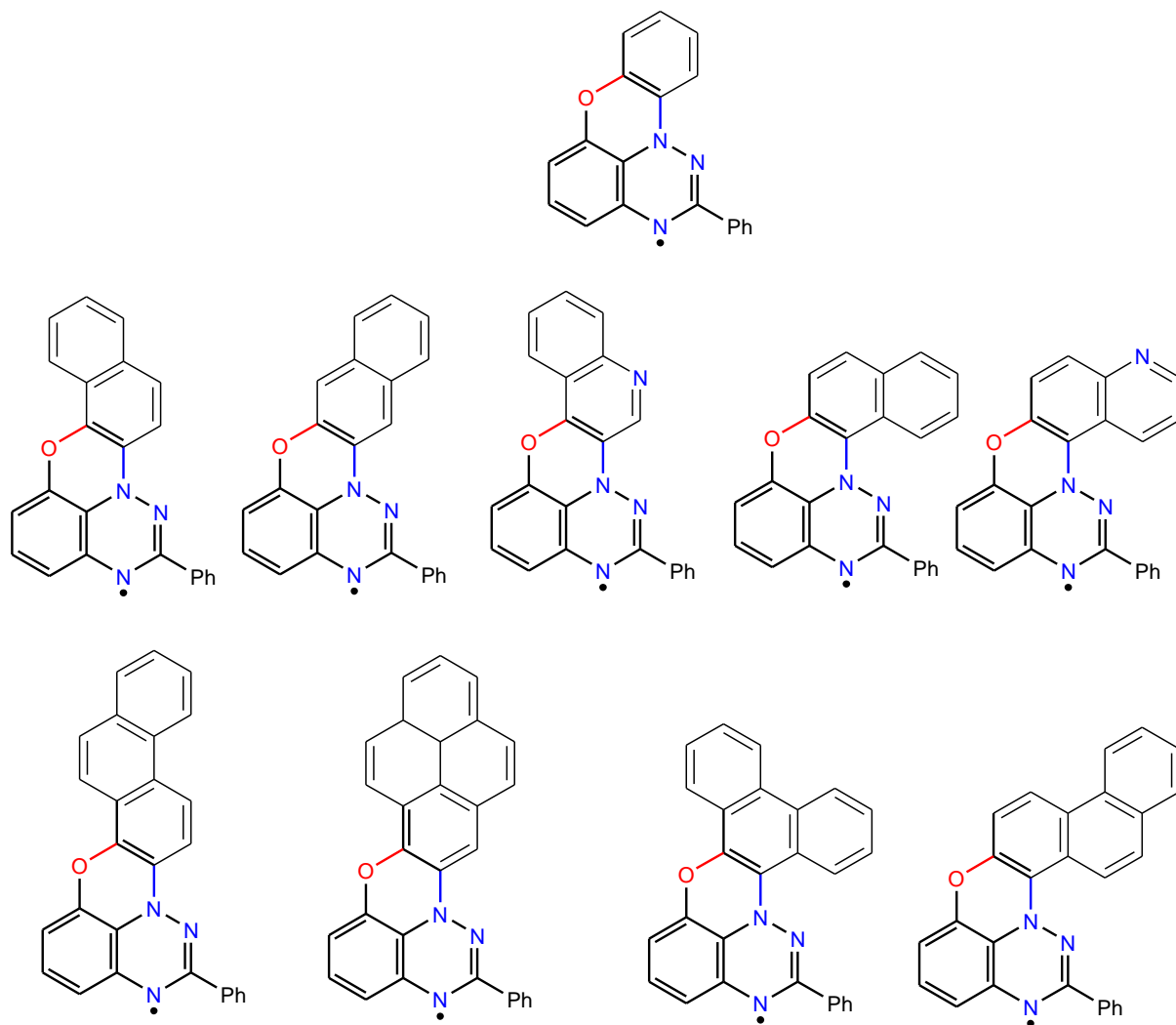


Figure 1.17. The structure of the O-fused and its π -extended derivatives.

The functionalized planar Blatter radicals have been used as structural elements for liquid crystals (Figure 1.18).⁶⁴ The planarity of the open-shell core permits efficient π - π stacking, which results in the formation of bent-core mesogens and soft crystalline phases above 100 °C. They demonstrated that planarization of the Blatter radical by periannulation of the two benzene rings provides sufficient anisotropy for efficient nano-segregation of the aromatic and aliphatic components. This leads to the unprecedented, for stable radical derivatives, formation of an organized lamellar phase with close π - π stacking of the central angular elements and, consequently, strong spin-spin interactions and high charge mobility, as evident from magnetic and photoconductivity measurements.⁶⁴

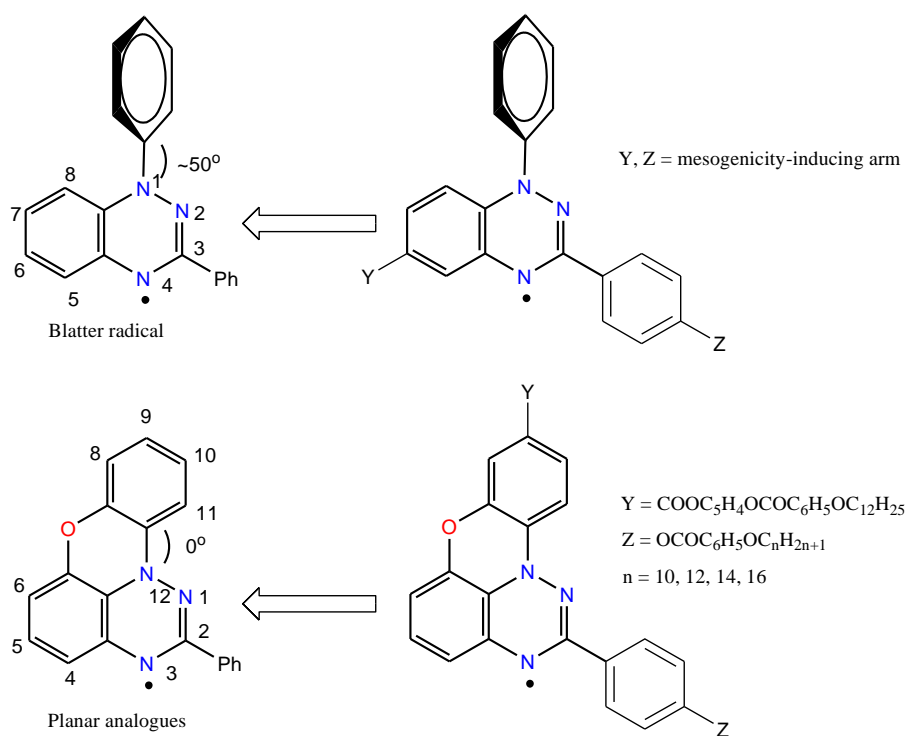


Figure 1.18. The structure of Blatter radical, planar Blatter radical, and two classes of liquid crystalline derivatives.⁶⁴

In general, increasing the electron donating ability of the substituent in bent-core mesogens, lowers the π - π^* excitation energy, cathodically shifts the redox potentials, increases spin delocalization beyond the [1,2,4]triazinyl ring and lowers BDE. All results indicate that the electron donating substituents lower excitation energies and redox potentials, and also increase radical stability by increasing electron spin delocalization and decreasing the N-H bond dissociation energy, and this discovery opens up opportunities for additional research on functionalized planar Blatter radicals especially [1,2,4]triazino[5,6,1-*kl*]phenothiazinyl radicals, and on their solid-state magnetic characteristics. Therefore, in the first part of this Thesis, we described a method for developing a new class of paramagnetic nanographenes, in which the [1,2,4]triazinyl is docked to polycyclic aromatic compounds to provide maximum spin delocalization, and we investigated their structure-property relationships.

In the second part of this Thesis, we present the synthesis and detailed characterization of five new derivatives of functionalized S-*peri*-annulated benzo[*e*][1,2,4]triazinyl and investigate the substituent effect on their spectroscopic and electrochemical properties. The idea behind this project was to contribute to a better understanding of the factors governing the crystal packing of the benzo[*e*][1,2,4]triazinyl derivatives and their impact on magnetic interactions.

For preparation of the functionalized derivatives of S-*peri*-annulated benzo[*e*][1,2,4]triazinyl, different derivatives of functionalized thiols were prepared to use as starting materials for the synthesis the 8-phenylsulfanyl-3-phenylbenzo[*e*][1,2,4]triazines. In this Thesis, two different methods are used for the preparation of thiols. There are however various methods to obtain thiols from different precursors, which are summarized in the next Section 1.6.

1.6. Preparation of aromatic thiols

Different aromatic species, such as haloaromatics, primary aromatic amines, aromatic hydroxyl groups, and aromatic hydrocarbons, can be used to synthesize aromatic thiols through a specific pathway and conditions depending on the type of the aromatic substrate and their functional groups and substituents.⁹⁶

Using haloaromatics is one approach for synthesizing thiols. In haloaromatics with strong electron-withdrawing groups in their structures, conversion to thiols can be achieved by methods such as reactions with hydrogen sulphide ion, thiosulphate ion and thiourea. However, these procedures cannot yield thiols in the case of simple haloaromatics, and an alternative approaches must be taken. There are two effective ways to obtain these compounds either through the use of organolithium and organomagnesium reagents, or by using cuprous alkyl mercaptides followed by the cleavage of the alkyl aryl sulfides (Figure 1.19).⁹⁶

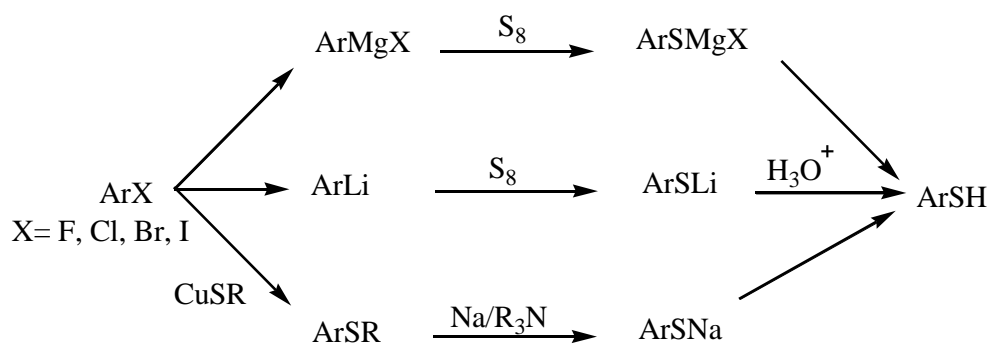


Figure 1.19. Reactions of organomagnesium and organolithium compounds with sulfur for synthesis both alkane and aromatic thiols.

Aromatic hydroxyl groups are also readily transformed into thiol groups by Newman-Kwart rearrangement and Schonberg rearrangement, which is the well-known route to thiophenols from phenols (Figure 1.20).⁹⁶

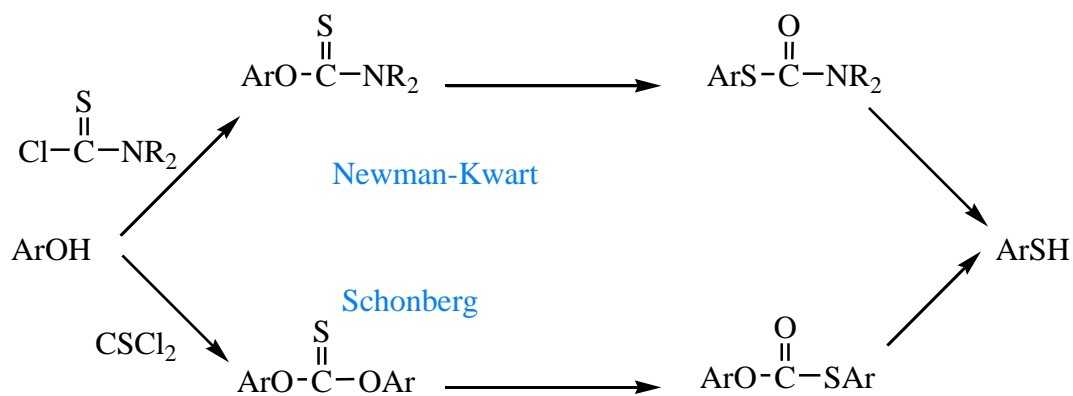


Figure 1.20. Newman-Kwart rearrangement and Schonberg rearrangement for synthesis thiophenols from phenols.

Another common method of thiol preparation involves aromatic electrophilic substitutions by sulfur electrophiles (Figure 1.21). These methods are constrained by the fact that aromatics with electron-withdrawing groups do not react and that only a limited number of isomers can be obtained.⁹⁶

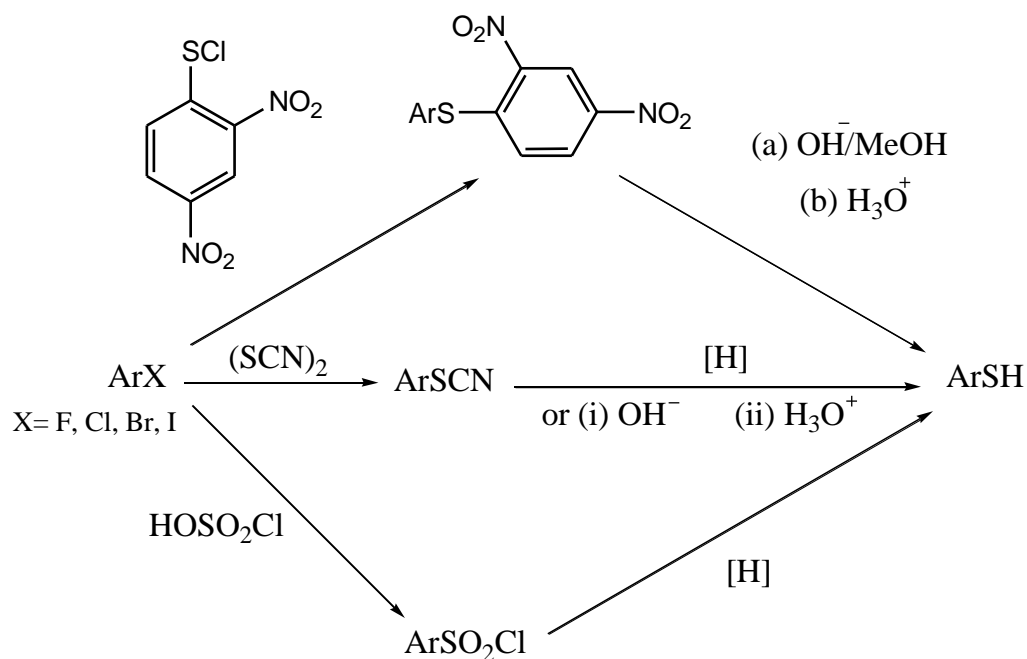


Figure 1.21. Synthesis of thiols by sulfur electrophiles via aromatic electrophilic substitutions.

Other examples of electrophilic aromatic substitutions leading to thiols include the reaction of sulfur dichloride with phenols and anilines (Figure 1.22).⁹⁶

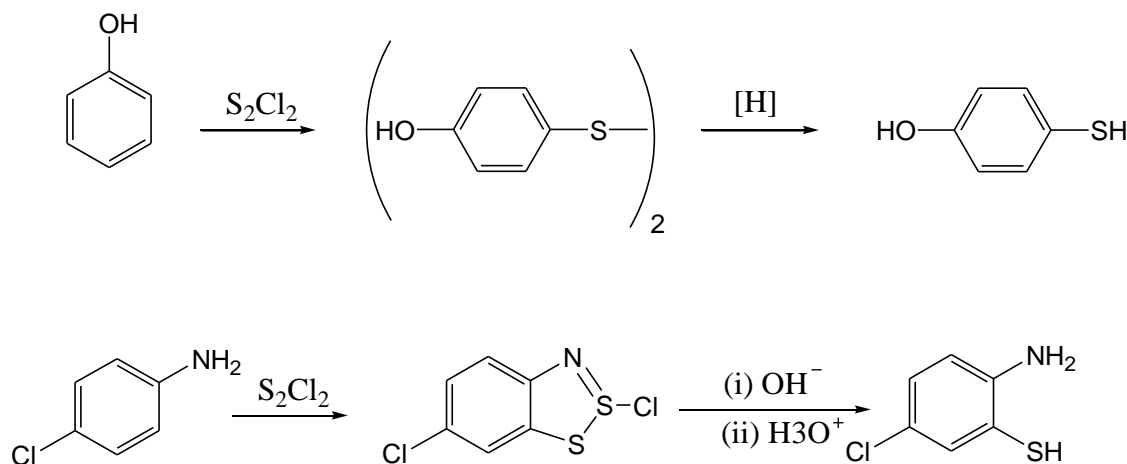


Figure 1.22. Synthesis of thiols by the reaction of disulfur dichloride with phenols and anilines.

There are a number of modifications from primary aromatic amines that each involve the reaction of the corresponding diazonium salt with a sulfur nucleophile (Figure 1.23). The xanthate reaction is the oldest among these processes.⁹⁶ Even if it is still the most popular approach, all of them offer a lot of potential. More focus should be placed on alternative techniques due to the risk of explosions in the xanthate process.⁹⁶

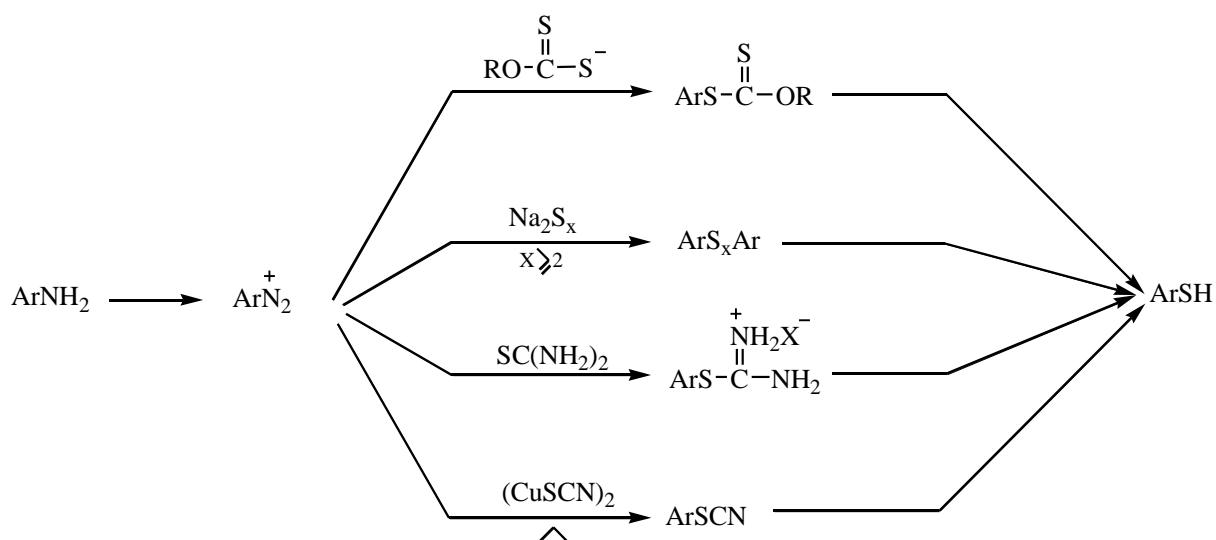


Figure 1.23. Synthesis of thiols by the reaction of a diazonium salt with a sulfur nucleophile.

1.6.1. Preparation of thiols *via* xanthates from aromatic diazonium salts

Arene-thiols are obtained by converting the diazonium salts to xanthates (Figure 1.24).⁹⁷⁻⁹⁹ This method uses an alkali metal alkyl xanthate. The potassium ethyl xanthate is typically employed⁹⁸ and it has been advised against heating solutions of potassium ethyl xanthate and aryl diazonium salts because explosions can occur.

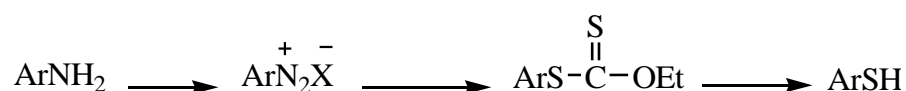


Figure 1.24. Synthesis of thiols by converting the appropriate xanthates from diazonium salts.

There are two common ways to prepare thiols from xanthates. These techniques include (a) basic hydrolysis and (b) reduction, especially when utilizing lithium aluminum hydride. Since many substituents are inert to the hydroxide ion under the conditions needed for hydrolyses, sodium (or potassium) hydroxide is typically employed to hydrolyze the xanthates.⁹⁸⁻¹⁰⁰

1.6.2. Preparation of thiols from disulfides and polysulfides

Reduction and other sulfur-sulfur bond cleavage reactions make it easy to convert disulfides to thiols. In some circumstances, disulfides have been obtained instead of thiols, which are often formed later by reducing the disulfides (Figure 1.25).⁹⁶

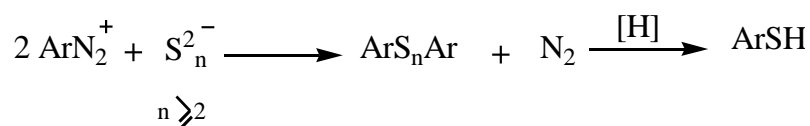


Figure 1.25. Synthesis of thiols by reducing the disulfides.

There are numerous reagents and techniques for reducing disulfides, such as lithium aluminum hydride, sodium borohydride, zinc and acid, alcohol,¹⁰¹⁻¹⁰⁴ tin,¹⁰¹ and other metals,¹⁰⁵ and acids, among others.

1.6.3. Preparation of thiols through thiocyanates

Thiocyanogen and thiocyanogen halides react with aromatic hydrocarbons containing strong electron-donating groups, such as the hydroxy and amino groups, to produce aryl thiocyanate, even in the presence of NO_2 , Cl, Br, and CO_2Et substituents.^{96,106} Normally, a metal thiocyanate and either bromine or chlorine are added to form *in situ* thiocyanogen (or thiocyanogen halide) (Figure 1.26). To prevent the development of a polymeric thiocyanogen material, low temperature should be applied. Only a few isomers can be produced since these reactions are electrophilic; for example, the thiocyanate usually attaches to the *para* position of amino or hydroxyl groups in the aromatic ring; if this position is blocked, *ortho* substitution results.⁹⁶

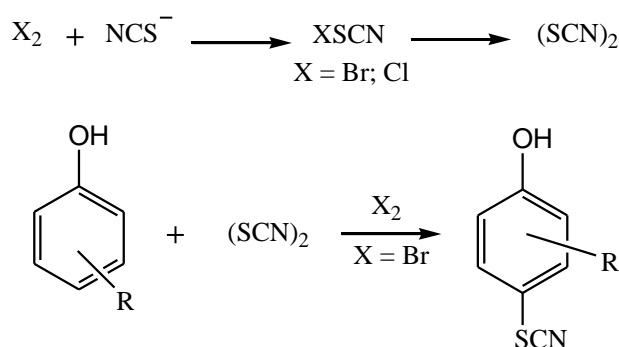
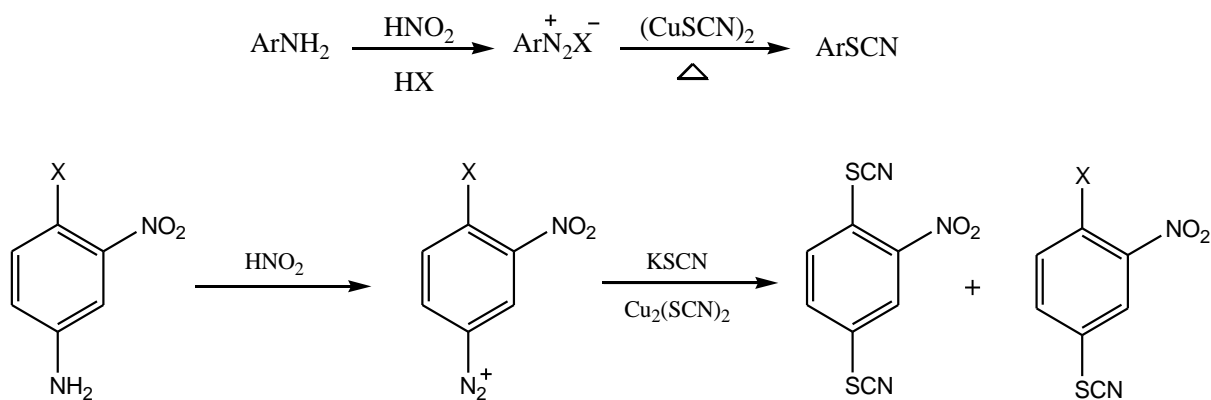


Figure 1.26. Synthesis of thiocyanogen.

The most versatile methods to produce aryl thiocyanates involve cuprous thiocyanates and diazotized amines in Gatterman or Sandmeyer reactions.^{96,107,108} Ferric thiocyanate can also be used. The availability of primary aromatic amines is the method's constraint. The halogen in *o*- and *p*-halobenzenediazonium salts can also be replaced by thiocyanates (Figure 1.27).^{96,109} Thus, diazotized 4-bromo- and 4-chloro-3-nitroaniline gave nitro-*para*-dithiocyanato benzene as well as the 4-halogeno-3-nitrophenyl thiocyanate on treatment with potassium and copper(I) thiocyanates (Figure 1.27). In this case, the strongly electron-withdrawing diazonium group allows the nucleophilic substitution of the halide.⁹⁶



X = Br; Cl

Figure 1.27. Synthesis of aryl thiocyanate involving cuprous thiocyanates and diazotized amines in Gatterman or Sandmeyer reactions.

1.6.4. Reduction of thiocyanates to thiols

One of the reducing agents that can be used to convert thiocyanates into thiols is lithium aluminum hydride. Such different compounds as *p*-tolyl thiocyanate¹¹⁰ and 1-hydroxy-4-thiocyanato-2,3,5,6-tetramethylbenzene¹⁰⁶ are reduced by lithium aluminum hydride in ether in good yields to the corresponding thiols (Figure 1.28).

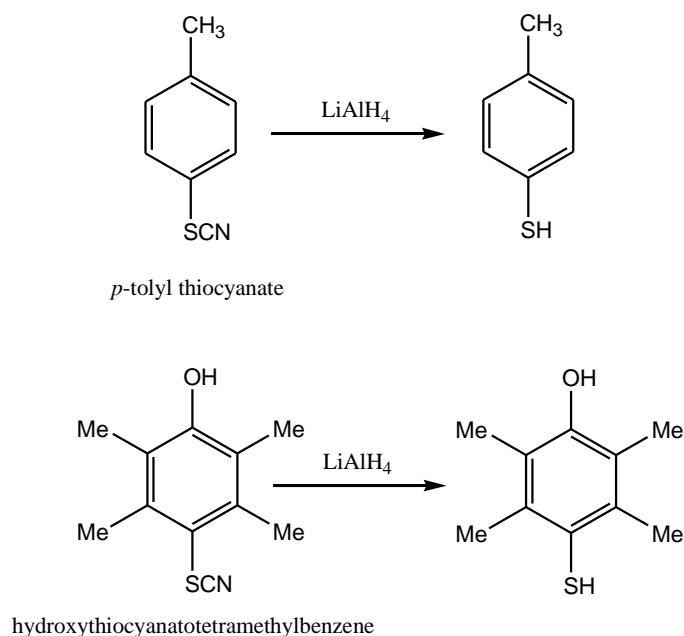


Figure 1.28. Synthesis of thiols by reducing aryl thiocyanate by lithium aluminum hydride.

Sodium borohydride, a milder reducing agent, was utilized as the reductant for diethyl 1-benzyl-2-thiocyanatopyrrole-3,4-dicarboxylate without damaging the ester groups (Figure 1.29).⁹⁶

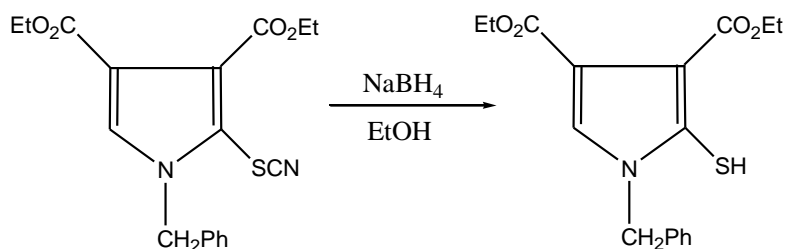


Figure 1.29. Synthesis of thiol by reducing diethyl 1-benzyl-2-thiocyanatopyrrole-3,4-dicarboxylate by sodium borohydride.

Alkyl and aryl thiocyanates were successfully reduced using sodium in liquid ammonia and yields of more than 70% were reported for hydroxyaromatic thiols. However, this method also has an impact on halogens- and the nitro-groups. Alkaline hydrolysis of aryl thiocyanates was demonstrated to produce thiophenols in good yields. The alkaline hydrolysis of *p*-di-thiocyanato benzene led to benzene-1,4-dithiol.⁹⁶ However, the disulfide was obtained when alkali was applied to aryl thiocyanates that contained electron-withdrawing groups (Figure 1.30).^{96,108} Reduction can also be performed in the presence of zinc and acid. *Para*-nitrobenzyl thiocyanate was successfully hydrolyzed by acid^{96,111} and *p*-nitrobenzyl thiocarbamate was observed an intermediate in this process.

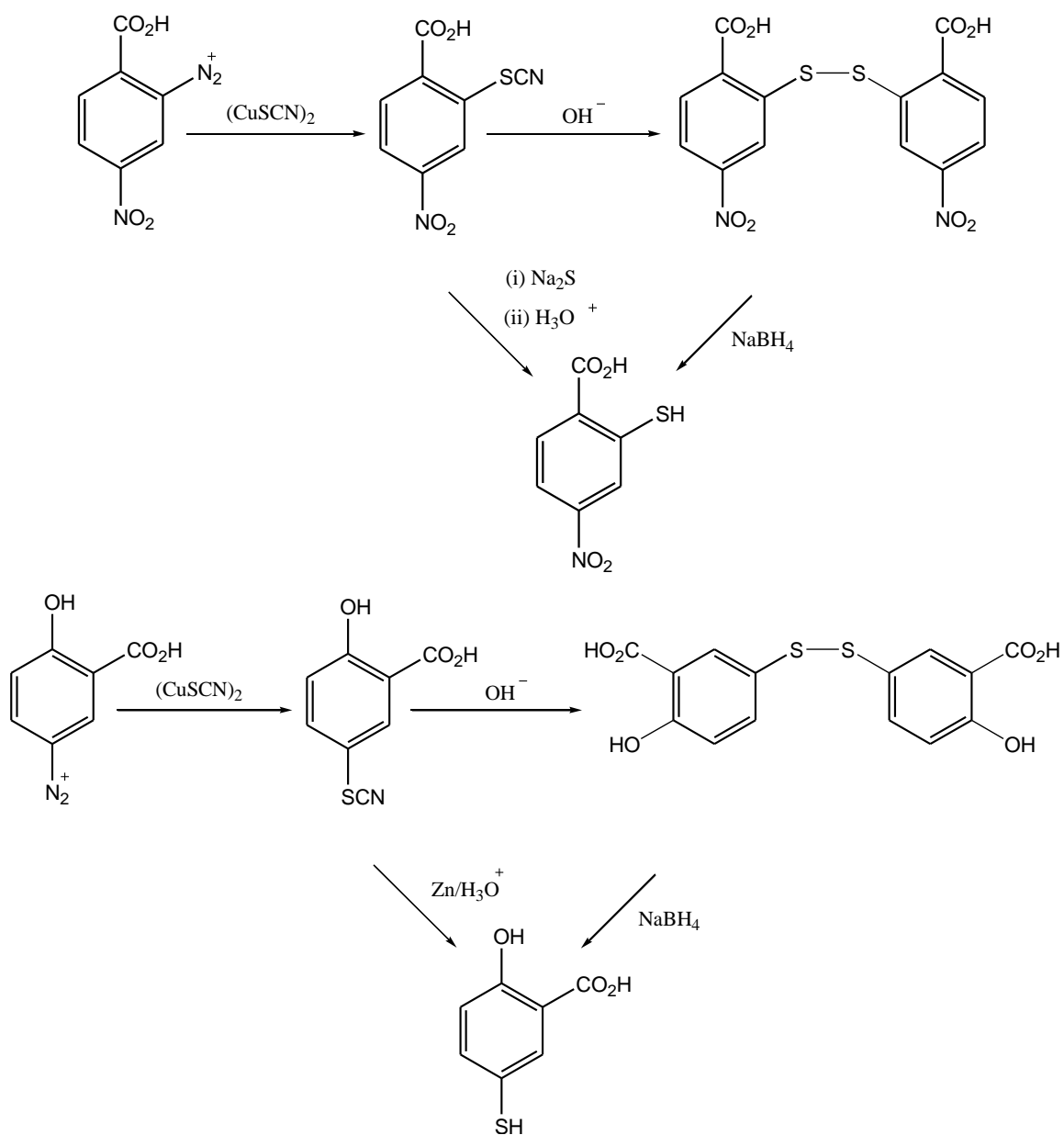


Figure 1.30. Synthesis of thiols by alkaline hydrolysis of aryl thiocyanates.

1.7. References

- (1) Stepien, M.; Gonka, E.; Żyła, M.; Sprutta, N. *Chemical Reviews*. **2017**, *117*(4), 3479-3716.
- (2) Mullen, K. *ACS Nano*. **2014**, *8*(7), 6531-6541.
- (3) Müllen, K.; Rabe, J. P. *Accounts of Chemical Research*. **2008**, *41*(4), 511-520.
- (4) Figueira-Duarte, T. M.; Mullen, K. *Chemical Reviews*. **2011**, *111*(11), 7260-7314.
- (5) Narita, A.; Wang, X. Y.; Feng, X.; Müllen, K. *Chemical Society Reviews*. **2015**, *44*(18), 6616-6643.
- (6) Kuninobu, Y.; Sueki, S. *Synthesis*. **2015**, *47*(24), 3823-3845.
- (7) Dewar, M. J. *Journal of the American Chemical Society*. **1952**, *74*(13), 3345-3350.
- (8) Li, Z.; Bally, T.; Houk, K. N.; Borden, W. T. *The Journal of Organic Chemistry*. **2016**, *81*(20), 9576-9584.
- (9) Huang, M.; Penning, T. M. *Encyclopedia of Food Safety*. **2014**, *2*, 416-423.
- (10) Gutzler, R.; Perepichka, D. F. *Journal of the American Chemical Society*. **2013**, *135*(44), 16585-16594.
- (11) Gomberg, M. *Journal of the American Chemical Society*. **1900**, *22*(11), 757-771.
- (12) Kahr, B.; Van Engen, D.; Gopalan, P. *Chemistry of Materials*. **1993**, *5*(5), 729-732.
- (13) Grubbs, R. B. *Polymer Reviews*. **2011**, *51*(2), 104-137.
- (14) Rugg, B. K.; Krzyaniak, M. D.; Phelan, B. T.; Ratner, M. A.; Young, R. M.; Wasielewski, M. R. *Nature Chemistry*. **2019**, *11*(11), 981-986.
- (15) Joo, Y.; Agarkar, V.; Sung, S. H.; Savoie, B. M.; Boudouris, B. W. *Science*, *359*(6382). **2018**, 1391-1395.
- (16) Qu, Y.; Li, Y.; Tan, X.; Zhai, W.; Han, G.; Hou, J.; Liu, Y. *Chemistry—A European Journal*. **2019**, *25*(33), 7888-7895.
- (17) Samouilov, A.; Ahmad, R.; Boslett, J.; Liu, X.; Petryakov, S.; Zweier, J. L. *Magnetic Resonance in Medicine*. **2019**, *82*(2), 842-853.

- (18) Ohira, S.; Nakayama, K.; Ise, T.; Ishida, T.; Nogami, T.; Watanabe, I.; Nagamine, K. *Polyhedron*. **2001**, *20*(11-14), 1223-1227.
- (19) Matsumura, T.; Tanaka, H.; Kaneko, K.; Yudasaka, M.; Iijima, S.; Kanoh, H. *The Journal of Physical Chemistry C*. **2007**, *111*(28), 10213-10216.
- (20) Jiao, Y.; Li, W. L.; Xu, J. F.; Wang, G.; Li, J.; Wang, Z.; Zhang, X. *Angewandte Chemie International Edition*. **2016**, *55*(31), 8933-8937.
- (21) Yan, M.; Lo, J. C.; Edwards, J. T.; Baran, P. S. *Journal of the American Chemical Society*. **2016**, *138*(39), 12692-12714.
- (22) Gu, Q. S.; Li, Z. L.; Liu, X. Y. *Accounts of Chemical Research*. **2019**, *53*(1), 170-181.
- (23) Romero, N. A.; Nicewicz, D. A. *Chemical Reviews*. **2016**, *116*(17), 10075-10166.
- (24) Jiang, H.; Studer, A. *CCS Chemistry*. **2019**, *1*(1), 38-49.
- (25) Matyjaszewski, K.; Xia, J. *Chemical Reviews*. **2001**, *101*(9), 2921-2990.
- (26) Feng, G.; Cheng, P.; Yan, W.; Boronat, M.; Li, X.; Su, J. H.; Yu, J. *Science*. **2016**, *351*(6278), 1188-1191.
- (27) Ratera, I.; Veciana, J. *Chemical Society Reviews*. **2012**, *41*(1), 303-349.
- (28) Hicks, R. G. *Organic & Biomolecular Chemistry*. **2007**, *5*(9), 1321-1338.
- (29) Power, P. P. *Chemical Reviews*. **2003**, *103*(3), 789-810.
- (30) Tang, B.; Zhao, J.; Xu, J. F.; Zhang, X. *Chemical Science*. **2020**, *11*(5), 1192-1204.
- (31) Kato, K.; Osuka, A. *Angewandte Chemie International Edition*. **2019**, *58*(27), 8978-8986.
- (32) Nishide, H.; Iwasa, S.; Pu, Y. J.; Suga, T.; Nakahara, K.; Satoh, M. *Electrochimica acta*. **2004**, *50*(2-3), 827-831.
- (33) Janoschka, T.; Martin, N.; Martin, U.; Friebe, C.; Morgenstern, S.; Hiller, H.; Schubert, U. S. *Nature*, *527*(7576). **2015**, 78-81.
- (34) Winsberg, J.; Hagemann, T.; Janoschka, T.; Hager, M. D.; Schubert, U. S. *Angewandte Chemie International Edition*. **2017**, *56*(3), 686-711.
- (35) Andersen, P.; Klewe, B. E. R. N. T. *Acta Chem. Scand*. **1967**, *21*(10), 2.

- (36) Veciana, J.; Carilla, J.; Miravittles, C.; & Molins, E. *Journal of the Chemical Society, Chemical Communications*. **1987**, (11), 812-814.
- (37) Sogo, P. B.; Nakazaki, M.; Calvin, M. *The Journal of Chemical Physics*. **1957**, 26(5), 1343-1345.
- (38) Reid, D. H. *Tetrahedron*. **1958**, 3(3), 339-352.
- (39) Shirman, E.; Ustinov, A.; Ben-Shitrit, N.; Weissman, H.; Iron, M. A.; Cohen, R.; Rybtchinski, B. *The Journal of Physical Chemistry B*. **2008**, 112(30), 8855-8858.
- (40) Schmidt, D.; Son, M.; Lim, J. M.; Lin, M. J.; Krummenacher, I.; Braunschweig, H.; Würthner, F. *Angewandte Chemie International Edition*. **2015**, 54(47), 13980-13984.
- (41) Lee, S.; Miao, F.; Phan, H.; Herng, T. S.; Ding, J.; Wu, J.; Kim, D. *ChemPhysChem*. **2017**, 18(6), 591-595.
- (42) Kim, Y.; Lee, E. *Chemistry—A European Journal*. **2018**, 24(72), 19110-19121.
- (43) Kumar, S.; Ajayakumar, M. R.; Hundal, G.; Mukhopadhyay, P. *Journal of the American Chemical Society*. **2014**, 136(34), 12004-12010.
- (44) Seifert, S.; Schmidt, D.; Würthner, F. *Chemical Science*. **2015**, 6(3), 1663-1667.
- (45) Schmidt, D.; Bialas, D.; Würthner, F. *Angewandte Chemie*. **2015**, 127(12), 3682-3685.
- (46) Rogers, F. J.; Norcott, P. L.; Coote, M. L. *Organic & Biomolecular Chemistry*. **2020**, 18(41), 8255-8277.
- (47) Kuhn, R.; Trischmann, H. *Angewandte Chemie*. **1963**, 75(6), 294-295.
- (48) Coppinger, G. M. *Journal of the American Chemical Society*. **1957**, 79(2), 501-502.
- (49) Zhang, K.; Monteiro, M. J.; Jia, Z. *Polymer Chemistry*. **2016**, 7(36), 5589-5614.
- (50) Nilsen, A.; Braslau, R. *Journal of Polymer Science Part A: Polymer Chemistry*. **2006**, 44(2), 697-717.
- (51) Ji, Y.; Long, L.; Zheng, Y. *Materials Chemistry Frontiers*. **2020**, 4(12), 3433-3443.
- (52) Blatter, H. M.; Lukaszewski, H. *Tetrahedron Letters*. **1968**, 9(22), 2701-2705.
- (53) Neugebauer, F. A.; Umminger, I. *Chemische Berichte*. **1981**, 114(7), 2423-2430.

- (54) Neugebauer, F. A.; Rimmler, G. *Magnetic Resonance in Chemistry*. **1988**, 26(7), 595-600.
- (55) Neugebauer, F. A.; Umminger, I. *Chemische Berichte*. **1980**, 113(4), 1205-1225.
- (56) Berezin, A. A.; Zissimou, G.; Constantinides, C. P.; Beldjoudi, Y.; Rawson, J. M.; Koutentis, P. A. *The Journal of Organic Chemistry*. **2014**, 79(1), 314-327.
- (57) Bodzioch, A.; Zheng, M.; Kaszyński, P.; Utecht, G. *The Journal of Organic Chemistry*. **2014**, 79(16), 7294-7310.
- (58) Demetriou, M.; Berezin, A. A.; Koutentis, P. A.; Krasia-Christoforou, T. *Polymer International*. **2014**, 63(4), 674-679.
- (59) Friebe, C.; Schubert, U. S. *Electrochemical Energy Storage: Next Generation Battery Concepts*. **2019**, 65-99.
- (60) Low, J. Z.; Kladnik, G.; Patera, L. L.; Sokolov, S.; Lovat, G.; Kumarasamy, E.; Venkataraman, L. *Nano Letters*. **2019**, 19(4), 2543-2548.
- (61) Jasinski, M.; Szczytko, J.; Pocięcha, D.; Monobe, H.; Kaszynski, P. *Journal of the American Chemical Society*. **2016**, 138(30), 9421-9424.
- (62) Kapuściński, S.; Gardias, A.; Pocięcha, D.; Jasiński, M.; Szczytko, J.; Kaszyński, P. *Journal of Materials Chemistry C*. **2018**, 6(12), 3079-3088.
- (63) Kapuściński, S.; Szczytko, J.; Pocięcha, D.; Jasiński, M.; Kaszyński, P. *Materials Chemistry Frontiers*. **2021**, 5(17), 6512-6521.
- (64) Shivakumar, K. I.; Pocięcha, D.; Szczytko, J.; Kapuściński, S.; Monobe, H.; Kaszyński, P. *Journal of Materials Chemistry C*. **2020**, 8(3), 1083-1088.
- (65) Gallagher, N.; Zhang, H.; Junghoefer, T.; Giangrisostomi, E.; Ovsyannikov, R.; Pink, M.; Rajca, A. *Journal of the American Chemical Society*. **2019**, 141(11), 4764-4774.
- (66) Gallagher, N. M.; Bauer, J. J.; Pink, M.; Rajca, S.; Rajca, A. *Journal of the American Chemical Society*. **2016**, 138(30), 9377-9380.
- (67) Hu, X.; Zhao, L.; Chen, H.; Ding, Y.; Zheng, Y. Z.; Miao, M. S.; Zheng, Y. *Journal of Materials Chemistry C*. **2019**, 7(22), 6559-6563.

- (68) Gardias, A.; Kaszyński, P.; Obijalska, E.; Trzybiński, D.; Domagała, S.; Woźniak, K.; Szczytko, J. *Chemistry—A European Journal*. **2018**, *24*(6), 1317-1329.
- (69) Kaszyński, P.; Constantinides, C. P.; Young Jr, V. G. *Angewandte Chemie International Edition*. **2016**, *55*(37), 11149-11152.
- (70) Constantinides, C. P.; Koutentis, P. A.; Rawson, J. M. *Chemistry—A European Journal*. **2012**, *18*(48), 15433-15438.
- (71) Constantinides, C. P.; Koutentis, P. A.; Krassos, H.; Rawson, J. M.; Tasiopoulos, A. J. *The Journal of Organic Chemistry*. **2011**, *76*(8), 2798-2806.
- (72) Koutentis, P. A.; Re, D. L. *Synthesis*. **2010**, *2010*(12), 2075-2079.
- (73) Constantinides, C. P.; Koutentis, P. A.; Loizou, G. *Organic & Biomolecular Chemistry*. **2011**, *9*(9), 3122-3125.
- (74) Constantinides, C. P.; Carter, E.; Murphy, D. M.; Manoli, M.; Leitus, G. M.; Bendikov, M.; Koutentis, P. A. *Chemical Communications*. **2013**, *49*(77), 8662-8664.
- (75) Constantinides, C. P.; Koutentis, P. A.; Rawson, J. M. *Chemistry—A European Journal*. **2012**, *18*(23), 7109-7116.
- (76) Constantinides, C. P.; Berezin, A. A.; Manoli, M.; Leitus, G. M.; Zissimou, G. A.; Bendikov, M.; Koutentis, P. A. *Chemistry—A European Journal*. **2014**, *20*(18), 5388-5396.
- (77) Zheng, Y.; Miao, M. S.; Kemei, M. C.; Seshadri, R.; Wudl, F. *Israel Journal of Chemistry*. **2014**, *54*(5-6), 774-778.
- (78) Constantinides, C. P.; Berezin, A. A.; Manoli, M.; Leitus, G. M.; Bendikov, M.; Rawson, J. M.; Koutentis, P. A. *New Journal of Chemistry*. **2014**, *38*(3), 949-954.
- (79) Berezin, A. A.; Constantinides, C. P.; Mirallai, S. I.; Manoli, M.; Cao, L. L.; Rawson, J. M.; Koutentis, P. A. *Organic & Biomolecular Chemistry*. **2013**, *11*(39), 6780-6795.
- (80) Berezin, A. A.; Constantinides, C. P.; Drouza, C.; Manoli, M.; Koutentis, P. A. *Organic Letters*. **2012**, *14*(21), 5586-5589.
- (81) Constantinides, C. P.; Berezin, A. A.; Zissimou, G. A.; Manoli, M.; Leitus, G. M.; Bendikov, M.; Koutentis, P. A. *A. Journal of the American Chemical Society*. **2014**, *136*(34), 11906-11909.

- (82) Yan, B.; Cramen, J.; McDonald, R.; Frank, N. L. *Chemical Communications*. **2011**, 47(11), 3201-3203.
- (83) Takahashi, Y.; Miura, Y.; Yoshioka, N. *New Journal of Chemistry*. **2015**, 39(6), 4783-4789.
- (84) Mukai, K.; Inoue, K.; Achiwa, N.; Jamali, J. B.; Krieger, C.; Neugebauer, F. A. *Chemical Physics Letters*. **1994**, 224(5-6), 569-575.
- (85) Constantinides, C. P.; Berezin, A. A.; Zissimou, G. A.; Manoli, M.; Leitus, G. M.; Koutentis, P. A. *Molecules*. **2016**, 21(5), 636.
- (86) Savva, A. C.; Mirallai, S. I.; Zissimou, G. A.; Berezin, A. A.; Demetriades, M.; Kourtellaris, A.; Koutentis, P. A. *The Journal of Organic Chemistry*. **2017**, 82(14), 7564-7575.
- (87) Grant, J. A.; Lu, Z.; Tucker, D. E.; Hockin, B. M.; Yufit, D. S.; Fox, M. A.; O'Donoghue, A. C. *Nature Communications*. **2017**, 8(1), 15088.
- (88) Takahashi, Y.; Miura, Y.; Yoshioka, N. *Chemistry Letters*. **2014**, 43(8), 1236-1238.
- (89) Constantinides, C. P.; Obijalska, E.; Kaszynski, P. *Organic Letters*. **2016**, 18(5), 916-919.
- (90) Bartos, P.; Anand, B.; Pietrzak, A.; Kaszynski, P. *Organic Letters*. **2019**, 22(1), 180-184.
- (91) Bartos, P.; Young Jr, V. G.; Kaszynski, P. *Organic Letters*. **2020**, 22(10), 3835-3840.
- (92) Bartos, P.; Celeda, M.; Pietrzak, A.; Kaszyński, P. *Organic Chemistry Frontiers*. **2022**, 9(4), 929-938.
- (93) Bartos, P.; Hande, A. A.; Pietrzak, A.; Chrostowska, A.; Kaszyński, P. *New Journal of Chemistry*. **2021**, 45(48), 22876-22887.
- (94) Zissimou, G. A.; Bartos, P.; Pietrzak, A.; Kaszyński, P. *The Journal of Organic Chemistry*. **2022**, 87(7), 4829-4837.
- (95) Gurry, M.; Aldabbagh, F. *Organic & Biomolecular Chemistry*. **2016**, 14(16), 3849-3862.
- (96) Wardell, J. L. *The Thiol Group (1974) Part 1*. **1974**, 1, 163-269.

- (97) Wilson, H. F.; Tarbell, D. S. *Journal of the American Chemical Society*. **1950**, 72(11), 5200-5205.
- (98) Crampton, M. R. *Journal of the Chemical Society B: Physical Organic*. **1971**, 2112-2116.
- (99) Leuckart, R. *Journal für Praktische Chemie*. **1890**, 41(1), 179-224.
- (100) Pan, H. L.; Namkung, M. J.; Fletcher, T. L. 3. *Journal of Medicinal Chemistry*. **1968**, 11(6), 1236-1237.
- (101) Bogert, M. T.; Smidth, L. *Journal of the American Chemical Society*. **1928**, 50(2), 428-436.
- (102) Otto, R. *Berichte der Deutschen Chemischen Gesellschaft*. **1877**, 10(1), 939-941.
- (103) Kolthoff, I. M.; May, D. R.; Morgan, P.; Laitinen, H. A.; O'Brien, A. S. *Industrial & Engineering Chemistry Analytical Edition*. **1946**, 18(7), 442-444.
- (104) Loven, J. M. *Journal für Praktische Chemie*. **1884**, 29(1), 366-378.
- (105) Kipnis, F.; Levy, I.; Ornfelt, J. *Journal of the American Chemical Society*. **1949**, 71(6), 2270-2270.
- (106) Wieland, T.; Bäuerlein, E. *Chemische Berichte*. **1964**, 97(8), 2103-2108.
- (107) Burawoy, A.; Turner, C. *Journal of the Chemical Society (Resumed)*. **1953**, 959-962.
- (108) Kaufmann, H. P.; Rossbach, E. *Berichte der Deutschen Chemischen Gesellschaft (A and B Series)*. **1925**, 58(8), 1556-1560.
- (109) Hantzsch, A.; Hirsch, B. *Berichte der Deutschen Chemischen Gesellschaft*. **1896**, 29(1), 947-952.
- (110) Strating, J.; Backer, H. J. *Recueil des Travaux Chimiques des Pays-Bas*. **1950**, 69(5), 638-648.
- (111) Bennett, G. M.; Berry, W. A. *Journal of the Chemical Society (Resumed)*. **1927**, 1666-1676.

2. Objectives and scope of work

The main goal of this Doctoral Thesis is research on synthetic access and systematic and detailed characterization of a new class of stable π -delocalized organic radicals for fundamental studies in the context of electronic and magnetic applications. In this context, the preparative routes for synthesis and detailed characterization of new derivatives of π -expanded and functionalized planar Blatter radicals are presented followed by the study on the influence of the chemical structure on their electronic and magnetic properties, and their spectroscopic, structural, electrochemical, and chemical behavior.

Our hypothesis states that the [1,2,4]triazinyl effectively introduces spin density into the annulated aromatic systems and allows to control the electronic properties of such nanographenes, such as spin delocalization, redox behavior, and electronic absorption by judicious choice of the size and type of the aromatic system in the molecular structure of the radicals.

The inspiration for the development of this class of structures comes from the rich experience of our team in the area of synthesis and physicochemical research of different derivatives of Blatter and planar Blatter radicals (Figure 2.1), which are becoming increasingly important structural elements for advanced functional materials. Their exceptional stability, spin delocalization, and attractive electrochemical and photophysical properties have recently been explored in the design of materials for molecular electronics.

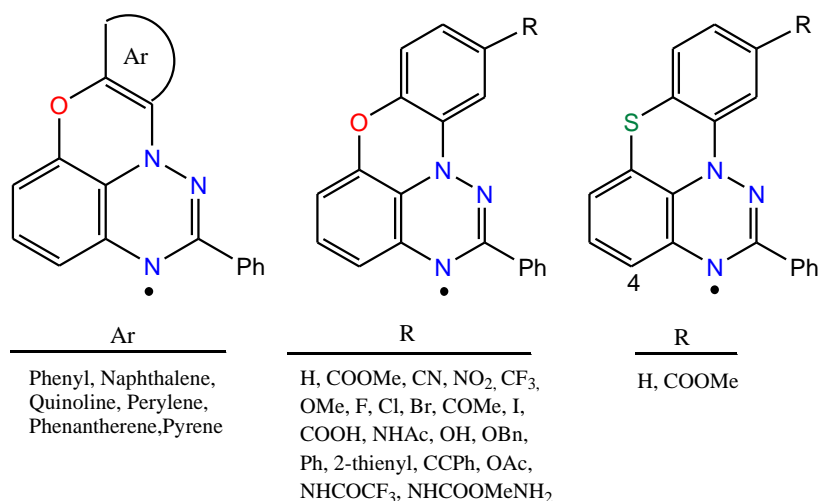
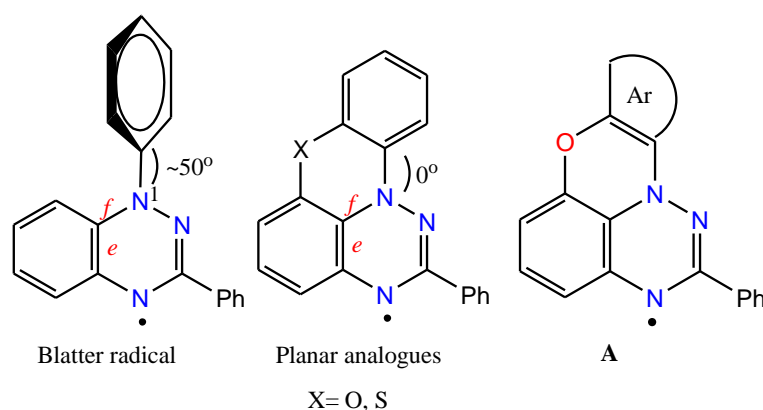


Figure 2.1. The structure of the planar analogues (X= O, S) of Blatter radical and their C(10) functionalized and π -extended derivatives.

In the first part of the Thesis, we planned to develop a new class of paramagnetic nanographenes, in which the [1,2,4]triazinyl is docked to a polycyclic aromatic compounds to provide maximum spin delocalization, and to understand their structure-property relationships. In this part of Thesis, simultaneous ring fusion at the *e* and *f* edges of [1,2,4]triazin-4-yl and planarization of the entire structure (Figure 2.2) leads to extension of the π -system, spin delocalization and greater control of the electronic properties of the [1,2,4]triazinyl-based radicals.

Previous works:



The first part of the thesis:

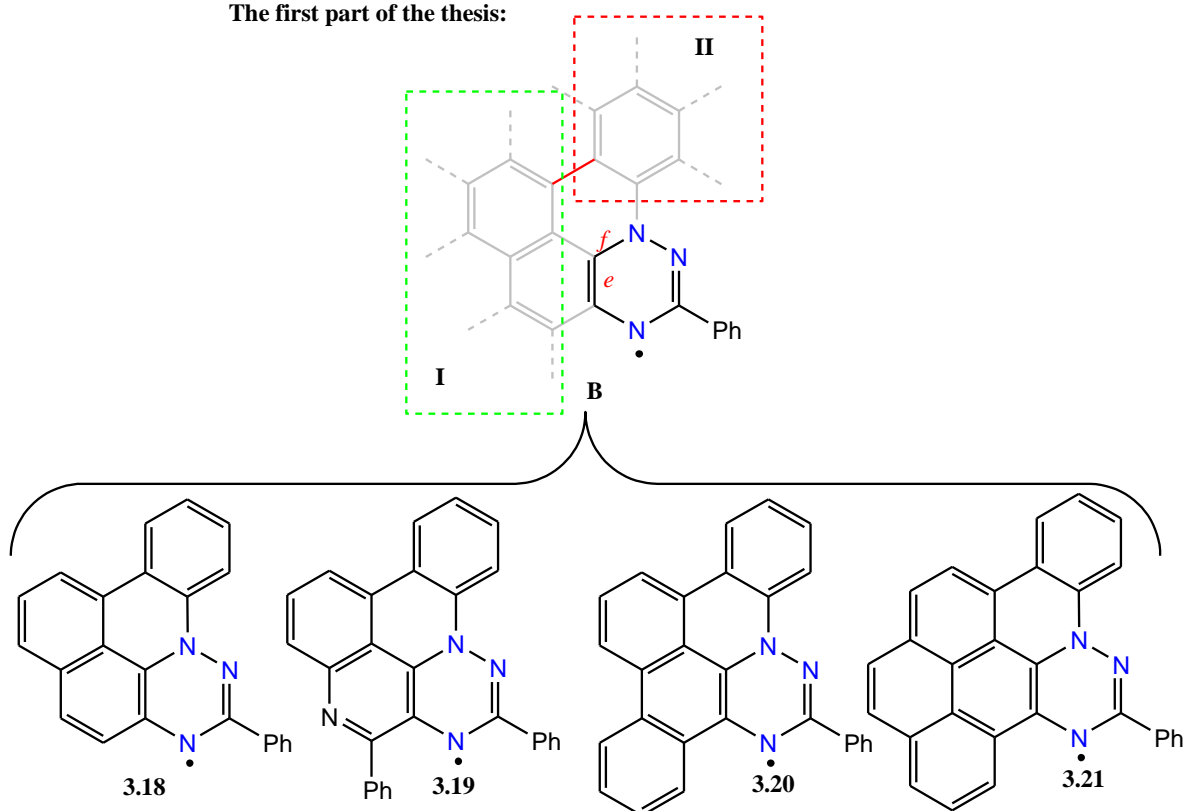


Figure 2.2. Blatter radical, planar Blatter radical and its π -extended at N(1) derivatives **A** and π -extended planar Blatter radical at the *e* and *f* edges of the 1,4-dihydro[1,2,4]triazin-4-yl unit in **B**.

Therefore, we expected to have greater spin delocalization and greater control of the electronic properties of the [1,2,4]triazinyl-based radicals. We anticipated to observe bathochromic shift to the near-IR region of the electronic absorption spectra and anodic shift of the reduction potential in the synthesized derivatives of Blatter radicals.

In the second part of this Thesis, we present preparative routes for synthesis and detailed characterization of five new derivatives of functionalized *S-peri*-annulated benzo[*e*][1,2,4]triazinyl containing CO₂Me, CN, CF₃ and NO₂ groups at the C(10) or C(9) positions through a TMS₃SiH-assisted cyclization of aryl iodides (Figure 2.3), and investigate the effect of substituent on their spectroscopic and electrochemical properties. The results from the previous works revealed, diverse packing motifs in the solid-state structures, which depend on the size and steric demands of the aryl substituent, impact on magnetic interactions. The idea behind this project was to better understand factors governing the crystal packing of the benzo[*e*][1,2,4]triazinyl derivatives and their impact on magnetic interactions in the solid state.

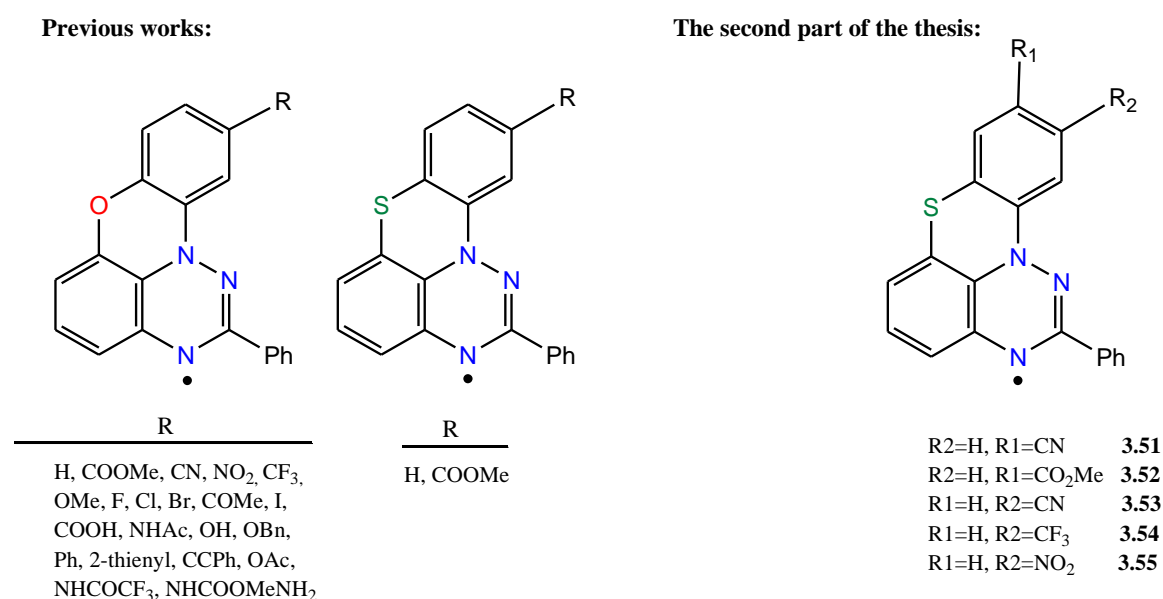


Figure 2.3. Synthesis of functional derivatives of planarized Blatter radical.

3. Discussion of the results of own research

There are two main projects in this Thesis. The first project is about synthesis and characterization of new π -expanded Blatter radicals through ring annulation of the derivatives of the benzo[*e*][1,2,4]triazinyl, and their spectroscopic, structural, electrochemical, and chemical properties. The first project is divided into two separate parts, which describe the synthesis of the radicals with similar structures but using different methodologies.

The second project in this Thesis, is about synthesis and characterization of five new derivatives of functionalized *S-peri*-annulated benzo[*e*][1,2,4]triazinyl and investigate the effect of substituent on their spectroscopic and electrochemical properties. The final radicals are characterized with spectroscopic (UV-vis and electron paramagnetic resonance, EPR) and electrochemical methods.

3.1. Ring expansion of the planar Blatter radical

3.1.1. Post-radical-generation ring-extended planar Blatter radicals

Here, synthesis of four derivatives of π -expanded Blatter radicals and their attempted cyclization to form π -expanded planar Blatter radicals are presented. The Blatter radicals are synthesized by azaphilic addition of organolithium to ring-fused [1,2,4]triazines, which were obtained by two different methods (Figure 3.1).

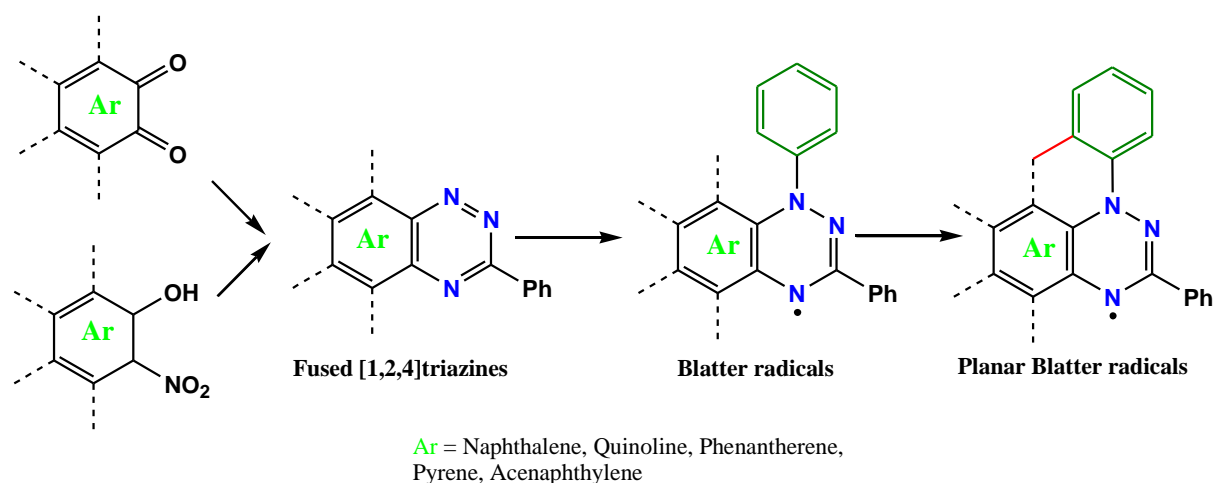


Figure 3.1. Synthesis of π -expanded planar Blatter radicals.

Subsequent ring annulation at the *e* and *f* edges of the 1,4-dihydro[1,2,4]triazin-4-yl (Figure 3.2), leads to further expansion of the π -system, greater spin delocalization, wider control of the electronic properties of [1,2,4]triazinyl-based radicals and enables the development of new materials with tunable properties, such as configurational stability, transannular electronic interactions, redox and photophysical behavior. To assess the effect of π expansion on the electronic properties, the radicals were characterized using spectroscopic (UV-vis and electron paramagnetic resonance, EPR) and electrochemical methods.

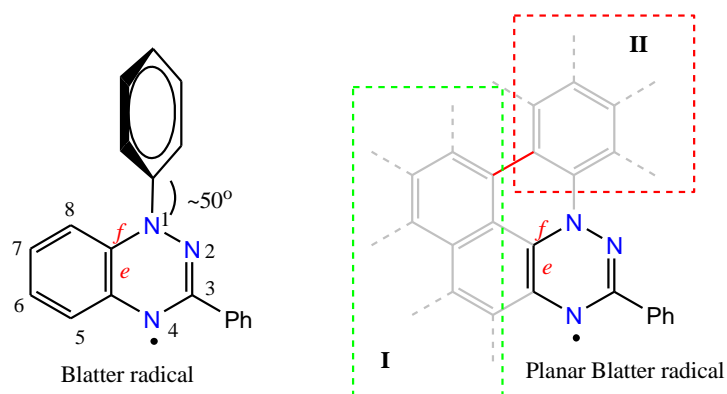


Figure 3.2. Blatter radical and π -extended planar Blatter radical formed by ring annulation at the *e* and *f* edges of the 1,4-dihydro[1,2,4]triazin-4-yl unit.

In this synthetic method, the installation of aromatic rings fused at the *e* edge of the 1,4-dihydro[1,2,4]triazin-4-yl is accomplished by proper choice of substrates which have naphthalene, quinoline, phenanthrene, pyrene and acenaphthalene backbones in their structures. For connection of two π molecular fragments (area I and area II, Figure 3.2), photocyclization reactions will be used (Figure 3.3).

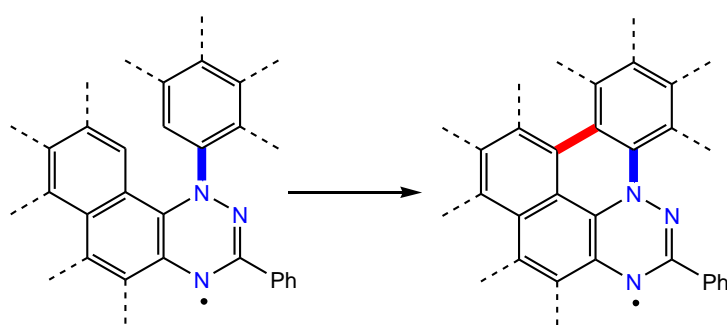


Figure 3.3. Connection of two π molecular fragments in the presence of the unpaired electron.

3.1.1.1. Synthesis of ring-fused [1,2,4]triazines

In order to obtain and study of the expansion the aromatic systems in Blatter radical, aromatic compounds with different sizes of π -system were used as substrates for the preparation of the π -extended [1,2,4]triazines, which were then converted to the desired radicals by the azaphilic addition of aryllithium reagents to the ring-fused [1,2,4]triazines followed by oxidation of the resulting anions. Two different methods were used for synthesis of the [1,2,4]triazines. The quinolino and naphtho derivatives of the [1,2,4]triazine were synthesized from the corresponding hydrazide derivatives with subsequent cyclization under reductive condition.¹ The phenanthro, pyreno and acenaphtho analogues were prepared by reacting the corresponding diones with benzamidrazone using modified literature procedures.²

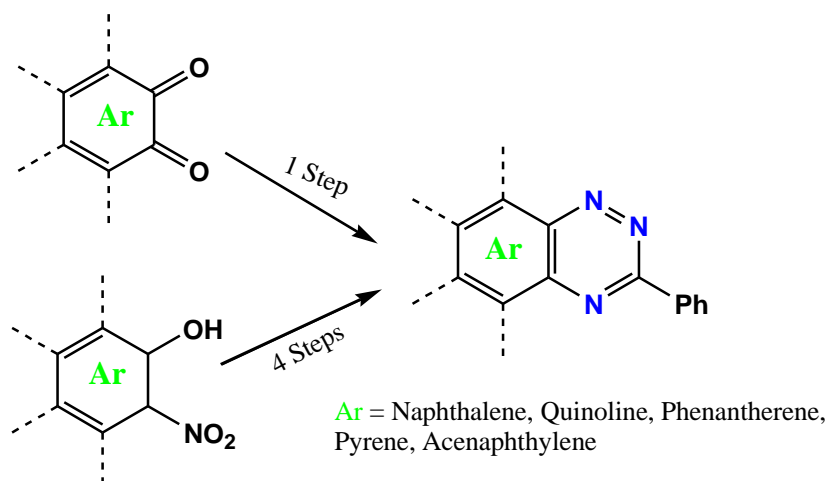
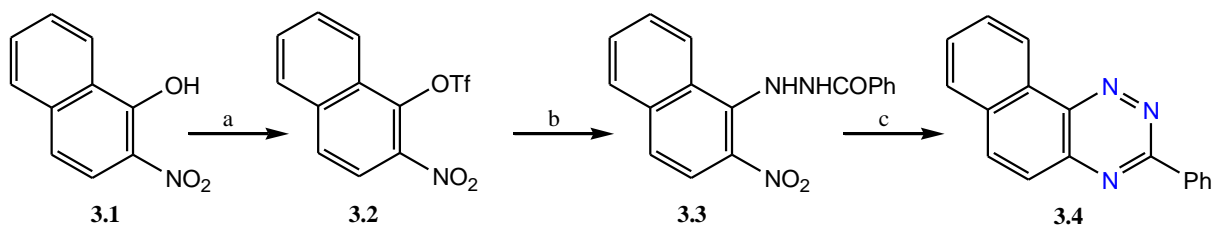


Figure 3.4. Two methods for preparation of ring-fused triazines.

3.1.1.1.1. Synthesis of 3-phenylnaphtho[2,1-*e*][1,2,4]triazine

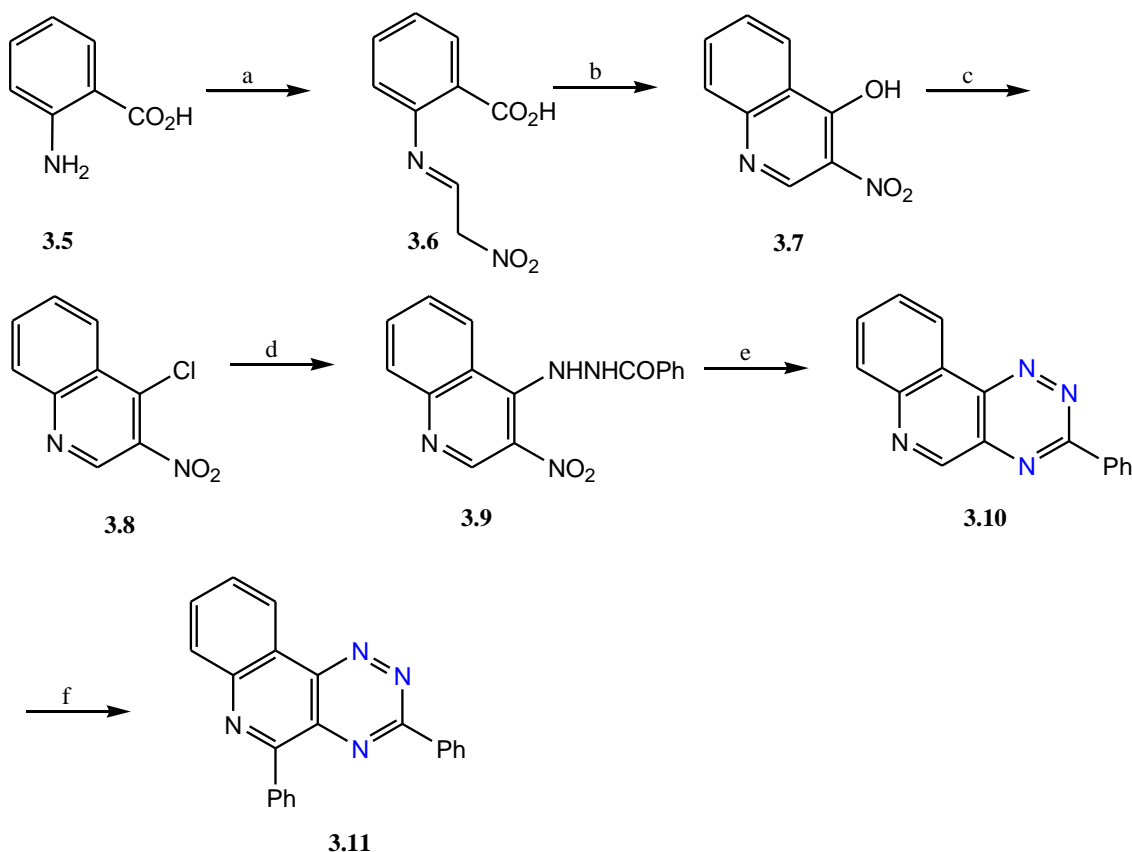
The triazine **3.4** (Scheme 3.1) was prepared in two steps and 66% overall yield from triflate ester **3.2**, which was N-arylated with benzhydrazide to form the hydrazide **3.3** with subsequent cyclization to triazine **3.4** under reductive conditions. Triflate ester **3.2** was obtained from the commercially available 2-nitro-1-naphthol **3.1** in and triflic anhydride in 91% yield.^{1,3}



Scheme 3.1. Synthesis of 3-phenylnaphtho[2,1-*e*][1,2,4]triazine. Reagents and conditions: (a) Et₃N, DCM, triflic anhydride, (b) benzhydrazide, DMSO, (c) 1. Sn, AcOH, 2. NaIO₄, DCM/MeOH (1:1).

3.1.1.1.2. Synthesis of 3,5-diphenyl-[1,2,4]triazino[5,6-*c*]quinoline

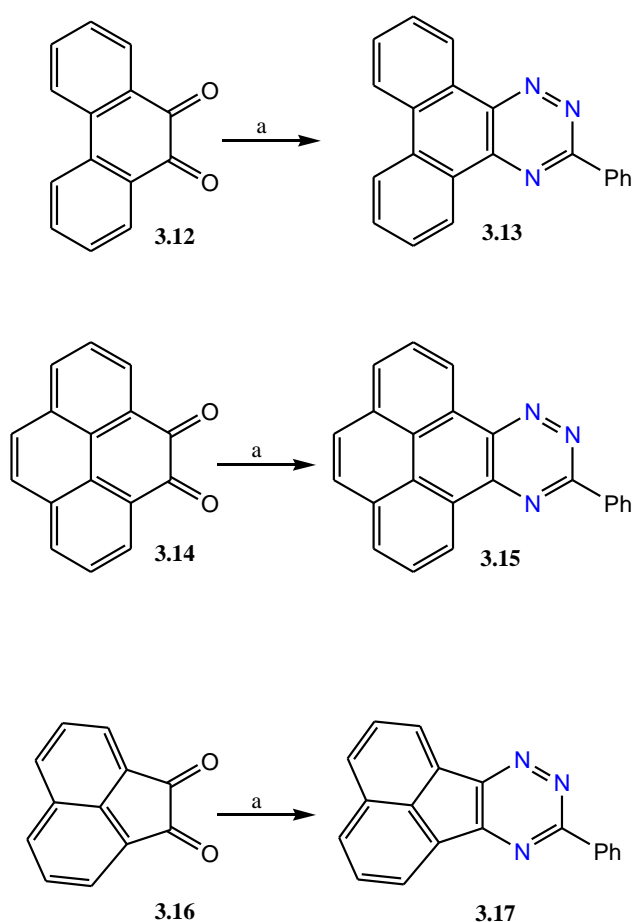
Triazine **3.10** was prepared in two steps and 44% overall yield from the hydrazide **3.9** with subsequent cyclization under reductive conditions.¹ The hydrazide **3.9** was prepared by N-arylation of the 4-chloro-3-nitroquinoline **3.8** in the presence of benzhydrazide.¹ Anthranilic acid **3.5** converted to 3-nitroquinolin-4-ol **3.7** in two steps in 24% overall yield and then chlorinated by POCl₃ and PCl₅ to form 4-chloro-3-nitroquinoline **3.8** in 60% yield (Scheme 3.2).^{4,5} The triazine **3.11** was obtained in 27% yield from triazine **3.10** by reacting the triazine with PhLi solution in n-butyl ether, which is the same method for synthesis the radicals.⁶ However, instead of the radical, triazine **3.11** was obtained as a result of the Chichibabin reaction.



Scheme 3.2. Synthesis of 3-phenyl-[1,2,4]triazino[5,6-*c*]quinoline and 3,5-diphenyl-[1,2,4]triazino[5,6-*c*]quinoline. Reagents and conditions: (a) methazoic acid, HCl, (b) acetic anhydride, NaOAc, (c) POCl₃, PCl₅, (d) benzohydrazide, DMSO, (e) 1. Sn, AcOH, 2. NaIO₄, DCM/MeOH (1:1), (f) PhLi solution, THF.

3.1.1.1.3. Synthesis of ring-fused [1,2,4]triazines through diketones

The triazines (**3.13**, **3.15** and **3.17**) were synthesized by reacting the corresponding diones (**3.12**, **3.14** and **3.16**) with benzamidrazone in methanol. Benzamidrazone was prepared from benzonitrile and hydrazine hydrate according to a literature procedure (Scheme 3.3).² Phenanthrene-9,10-dione (**3.12**) and acenaphthylene-1,2-dione (**3.16**) were obtained commercially but pyrene-4,5-dione (**3.14**) was prepared in 40% yield by oxidation of pyrene with NaIO₄ in the presence of RuCl₃·xH₂O in H₂O, according to a general literature procedure.²



Scheme 3.3. Synthesis of 3-phenylphenanthro[9,10-*e*][1,2,4]triazine, 11-phenyl-9,10,12-triaza-benzo[*e*]pyrene and 9-phenylacenaphtho[1,2-*e*][1,2,4]triazine. Reagents and conditions: (a) benzamidrazone, MeOH, rt.

3.1.1.1.4. Electronic absorption spectroscopy of fused [1,2,4]triazines (UV–vis).

A Jasco V770 spectrophotometer was used to record the UV-vis absorption spectra of triazines. Solutions were prepared in spectroscopic grade CH_2Cl_2 at concentrations ranging from 1.0 to $3.0 \times 10^{-5} \text{ mol} \cdot \text{L}^{-1}$ and the measurements were taken shortly after. The measured UV-vis spectra were fitted to the Beer–Lambert law ($A = \epsilon cl$), the molar absorption coefficient (ϵ) was derived from the linear plots. Results are shown in Table 3.1 and Figures 3.5–3.10.

Triazines exhibit low-intensity absorption bands in the visible range. The only exception is the spectrum of the pyrene derivative **3.15**, which exhibits a relatively intense absorption peak at 428 nm ($\log \epsilon = 2.64$) and indicates that the size of the aromatic rings have some effect on the electronic absorption energy of the molecules. In **3.15** fusing a pyrene ring at the *e* edge of the triazines results in a bathochromic shift of the absorption maximum at 428 nm. The lowest energy maximum of absorption in triazines lies between 424 and 469 nm due to aromatic rings which cause bathochromic shift of the absorption maximum (Table 3.1).

Table 3.1. Lowest energy absorption maximum wavelength of triazines.

Compound	λ_{max} (nm)
3.4 (Naphthalene)	433.5
3.10 (Quinoline)	469
3.11 (Quinoline)	469
3.13 (Phenanthrene)	424
3.15 (Pyrene)	428
3.17 (Acenaphthylene)	345

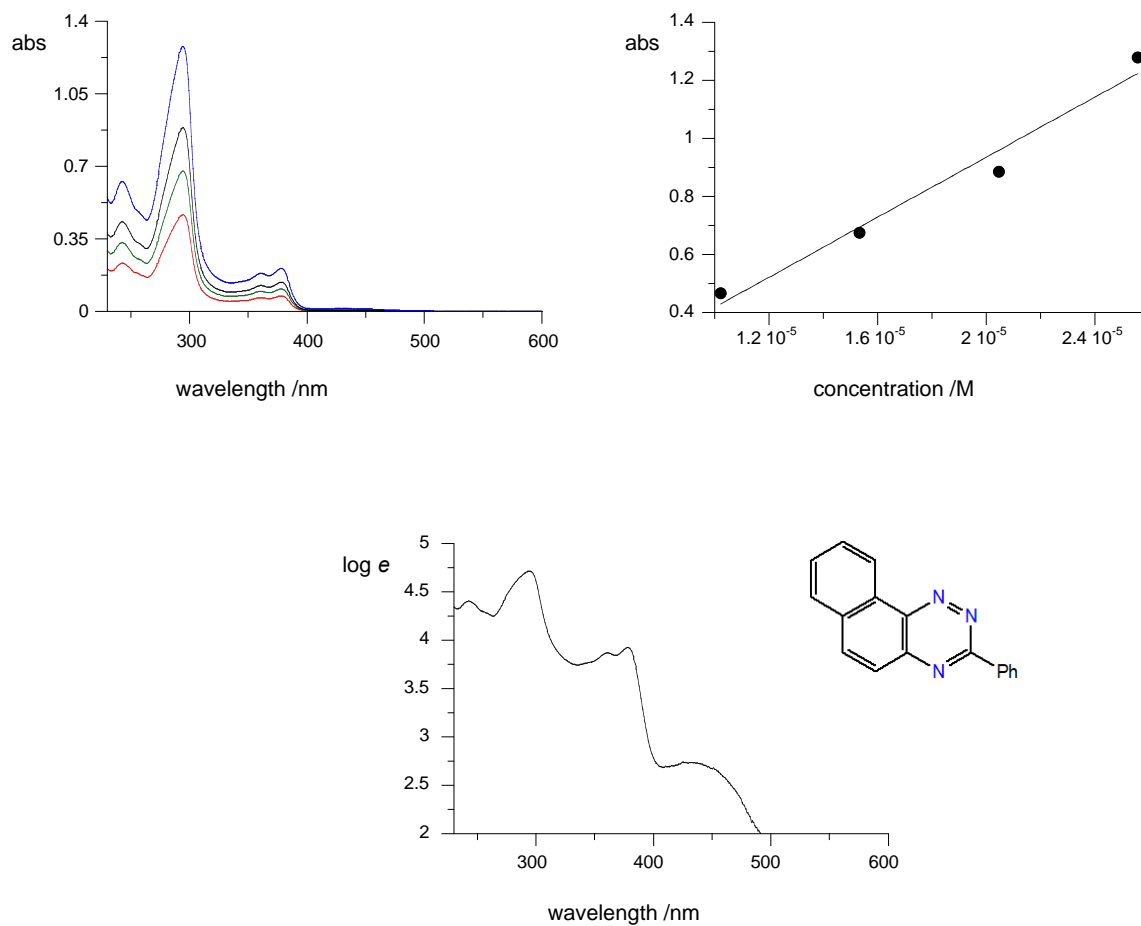


Figure 3.5. Clockwise: electronic absorption spectra for **3.4** in CH_2Cl_2 at four different concentrations (top left), determination of molar extinction coefficient ϵ at $\lambda = 294 \text{ nm}$ (top right, best fit function: $\epsilon = 51726 \times \text{conc}$, $r^2 = 0.986$) and molar extinction $\log(\epsilon)$ plot (bottom).

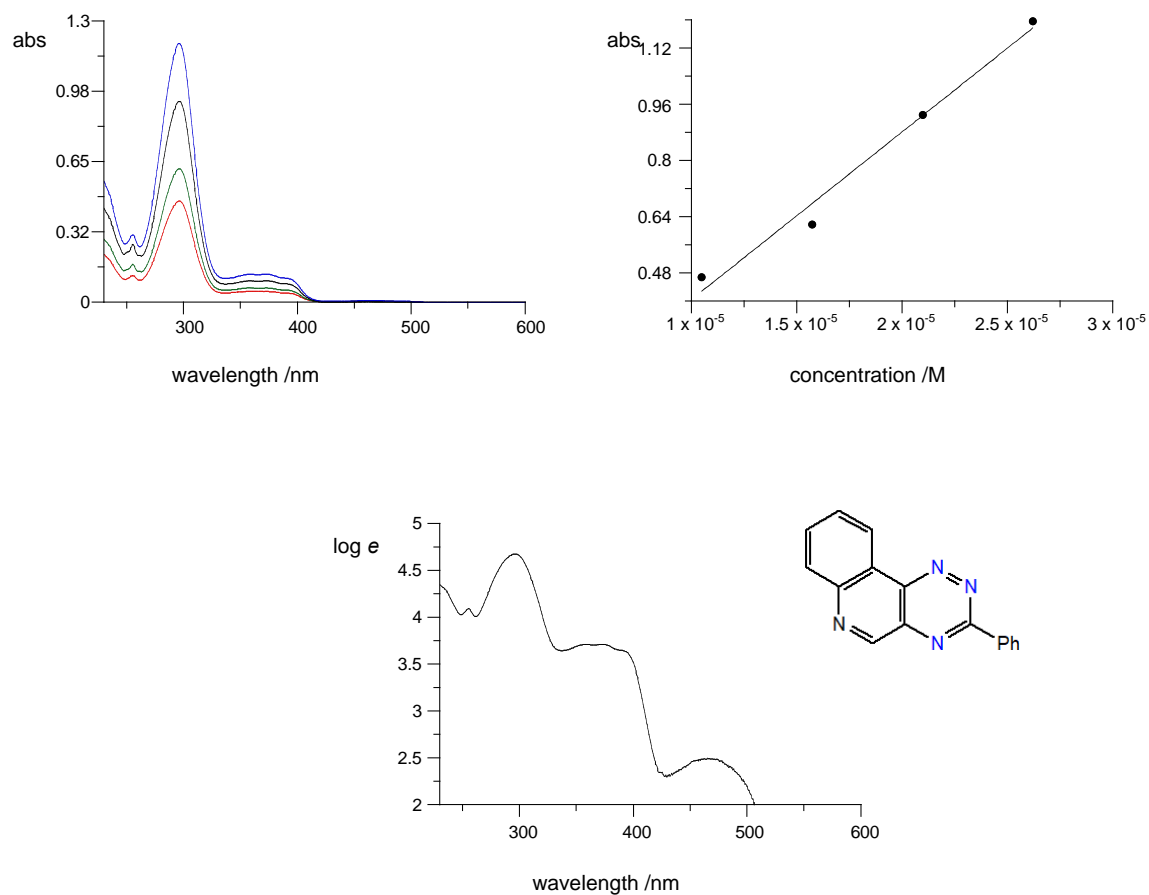


Figure 3.6. Clockwise: electronic absorption spectra for **3.10** in CH₂Cl₂ at four different concentrations (top left), determination of molar extinction coefficient ϵ at $\lambda = 296$ nm (top right, best fit function: $\epsilon = 47683 \times \text{conc}$, $r^2 = 0.982$) and molar extinction $\log(\epsilon)$ plot (bottom).

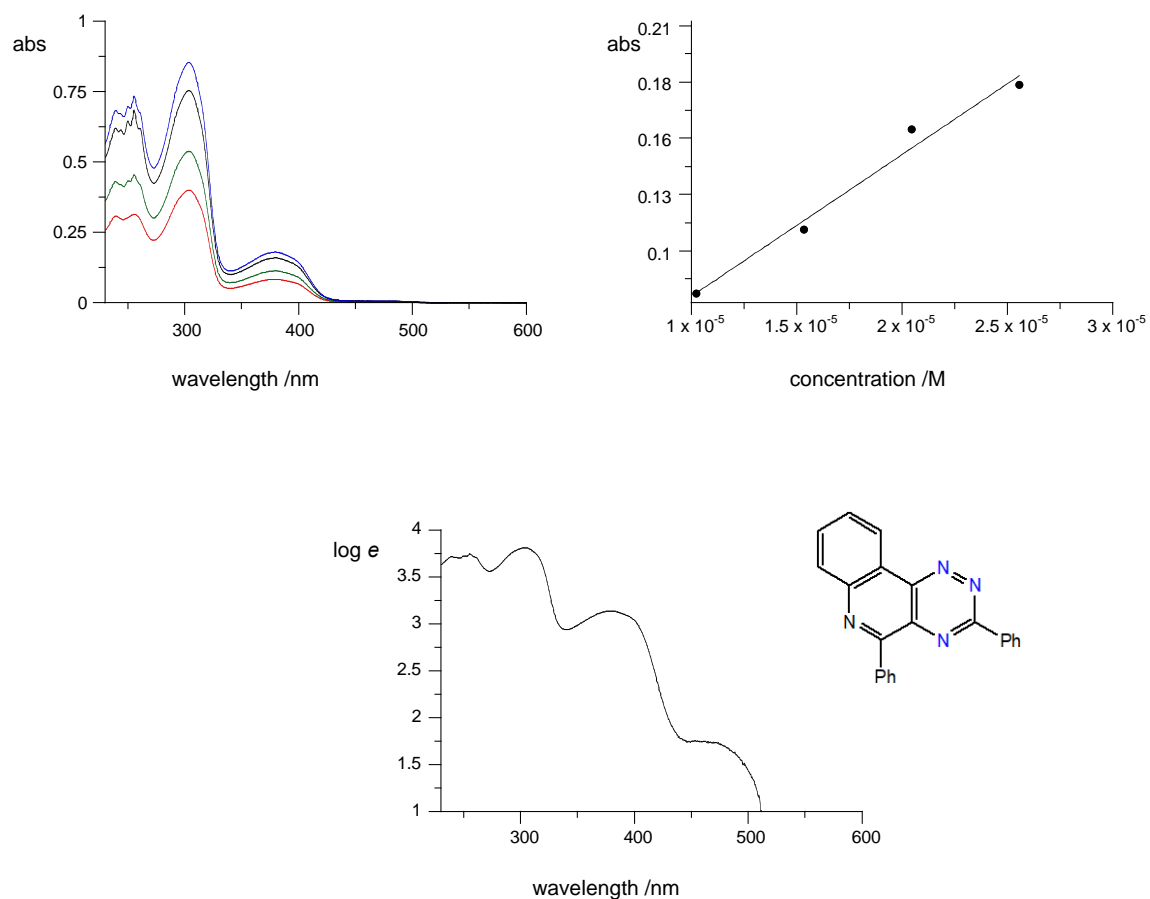


Figure 3.7. Clockwise: electronic absorption spectra for **3.11** in CH₂Cl₂ at four different concentrations (top left), determination of molar extinction coefficient ϵ at $\lambda = 379$ nm (top right, best fit function: $\epsilon = 6545 \times \text{conc}$, $r^2 = 0.980$) and molar extinction $\log(\epsilon)$ plot (bottom).

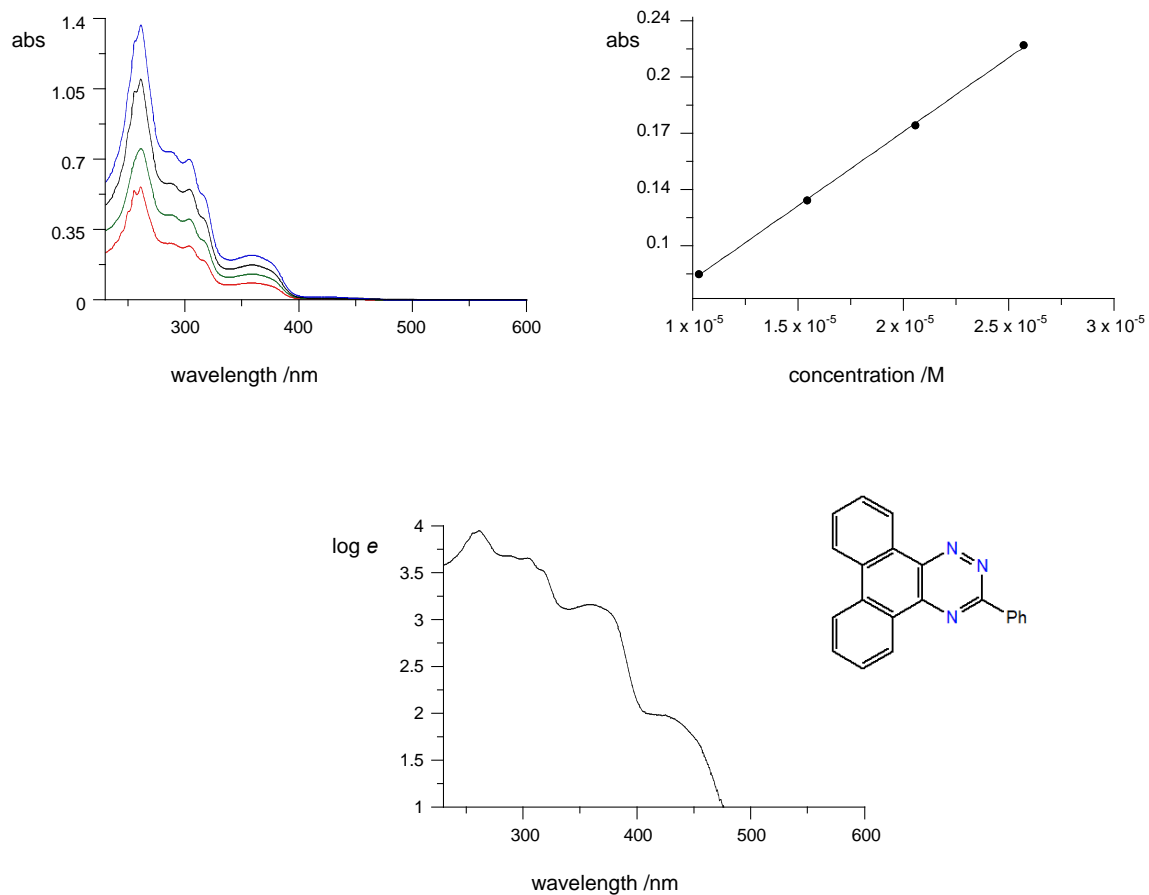


Figure 3.8. Clockwise: electronic absorption spectra for **3.13** in CH₂Cl₂ at four different concentrations (top left), determination of molar extinction coefficient ϵ at $\lambda = 359$ nm (top right, best fit function: $\epsilon = 8942 \times \text{conc}$, $r^2 = 0.9996$) and molar extinction $\log(\epsilon)$ plot (bottom).

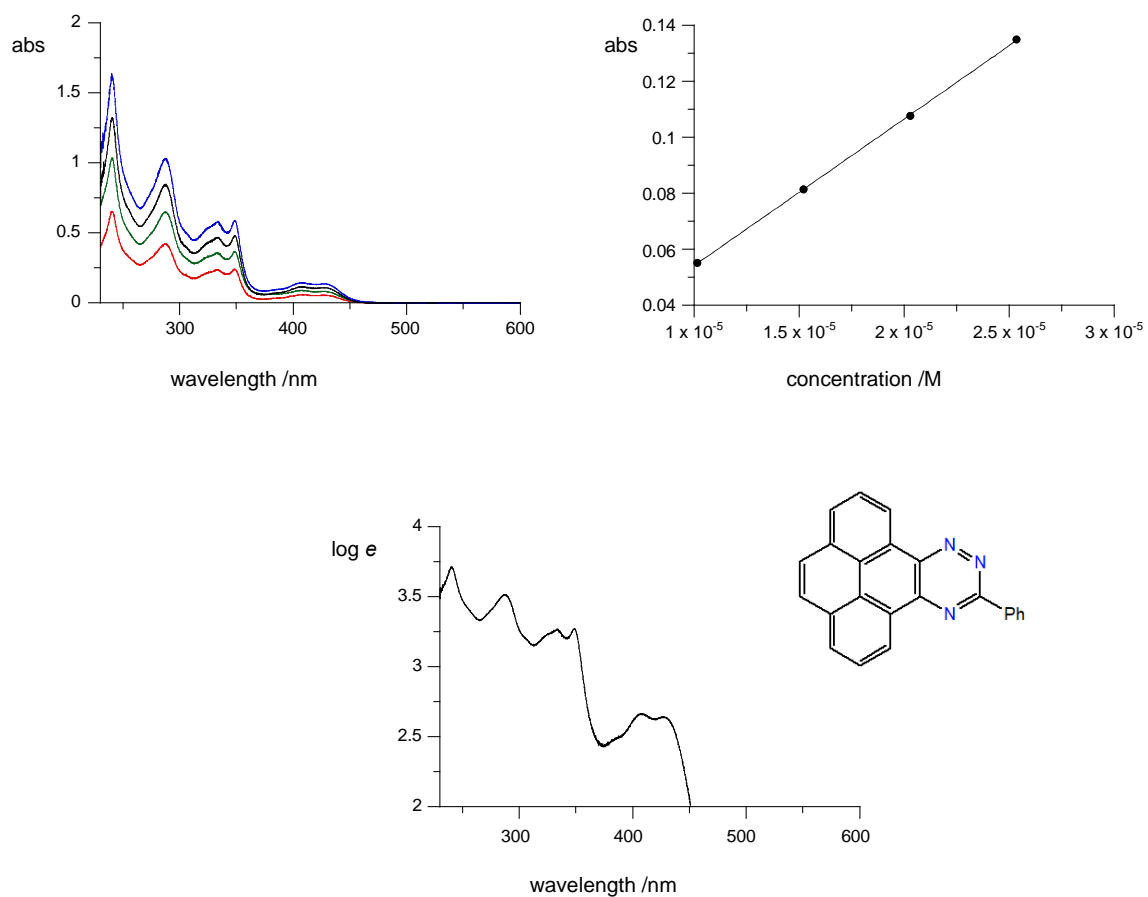


Figure 3.9. Clockwise: electronic absorption spectra for **3.15** in CH₂Cl₂ at four different concentrations (top left), determination of molar extinction coefficient ϵ at $\lambda = 430$ nm (top right, best fit function: $\epsilon = 5238 \times \text{conc}$, $r^2 = 0.9998$) and molar extinction log (ϵ) plot (bottom).

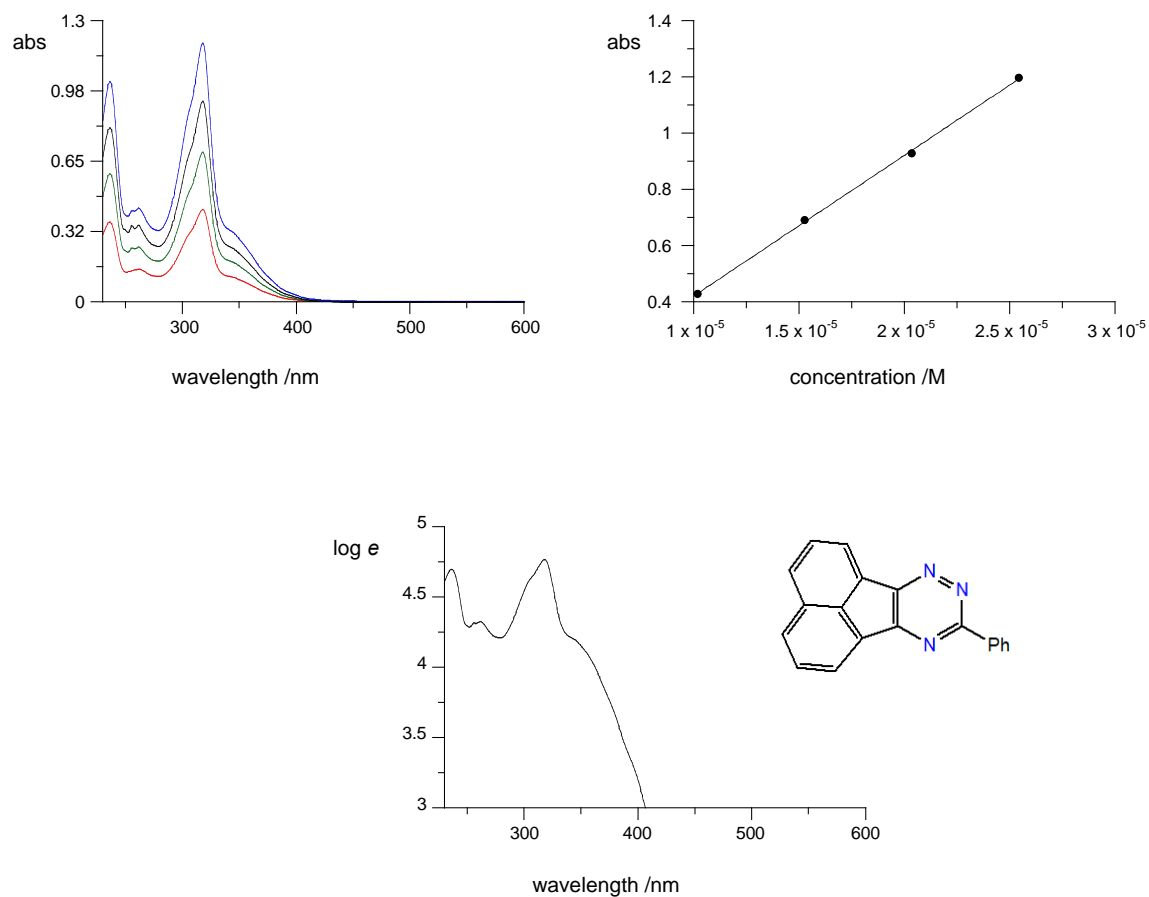


Figure 3.10. Clockwise: electronic absorption spectra for **3.17** in CH₂Cl₂ at four different concentrations (top left), determination of molar extinction coefficient ϵ at $\lambda = 318$ nm (top right, best fit function: $\epsilon = 50028 \times \text{conc}$, $r^2 = 0.9994$) and molar extinction $\log(\epsilon)$ plot (bottom).

3.1.1.2. Synthesis of radicals by azaphilic ArLi addition to fused [1,2,4]triazines

Preparation of radicals was accomplished by adding an organometallic reagent (PhLi solution in n-butyl ether) to the available triazines followed by oxidation of the resulting anion (Figure 3.11). The method is potentially general, permits introduction of a substituent at the N(1) position postcyclization step, and avoids the use of arylhydrazine.⁷ The radicals **3.18** and **3.19** exhibited limited stability in solutions and to chromatography, however it was possible to do fast purification by a short column with Et₃N-passivated silica and then washing the product with hot n-pentane for three times. Spectroscopic (UV-vis and EPR) and electrochemical methods and high-resolution mass spectrometry (HRMS) measurements for the final products, confirmed the formation of the radicals (Table 3.2).

Radicals (**3.20** – **3.22**) undergo slow decomposition in solutions as evidenced by the appearance of a blue spot and a strong baseline on the TLC, however it was possible to do spectroscopic (UV-vis and EPR) and electrochemical analyses and high-resolution mass spectrometry (HRMS) measurements for the final products indeed confirmed the formation of the radicals. Direct recrystallization of the reaction mixture failed to give the pure product, therefore the purification was performed by short column with Et₃N-passivated silica and then washing the product by hot n-pentane for three times. Radical **3.21** was the most stable radical, however was not possible to keep it at room temperature and in the present of light (Table 3.2).

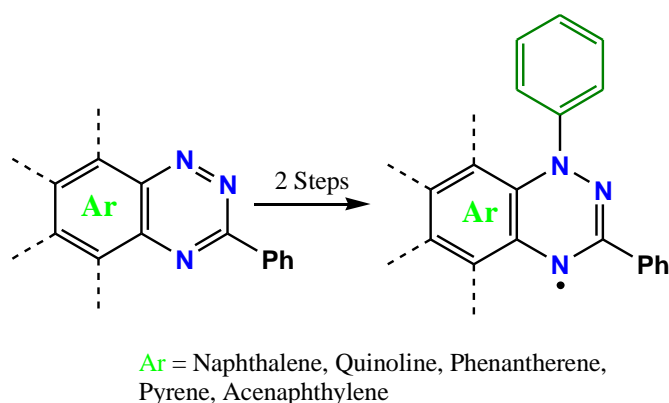
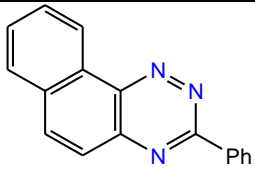
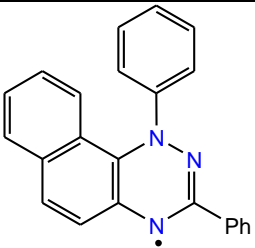
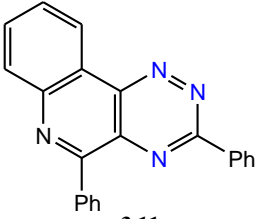
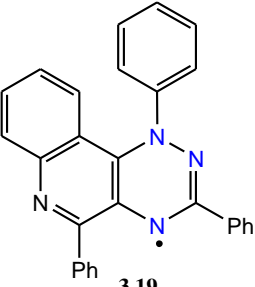
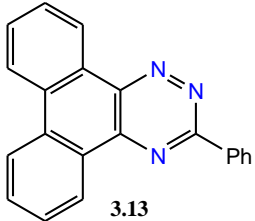
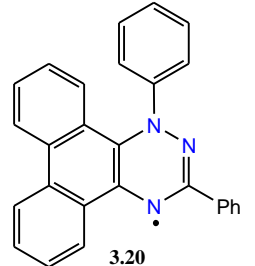
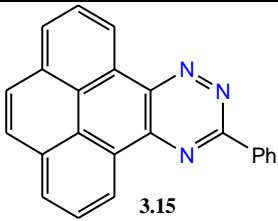
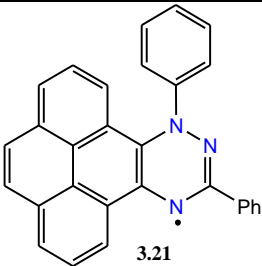
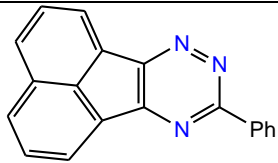
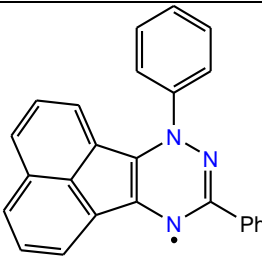


Figure 3.11. Synthesis of radicals. Reagents and conditions: (a) PhLi solution, THF, (b) air.

Table 3.2. Synthesis of radicals

Triazines	Radicals (Triazines + PhLi)	Comments
 <p>3.4</p>	 <p>3.18</p>	<ul style="list-style-type: none"> • Limited stability in solutions • Fast purification by short column with Et₃N-passivated silica • Washing by hot n-pentane for three times. • Light brown
 <p>3.11</p>	 <p>3.19</p>	<ul style="list-style-type: none"> • Limited stability in solutions • Fast purification by short column with Et₃N-passivated silica • Washing by hot n-pentane for three times. • Dark brown
 <p>3.13</p>	 <p>3.20</p>	<ul style="list-style-type: none"> • Limited stability in solutions • Fast purification by short column with Et₃N-passivated silica • Washing by hot n-pentane for three times. • Dark green
 <p>3.15</p>	 <p>3.21</p>	<ul style="list-style-type: none"> • Limited stability in solutions • Fast purification by short column with Et₃N-passivated silica • Washing by hot n-pentane for three times. • Red
 <p>3.17</p>	 <p>3.22</p>	<ul style="list-style-type: none"> • this radical did not form according to the lack of EPR signal.

3.1.1.2.1. Characterisation of the electronic structure of the radicals

The influence of radical system extension and connectivity on the electronic characteristics was studied using spectroscopic (UV-vis and EPR) and electrochemical methods.

3.1.1.2.1.1. Electronic absorption spectroscopy (UV-vis)

The effect of the extension of the π system in radicals on their electronic properties was investigated by spectroscopic (UV-vis) method. A Jasco V770 spectrophotometer was used to record the UV-vis absorption spectra of radicals. Solutions were prepared in spectroscopic grade CH_2Cl_2 at concentrations ranging from 1.0 to $3.0 \times 10^{-5} \text{ mol} \cdot \text{L}^{-1}$ and the measurements were taken shortly after. The measured UV-vis spectra were fitted to the Beer-Lambert law ($A = \epsilon cl$), the molar absorption coefficient (ϵ) was derived from the linear plots. Results are shown in Table 3.3 and Figures 3.12–3.15.

Table 3.3. Lowest energy absorption maximum wavelength of radicals.

Compound	λ_{max} (nm)
Blatter radical ^a	492
3.18 (Naphthalene)	490
3.19 (Quinoline)	384
3.20 (Phenanthrene)	762
3.21 (Pyrene)	548

^a Ref.⁶

Similar to other benzo[*e*][1,2,4]triazinyls, radicals exhibit low-intensity, broad absorption bands in the visible range (Figures 3.12–3.15). UV spectra most likely do not reflect spectra of pure radicals. Most likely they are of mixtures with decomposition products, *e.g.* **3.19**. The analysis of a series of the radicals, **3.18** (naphthalene analogue) \rightarrow **3.20** (phenanthrene analogue) \rightarrow **3.21** (pyrene analogue), indicates that the size of the rings have some, albeit modest, effects on the electronic absorption energy of the molecules. Thus, fusing more aromatic rings in **3.18**, **3.20**, and **3.21**, results in a higher intensity of the absorption bands in the visible range with maxima at approximately 490, 762, and 548 nm respectively, and also more bathochromic shift of the absorption maximum than Blatter radical. Among the radicals, phenanthrene derivative **3.20** shows a significant bathochromic shift with a maximum of absorption at 762 nm (Figure 3.14).

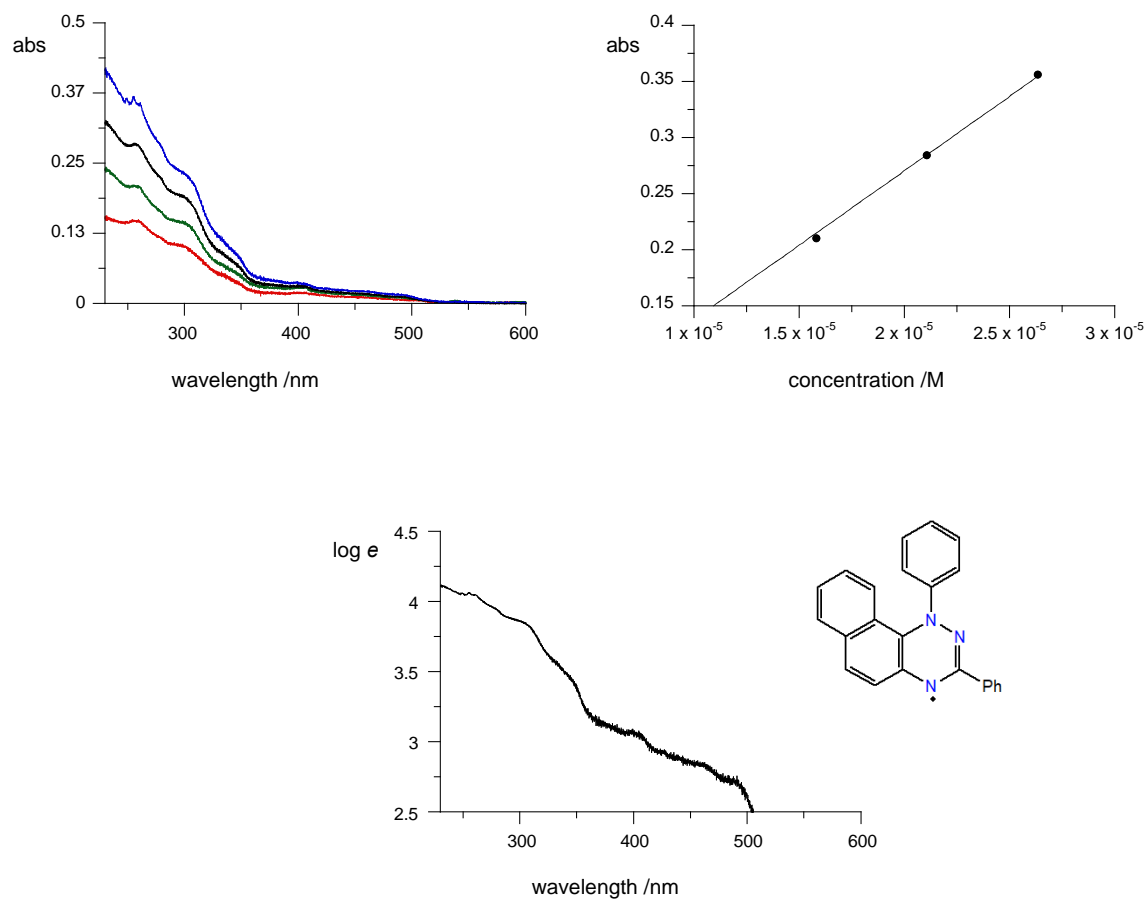


Figure 3.12. Clockwise: electronic absorption spectra for **3.18** in CH₂Cl₂ at three different concentrations (top left), determination of molar extinction coefficient ϵ at $\lambda = 258$ nm (top right, best fit function: $\epsilon = 13252 \times \text{conc}$, $r^2 = 0.9985$) and molar extinction $\log(\epsilon)$ plot (bottom).

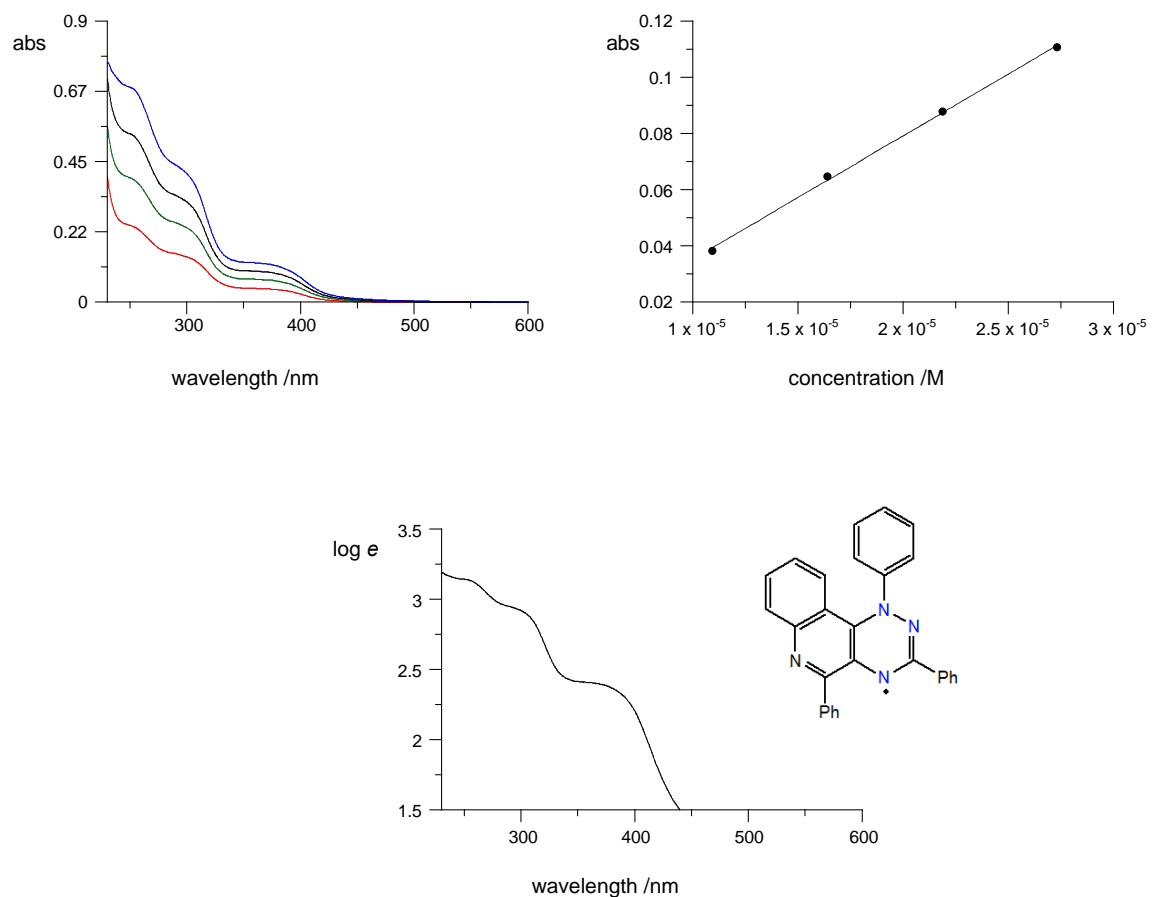


Figure 3.13. Clockwise: electronic absorption spectra for **3.19** in CH₂Cl₂ at four different concentrations (top left), determination of molar extinction coefficient ϵ at $\lambda = 384$ nm (top right, best fit function: $\epsilon = 4398 \times \text{conc}$, $r^2 = 0.999$) and molar extinction $\log(\epsilon)$ plot (bottom).

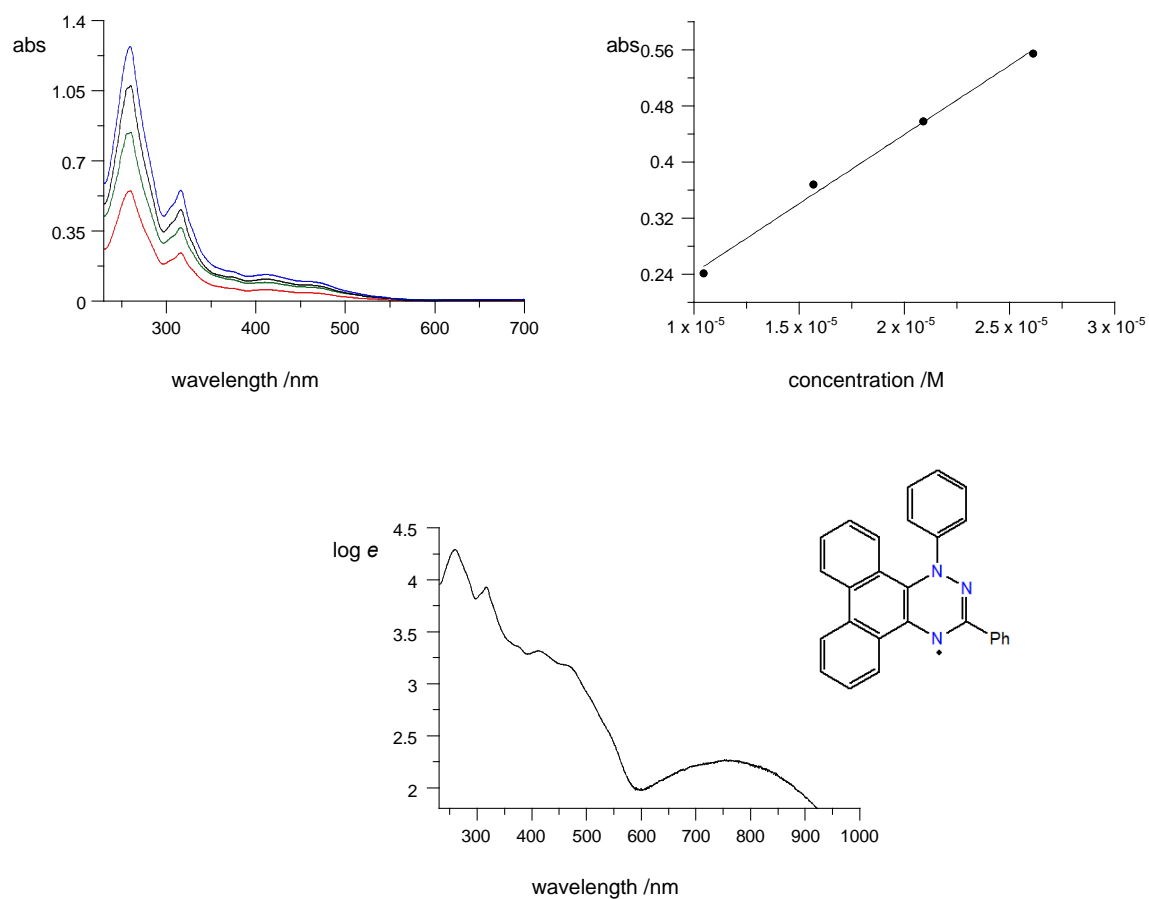


Figure 3.14. Clockwise: electronic absorption spectra for **3.20** in CH₂Cl₂ at four different concentrations (top left), determination of molar extinction coefficient ϵ at $\lambda = 316$ nm (top right, best fit function: $\epsilon = 19715 \times \text{conc}$, $r^2 = 0.994$) and molar extinction $\log(\epsilon)$ plot (bottom).

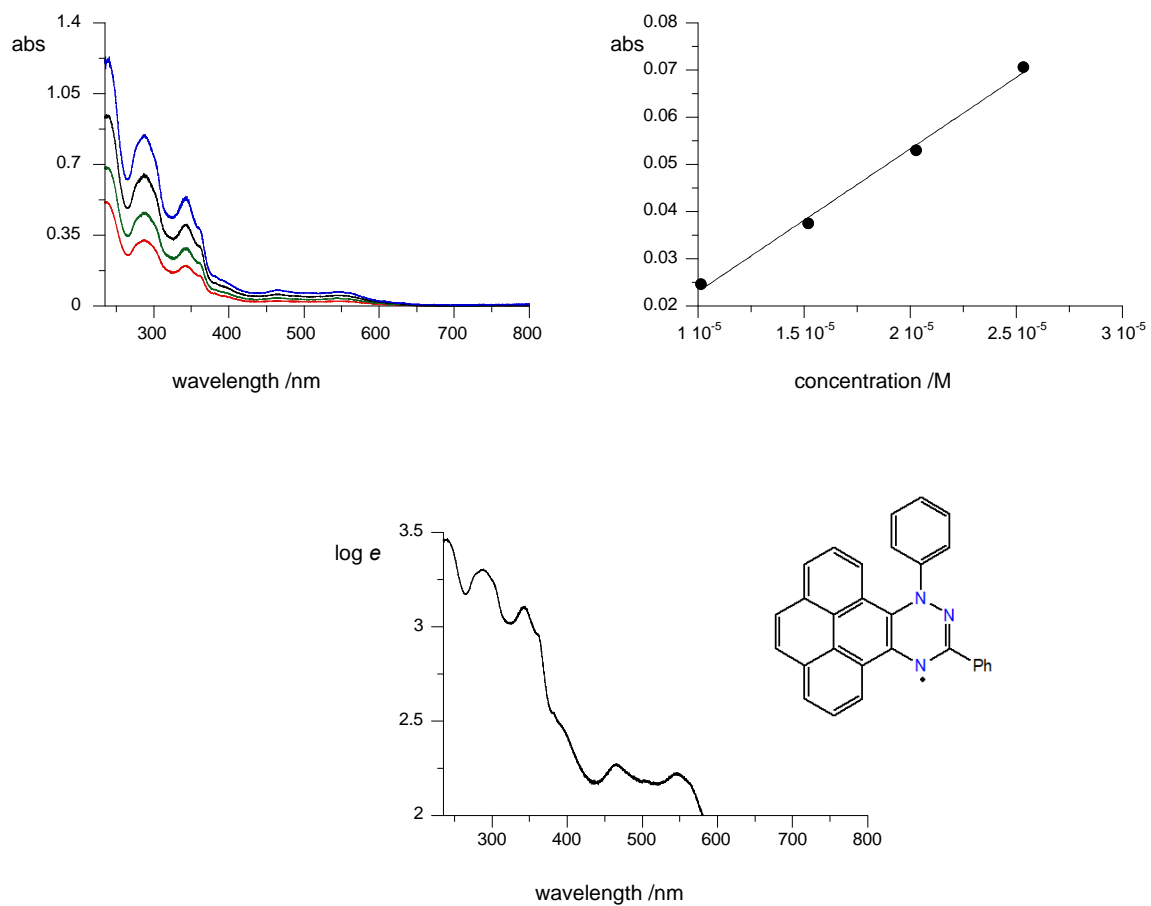


Figure 3.15. Clockwise: electronic absorption spectra for **3.21** in CH₂Cl₂ at four different concentrations (top left), determination of molar extinction coefficient ϵ at $\lambda = 548$ nm (top right, best fit function: $\epsilon = 3028 \times \text{conc}$, $r^2 = 0.997$) and molar extinction $\log(\epsilon)$ plot (bottom).

3.1.1.2.1.2. Electrochemistry (cyclic voltammetry measurements)

A Metrohm Autolab PGSTAT 128N potentiostat/galvanostat instrument was used for the electrochemical characterization of radicals. The concentrations of the radicals were 0.5 mM in dry and degassed, spectroscopic grade CH_2Cl_2 (7 mL) containing $[\text{n-Bu}_4\text{N}]^+ [\text{PF}_6]^-$ (50 mM) as an electrolyte. A three-electrode electrochemical cell was employed with a glassy carbon disk as working electrode (\varnothing 2 mm), Pt wire as the counter electrode and Ag/AgCl wire as the pseudoreference electrode. Temperature was *ca.* 20 °C and scan rate was 50 $\text{mV}\cdot\text{s}^{-1}$. All samples were measured twice, once without an internal reference and once with internal reference: $\text{FcMe}_{10}/\text{FcMe}_{10}^+$ ($E_{\text{FcMe}_{10}/\text{FcMe}_{10}^+} = -0.10 \text{ V vs SCE}$).⁸ Results are shown in Figures 3.16-3.19 and summarized in Table 3.4.

Table 3.4. Electrochemical properties of radicals^a

Compound	$E_{1/2}^{-1/0}$ (V)	$E_{1/2}^{0/+1}$ (V)	$E_{\text{HOMO}}^{\text{b}}$ (eV)
3.18 (naphthalene)	-	-0.08	-4.70
3.19 (quinoline)	-1.11	-	-
3.20 (phenanthrene)	-	-0.08	-4.70
3.21 (pyrene)	-	-0.08	-4.70

^a Potential vs SCE. ^b $E_{\text{HOMO/LUMO}} = -(E_{(\text{onset ox/red vs Fc}^+/\text{Fc})} + 5.1)$.

Cyclic voltammetry measurements revealed that oxidation process is reversible only for **3.18**, **3.20** and **3.21**, and reduction process is only for radical **3.19** (Figures 3.16-3.19, Table 3.4), which indicates the presence of impurities, such as decomposition products.

The data collected in Table 3.4 demonstrate that the extension of the π system in the radicals **3.18** (naphthalene analogue) \rightarrow **3.20** (phenanthrene analogue) \rightarrow **3.21** (pyrene analogue), does not impact the oxidation potential $E_{1/2}^{0/+1}$ nor the level of the HOMO. The electrochemical window was not calculated for these radicals because they do not have reversible reduction processes.

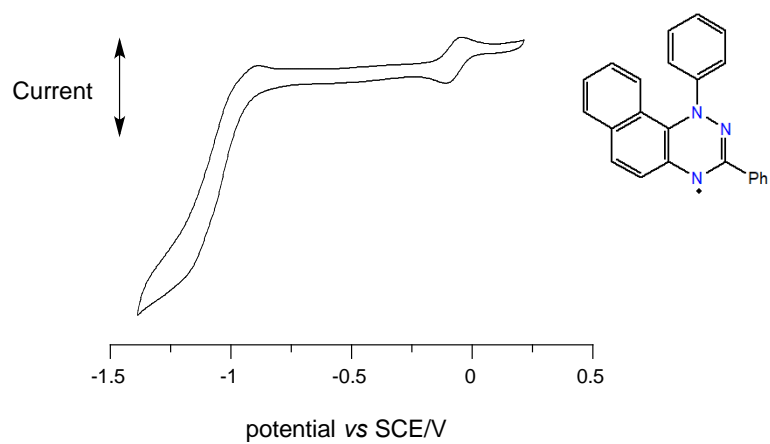


Figure 3.16. Cyclic voltammogram of **3.18** in CH_2Cl_2 .

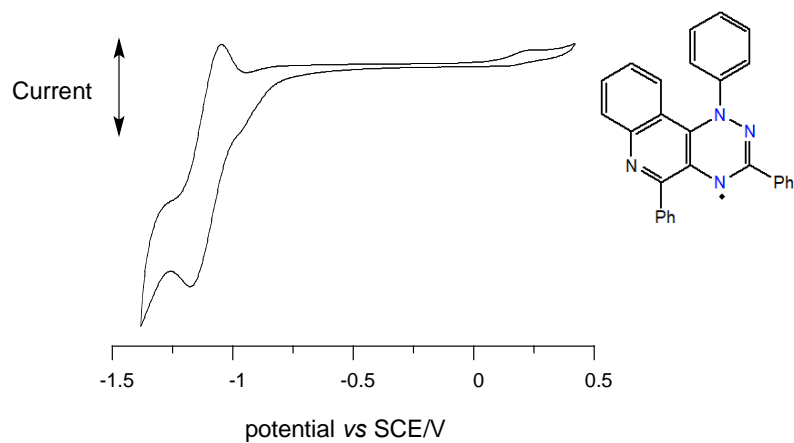


Figure 3.17. Cyclic voltammogram of **3.19** in CH_2Cl_2 .

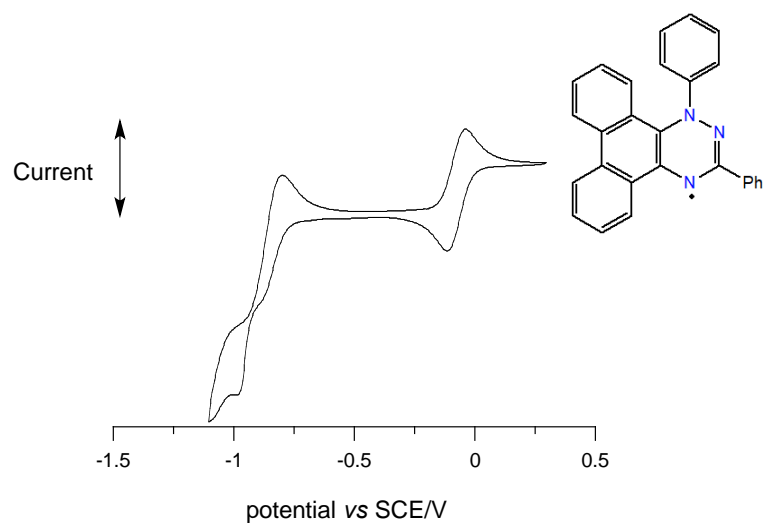


Figure 3.18. Cyclic voltammogram of **3.20** in CH_2Cl_2 .

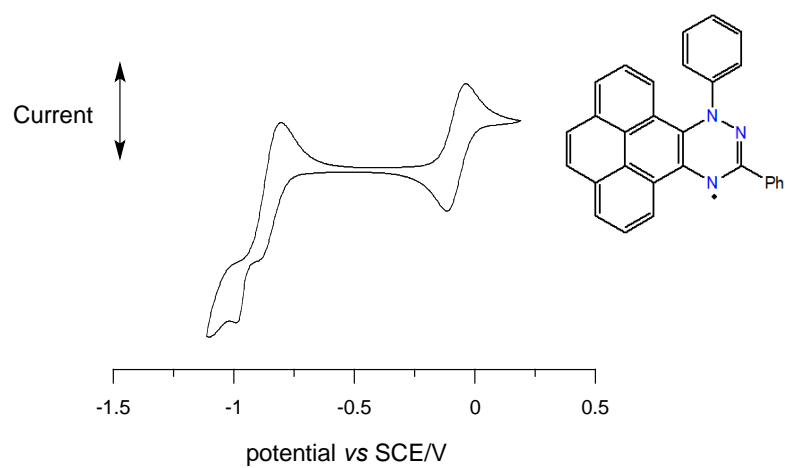
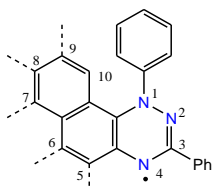


Figure 3.19. Cyclic voltammogram of **3.21** in CH_2Cl_2 .

3.1.1.2.1.3. Electron paramagnetic resonance spectroscopy (EPR)

The distribution of spin density in radicals was assessed with electron paramagnetic resonance spectroscopy. EPR spectra for radicals were recorded on an X-band EMX-Nano EPR spectrometer at ambient temperature on dilute and degassed solutions in distilled benzene in a concentration range of $2\text{-}5 \times 10^{-4}$ M. The microwave power was set with the Power Sweep program below the saturation of the signal, modulation frequency of 100 kHz, modulation amplitude of 0.5 G_{pp} and spectral width of 100 G. Accurate g -values were obtained using TEMPO as EMX-Nano internal standard. Simulations of the spectra were performed with the EMX-Nano software using DFT results (*vide infra*) as the starting point including all nitrogen and up to four hydrogen atoms. The resulting $hfcc$ values were perturbed several times until a global minimum for the fit was achieved. Experimental and simulated spectra are shown in Figures 3.20-3.23 and resulting $hfcc$ are listed in Table 3.5.

Table 3.5. Summary of hyperfine coupling constants (G) for radicals.



Compound	a_{N1}^a	a_{N2}^a	a_{N4}^a	a_H	a_H	a_H	a_H	g^b
Blatter radical ^c	7.65	4.87	4.90	1.32	1.58	1.03	0.58	2.0033
3.18 (naphthalene)	7.73	4.48	4.75	-0.77	1.31	1.31	1.31	2.0041
3.19 (quinoline)	7.19	2.45	5.15	-1.25	-1.25	-0.03	5.88	2.0042
3.20 (phenanthrene)	7.63	2.08	4.11	-1.77	-1.10	-3.22	8.02	2.0040
3.21 (pyrene)	7.68	2.11	4.52	-1.23	-0.91	-3.15	8.99	2.0037

^aAssignments follow the previous EPR and ENDOR studies on ^{15}N -labeled derivatives (ref.⁹), ^bReferenced to TEMPO as the internal standard. ^cRef.⁶

EPR spectra of radicals in benzene solutions revealed a typical complex pattern of signals resulting from splitting with three ^{14}N nuclei modulated with additional smaller splitting by ^1H nuclei, as shown in Figures 3.20-3.23. The analysis of the a_{N} hyperfine coupling constant (*hfcc*) for the series is consistent with those for Blatter radical⁶ (Table 3.5) and are in the range of ~ 7.1 to 7.7 G for $a_{\text{N}(1)}$ and ~ 2.1 to 4.4 G for $a_{\text{N}(2)}$ and ~ 4.1 to 5.4 G for $a_{\text{N}(4)}$.

The extension of the π system in the radicals has big effect on the $a_{\text{N}(1)}$ value and it is almost similar for all radicals while the sum of $a_{\text{N}(2)}$ and $a_{\text{N}(4)}$ decreases. The value for $a_{\text{N}(4)}$ for all radicals except **3.19** slightly decreases relative to the Blatter radical especially in phenanthrene analogue **3.20** which decreases from 4.90 to 4.11 G, reflecting the increasing delocalization of the spin from the [1,2,4]triazinyl ring. Just $a_{\text{N}(4)}$ value for **3.19** increases from 4.90 to 5.15 and it is because of the N atom in the quinoline structure at position C(6). The $a_{\text{N}(2)}$ value, for all radicals particularly decreases except for **3.18**, which decreases very little from 4.87 to 4.48 G.

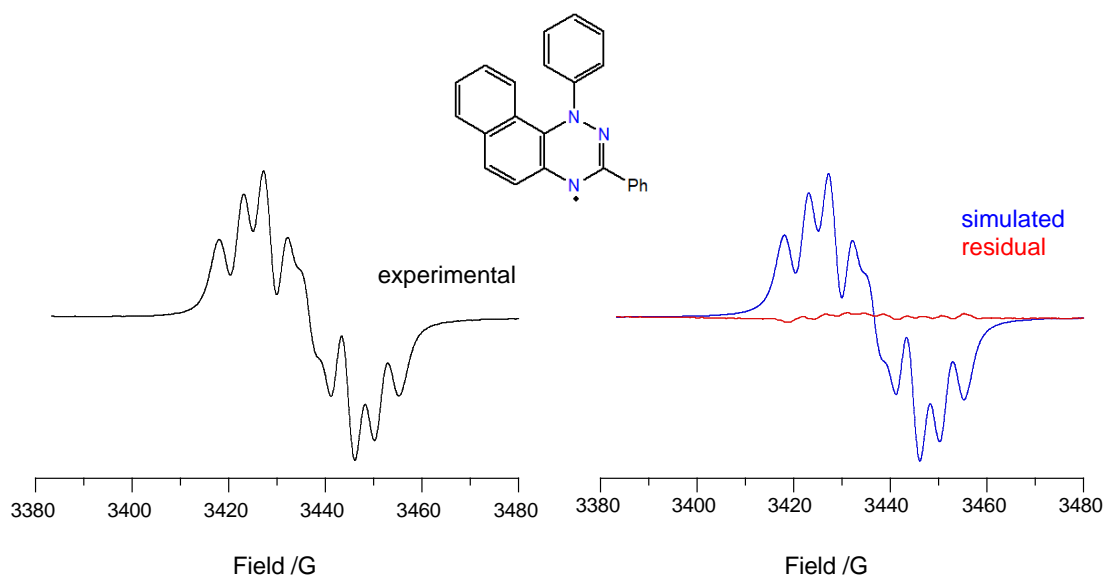


Figure 3.20. Experimental (black, left), simulated (blue, right) and difference (red, right) spectra for **3.18** recorded in benzene at *ca* 20 °C.

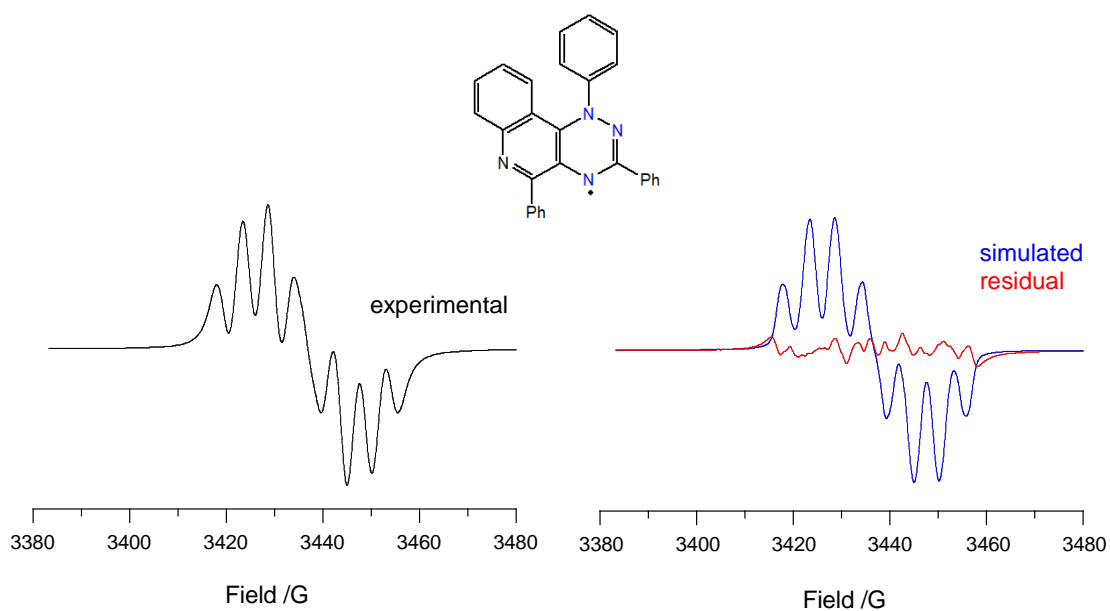


Figure 3.21. Experimental (black, left), simulated (blue, right) and difference (red, right) spectra for **3.19** recorded in benzene at *ca* 20 °C.

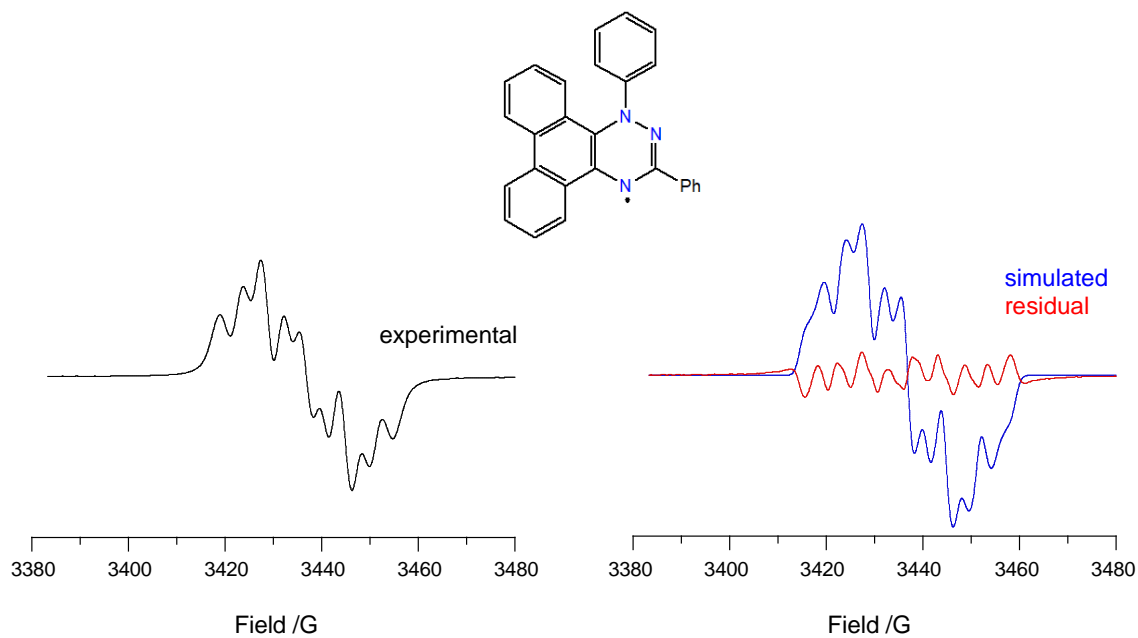


Figure 3.22. Experimental (black, left), simulated (blue, right) and difference (red, right) spectra for **3.20** recorded in benzene at *ca* 20 °C.

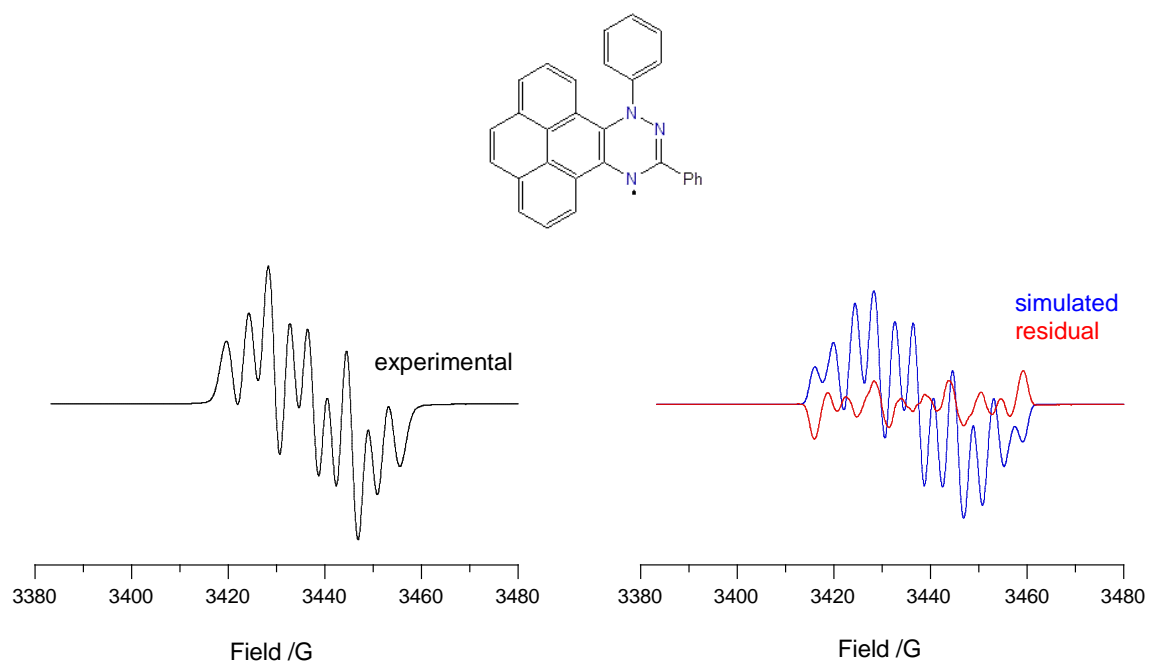
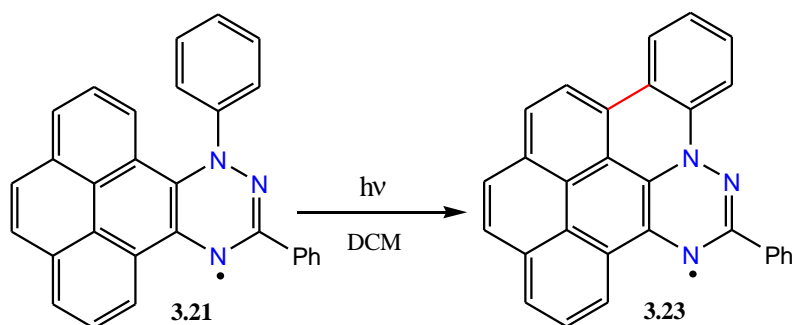


Figure 3.23. Experimental (black, left), simulated (blue, right) and difference (red, right) spectra for **3.21** recorded in benzene at *ca* 20 °C.

3.1.1.3. Synthesis of ring-fused π -extended Blatter radicals by photocyclization

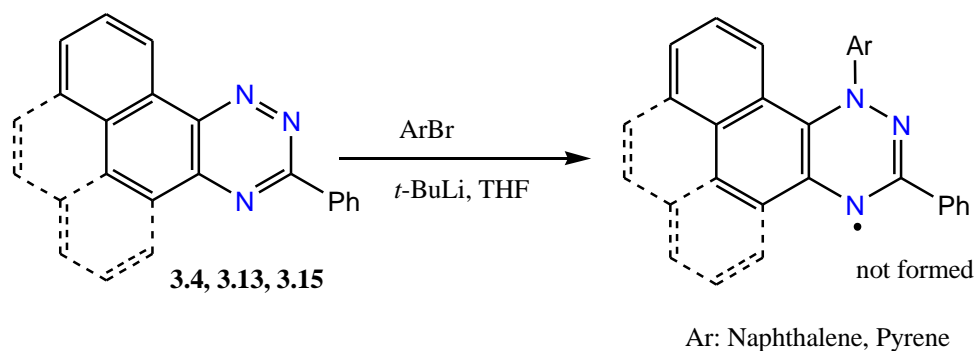
For connection of two π molecular fragments and planarization of the structure of the radicals, pyrenotriazinyl **3.21**, which was more stable than the other radicals, was used for Mallory photocyclization reaction. (Scheme 3.4). In this method, a 300 W halogen lamp was used to irradiate the 1 mM solution of the precursor in dry DCM while stirring it.¹⁰ The lamp was positioned around 30 cm from the flask. The reaction mixture warmed to 30–35 °C during irradiation and the irradiation was terminated after 24 h. The product was isolated using a short column with Et₃N-passivated silica. The resulting radical **3.23** was slowly decomposed in solutions during photocyclization and recrystallization, as evidenced by the appearance of a blue spot and a strong baseline on TLC. It was possible to perform high-resolution mass spectrometry (HRMS) measurements to support the proposed structure.



Scheme 3.4. Synthesis of planar pyrenotriazinyl **3.23** through photocyclization. Reagents and conditions: 300 W halogen lamp, 1mM solution of precursor in DCM (dry).

3.1.1.4. Synthesis of ring expanded Blatter radicals at N(1) position

For the expansion of the π -system at the N(1) position of the Blatter radical, three different available triazines (**3.4**, **3.13** and **3.15**) were used for azaphilic addition of aryllithium reagents prepared from appropriate aryl bromide and *t*-BuLi at -78 °C, followed by oxidation of the resulting anion (Scheme 3.5)⁷. Unfortunately, after adding aryllithium reagents, the expected anions and radicals did not form and just starting materials were recovered, and this result demonstrated the limitation of this method for π -extension at *f* edge, which may be related to the sterically congested positions.



Scheme 3.5. Ring expansion at the N(1) position of the triazinyl radicals. Reagents and conditions:
(a) arylbromide, *t*-BuLi, THF.

3.1.2 Synthesis of ring expanded planar Blatter radicals through cyclization

In this part, the detailed preparative procedures for the synthesis and partial characterization of a novel derivative of the π -expanded planar Blatter radical by ring annulation at the *e* edge and the N(1) position of the 1,4-dihydro[1,2,4]triazin-4-yl are described. The preparation of two π -extended triazines, out of which one was converted to the desired radical by photocyclization, was carried out using appropriate naphthalene derivative and aromatic bromic acids under standard Suzuki-Miyaura conditions (Figure 3.24).

It is possible to develop new materials with tunable properties including configurational stability, transannular electronic interactions, redox and photophysical behavior by ring annulation at the *e* and *f* edges of the 1,4-dihydro[1,2,4]triazin-4-yl. This also leads to further expansion of the π -system, greater spin delocalization, wider control of the electronic properties of such [1,2,4]triazinyl-based radicals. In order to understand how the π -expansion affects the electronic properties, the final radical is characterized using electron paramagnetic resonance (EPR) spectroscopy.

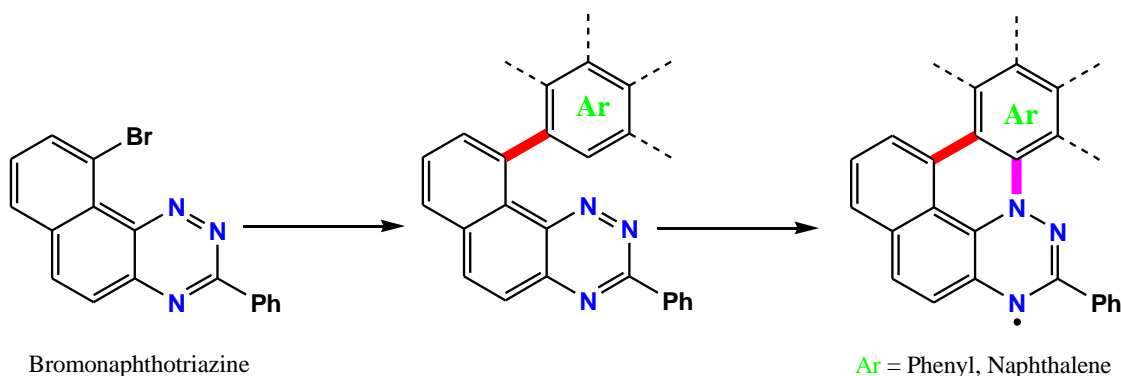
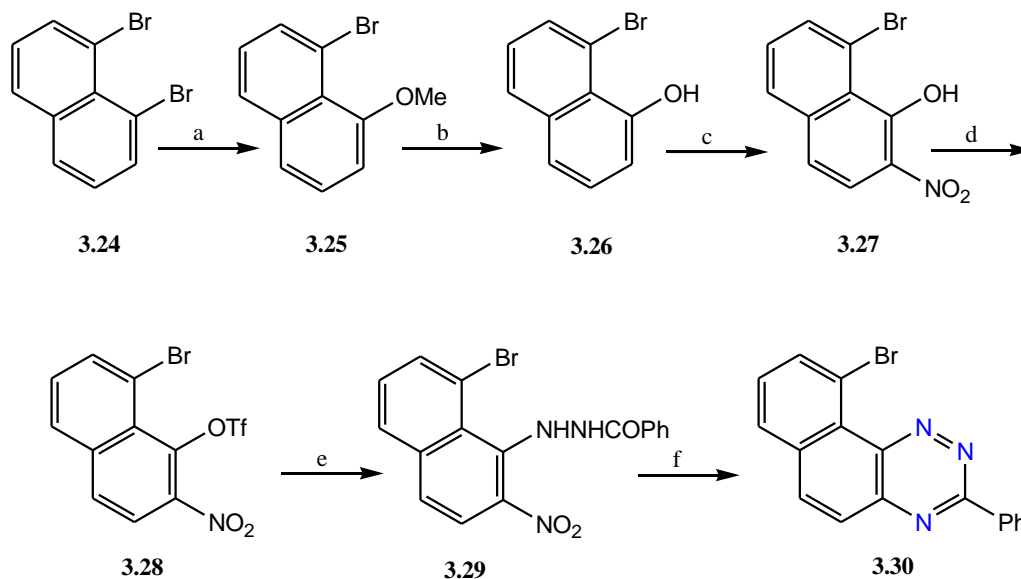


Figure 3.24. Synthesis of radicals *via* intramolecular azaphilic addition.

3.1.2.1. Synthesis of naphtho[2,1-*e*]triazine derivatives

3.1.2.1.1. Synthesis of 10-bromo-3-phenyl-naphtho[2,1-*e*][1,2,4]triazine

In this methodology the installation of aromatic rings fused at the *e* edge of the 1,4-dihydro[1,2,4]triazin-4-yl skeleton, is accomplished by the proper choice of the substrate. For this reason, 1,8-dibromonaphthalene **3.24** was used as the starting material. The key intermediate for synthesis of the radical is 10-bromo-3-phenyl-naphtho[2,1-*e*][1,2,4]triazine (**3.30**, Scheme 3.6), which was prepared by nucleophilic aromatic substitution of triflate **3.28** with benzhydrazide giving the coupled product **3.29**. Subsequently, the nitro group in hydrazide **3.29** was reduced, and then cyclodehydrated by acid-mediation to obtain the fused triazine **3.30** in 51 % yield.¹ Triflic ester **3.28** was obtained by converting the 8-bromo-2-nitronaphthol **3.26** in the presence of triflic anhydride in 38% yield.¹¹ 8-Bromo-1-naphthol **3.26** was synthesized by deprotection of the methyl group in 1-bromo-8-methoxy-naphthalene **3.25**,¹² which was obtained from 1,8-dibromonaphthalene **3.24**.¹³ 8-Bromo-1-naphthol was nitrated with a low yield in the presence of KHSO_4 , $\text{Ni}(\text{NO}_3)_2 \cdot 6\text{H}_2\text{O}$ (Scheme 3.6).¹⁴



Scheme 3.6. Synthesis of 10-bromo-3-phenyl-naphtho[2,1-*e*][1,2,4]triazine. Reagents and conditions: (a) CuI , NaOMe , MeOH , (b) BBr_3 , dry DCM , (c) KHSO_4 , CH_3CN , $\text{Ni}(\text{NO}_3)_2 \cdot 6\text{H}_2\text{O}$, (d) Et_3N , DCM , triflic anhydride, (e) benzhydrazide, DMSO , (f) 1. Sn , AcOH , 2. NaIO_4 , DCM/MeOH (1:1).

3.1.2.1.1.1. Synthesis of 8-bromo-1-naphthol

For synthesis of 8-bromo-1-naphthol **3.26** from 1,8-diaminonaphthalene **3.33**, three different methodologies were used (Figure 3.25, Scheme 3.7). Method A involved oxidative hydroxylation of the (8-bromonaphthalen-1-yl)boronic acid **3.32** which failed because it was overoxidized and the desired product did not form. In method B, 1-amino-8-bromonaphthalene **3.31** was used as the starting material to obtain the 8-bromo-1-naphthol **3.26** through the Sandmeyer reaction.¹⁵ However, in method B we obtained the desired product in low yield, and most of the substrate was decomposed. Method C relied on deprotection of methoxy group¹² in 1-bromo-8-methoxynaphthalene **3.25**. Method C contained one step more than method B (Sandmeyer) but the overall yield was higher than method B according to recovered unreacted substrate from the reaction mixture.

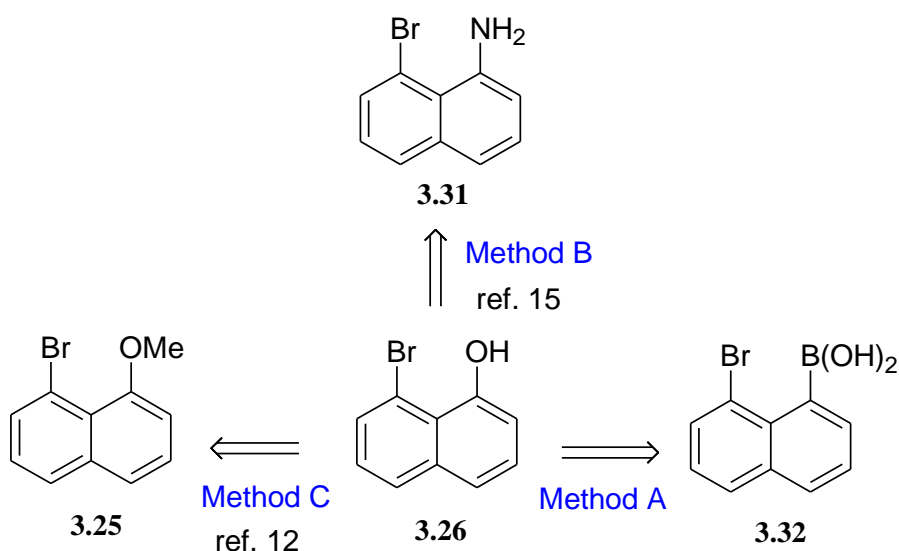
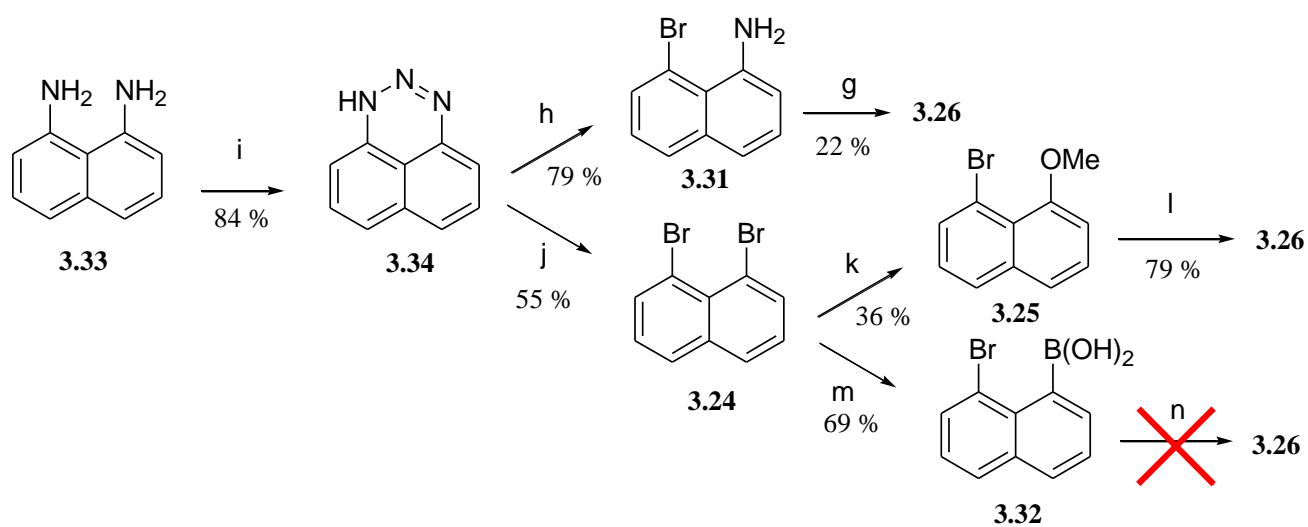


Figure 3.25. Different methods for synthesis of 8-bromo-1-naphthol.



Scheme 3.7. Different methods for synthesis of 8-bromo-1-naphthol. Reagents and conditions: (i) NaNO_2 , AcOH , 0°C ,³¹ (h) Cu (10 mol%), HBr , rt, 12h,³¹ (g) NaNO_2 , H_2SO_4 , H_2O ,¹⁵ (j) H_2SO_4 (6.9 M), NaNO_2 , CuBr , HBr (48%),³¹ (k) CuI , NaOMe , MeOH ,¹³ (l) BBr_3 , dry DCM , reflux,¹² (m) *n*-butyllithium, trimethylborate, NH_4Cl ,³² (n) AcOH , H_2O_2 .³³

3.1.2.1.1.2. Synthesis of 8-bromo-2-nitro-1-naphthol

Another challenging issue for the synthesis of the bromonaphthotriazie **3.30** was the nitration of 8-bromo-1-naphthol **3.26** to get the 8-bromo-2-nitro-naphthol **3.26**. Different methods were tried. The best yields were obtained using cerium (IV) ammonium nitrate¹⁶ and KHSO₄, Ni(NO₃)₂.6H₂O¹⁴ but they were not reproducible (Table 3.6).

Table 3.6. Synthesis of 8-bromo-2-nitro-naphthol

Catalyst and nitrating agent (eq)	Solvent	Conditions	Yield of 2- NO ₂ -1-Naphthol (%)	Comments
TBN (1)	CH ₃ CN	1 h, rt	8	The substrate did not recover
TBN (2)	THF, H ₂ O	2.5 h, rt	5	The substrate did not recover
KNO ₃ (1), (COCl) ₂ /DMF iminiumsalt (1.5)	CH ₃ CN	6-8 h, rt	7	The substrate did not recover
KIO ₄ (0.4-0.5 mol%) NaNO ₂ (2) KHSO ₄ (1)	CH ₃ CN	17- 30 h, 35C°	5	The substrate did not recover
Solid CAN (1) ¹⁶	-	2h, rt	20-24	Most of the substrate recovered
KHSO ₄ (0.012) ¹⁴ Ni(NO ₃) ₂ .6H ₂ O (1)	CH ₃ CN	10 min	17-20	Most of the substrate recovered
PTSA(0.012), Ni(NO ₃) ₂ .6H ₂ O (1)	Acetone	3 h, 56 °C	2	The substrate did not recover

TBN: tert-Butyl nitrite

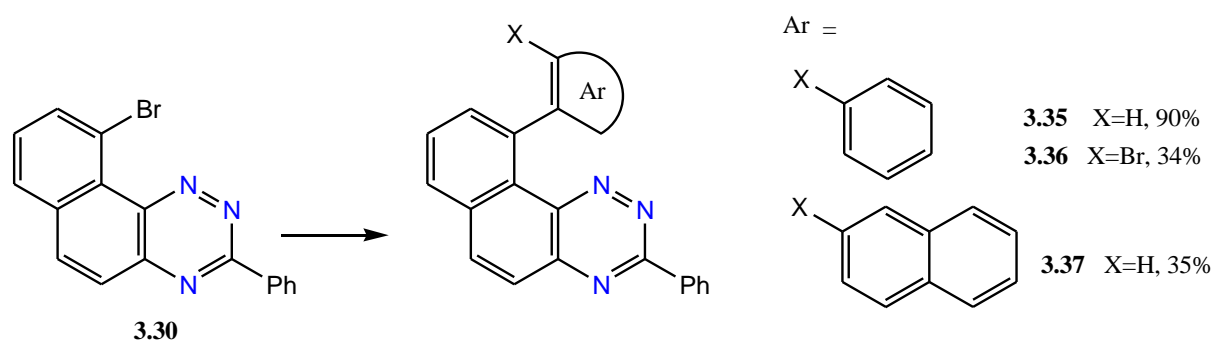
CAN: cerium (IV) ammonium nitrate

PTSA: p-toluenesulfonic acid

Acetonitrile was used as solvent, KHSO₄ as a catalyst, and Ni(NO₃)₂.6H₂O was added for nitration. This reaction was not reproducible due to obtaining different yield of the desired product and the best yield was around 17%.

3.1.2.1.2. Synthesis of naphtho[2,1-*e*][1,2,4]triazine derivatives *via* Suzuki-Miyaura coupling

Two aromatic boronic acid derivatives with different sizes in the π -system (naphthyl and phenyl) were used for ring expansion at the N(1) position of the Blatter radical and they were reacted with the 10-bromo-3-phenyl-naphtho[2,1-*e*][1,2,4]triazine **3.30** under standard Suzuki-Miyaura condition (Scheme 3.8).¹⁷

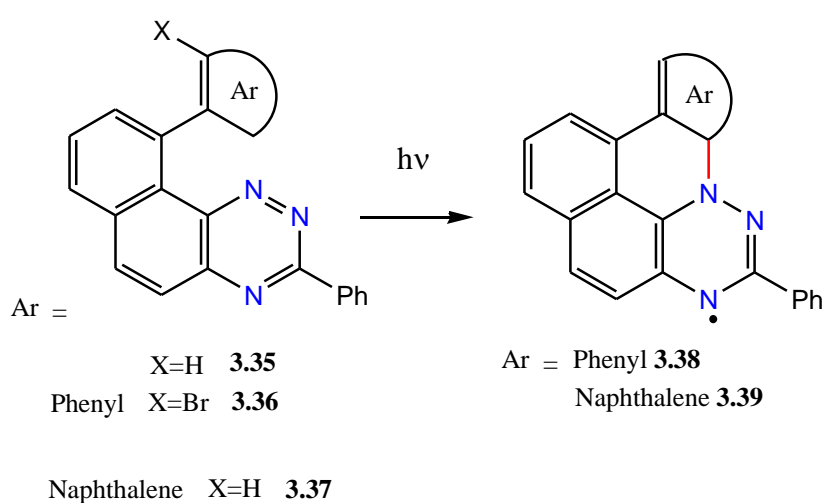


Scheme 3.8. Synthesis of triazines through Suzuki-Miyaura coupling. Reagents and conditions: Boronic acids, Pd(PPh₃)₄, K₂CO₃, THF/H₂O

For this reaction, 10-bromo-3-phenyl-naphtho[2,1-*e*][1,2,4]triazine **3.30** was treated with the appropriate boronic acid in the presence of Pd(PPh₃)₄ and K₂CO₃.¹⁷ The 10-phenyl-3-phenyl-naphtho[2,1-*e*][1,2,4]triazine was obtained in a better yield than 10-(2-bromo-phenyl)-3-phenyl-naphtho[2,1-*e*][1,2,4]triazine.

3.1.2.2. Synthesis of radicals through intramolecular photocyclization

Two radicals **3.38** and **3.39** were generated by photocyclization of triazines **3.35-3.37**.¹⁰ These radicals undergo slow decomposition in solutions during photocyclization, as evidenced by the appearance of a blue spot and a strong baseline on TLC. Direct recrystallization of the reaction mixture also failed to give the pure product. The radicals exhibited heat, air, and possibly moisture sensitivity, however it was possible to obtain electron paramagnetic resonance (EPR) analysis of one of the products, and high-resolution mass spectrometry (HRMS) measurements indeed confirmed the formation of the desired radical **3.38** (Scheme 3.9).



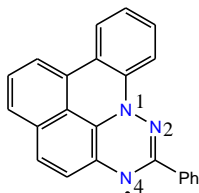
Scheme 3.9. Synthesis of radicals through intramolecular azaphilic radical addition. Conditions: 300 W halogen lamp, 1mM solution of precursor in DCM (dry)

3.1.2.2.1. Characterisation of the electronic structure of the radical

3.1.2.2.1.1. Electron paramagnetic resonance spectroscopy (EPR)

The distribution of spin density in radical **3.38** was assessed with electron paramagnetic resonance spectroscopy. EPR spectrum of the radical was recorded on an X-band EMX-Nano EPR spectrometer at ambient temperature on dilute and degassed solutions in distilled benzene in a concentration range of $2\text{-}5 \times 10^{-4}$ M. The microwave power was set with the Power Sweep program below the saturation of the signal, modulation frequency of 100 kHz, modulation amplitude of 0.5 G_{pp} and spectral width of 100 G. Accurate g-values were obtained using TEMPO as EMX-Nano internal standard. Simulations of the spectra were performed with the EMX-Nano software using DFT results (*vide infra*) as the starting point including all nitrogen and up to 4 hydrogen atoms. The resulting *hfcc* values were perturbed several times until a global minimum for the fit was achieved. Experimental and simulated spectra are shown in Figures 3.26 and resulting *hfcc* are listed in Table 3.7.

Table 3.7. Summary of hyperfine coupling constants (G) for radicals.



Compound	a_{N1}^a	a_{N2}^a	a_{N4}^a	aH	aH	aH	aH	g^b
Blatter radical ^c	7.65	4.87	4.90	1.32	1.58	1.03	0.58	2.0033
3.18 (naphthalene)	7.73	4.48	4.75	-0.77	1.31	1.31	1.31	2.0041
3.38	5.67	4.37	4.00	-0.03	0.09	0.47	0.00	2.0038

^aAssignments follow the previous EPR and ENDOR studies on ¹⁵N-labeled derivatives (ref.⁹), ^bReferenced to TEMPO as the internal standard. ^cRef.⁶

EPR spectrum of radical **3.38** in benzene solutions resulting from splitting with three ¹⁴N nuclei modulated with additional smaller splitting by ¹H nuclei, is shown in Figures 3.26. The analysis of the a_N hyperfine coupling constant (*hfcc*) for the series is consistent with those for Blatter radical⁶ (Table 3.7) and are in is ~ 5.6 G for $a_{N(1)}$ and ~ 4.3 G for $a_{N(2)}$ and ~ 4.9 G for $a_{N(4)}$.

Analysis of the results indicates that by connecting of two aromatic parts of the structure and planarize the structure of the molecule, the $a_{N(1)}$ value decreases from 7.73 for **3.18** to 6.82 G for **3.38** and the sum of $a_{N(1)}$ and $a_{N(3)}$ decrease as well, which revealed that the spin is delocalized by connection of two aromatic sites.

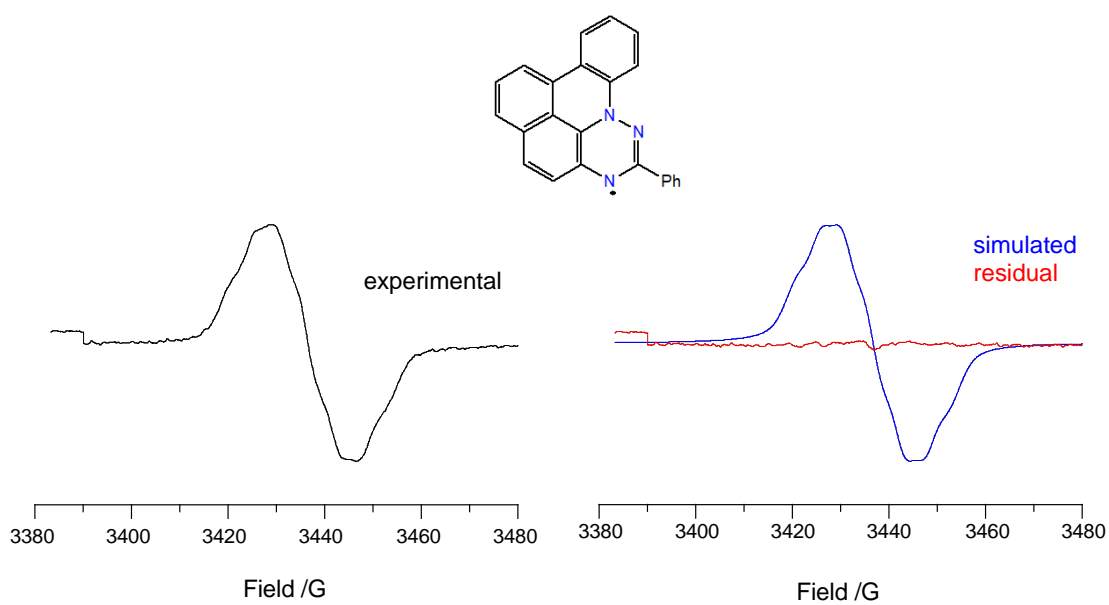


Figure 3.26. Experimental (black, left), simulated (blue, right) and difference (red, right) spectra for **3.38** recorded in benzene at *ca* 20 °C.

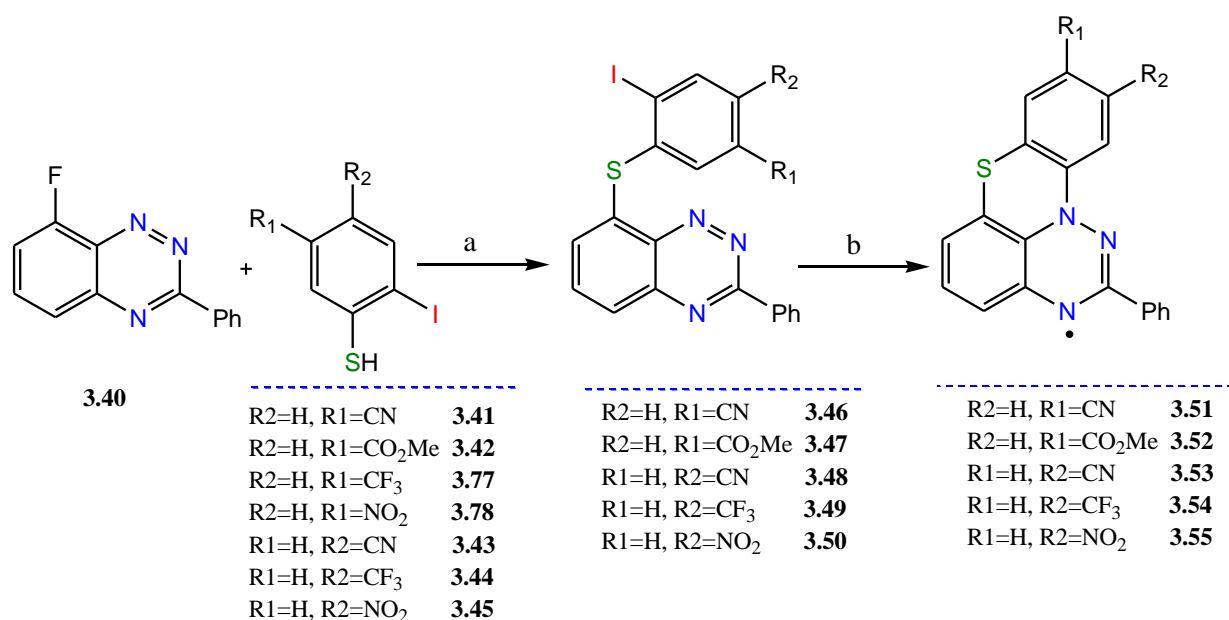
3.2. Functionalization of *S*-peri-annulated benzo[*e*][1,2,4]triazinyl radicals

As it was mentioned in the Introduction of the Thesis, a large torsion angle between the two π planes in the structure of Blatter radicals affects the molecular packing in the solid-state, which, in turn, impacts magnetic properties and also limits the spin delocalization. To remedy these problems, planarized Blatter radicals were prepared by the connection of the C(8) and C(*ortho*) positions with an oxygen or sulfur atom in the Blatter radical¹ (Figure 3.2).

Many derivatives of the Blatter radical, such as those with different aryl substituents at the N(1) position, have been investigated for their solid-state structures and magnetic behavior. The results revealed diverse packing motifs in the solid-state, depending on the size and steric demands of the aryl substituent, which impact on magnetic interactions.⁷

Herein, we present the synthesis and detailed characterization of five new derivatives of functionalized *S*-peri-annulated benzo[*e*][1,2,4]triazinyl containing CO₂Me, CN, CF₃ and NO₂ groups at the C(10) or C(9) positions through a TMS₃SiH-assisted cyclization of aryl iodides, and investigate the effect of the substituent on their spectroscopic and electrochemical properties.

The goal was a better understanding of factors governing the crystal packing of the benzo[*e*][1,2,4]triazinyl derivatives and their impact on magnetic interactions (Scheme 3.10).

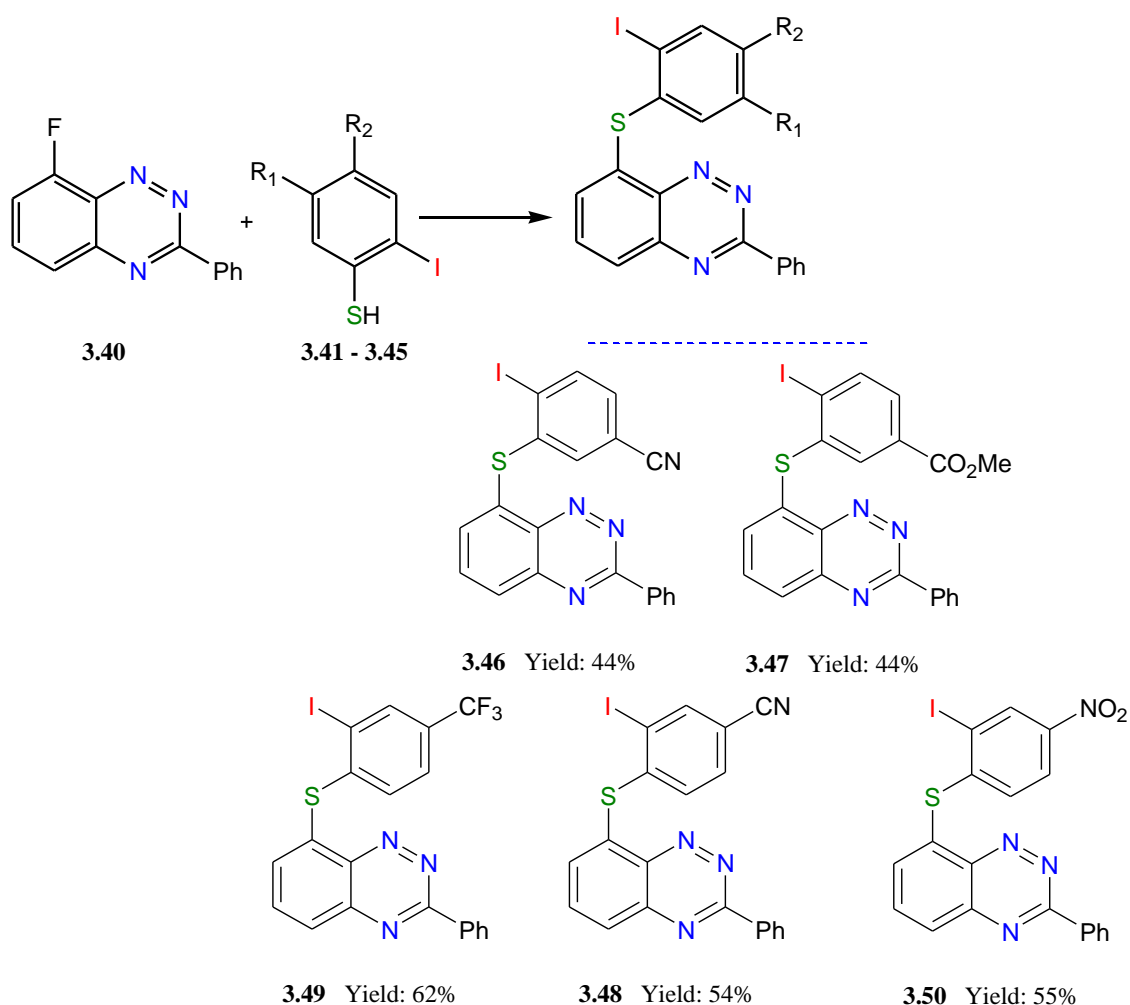


Scheme 3.10. Synthesis of functional derivatives of sulfur-containing planarized Blatter radical.
Reagents and conditions: (a) DMSO, NaH, (b) TMS₃SiH, AIBN.

Radicals **3.51-3.55** can be obtained by reacting the [1,2,4]triazine **3.40** with appropriate thiols in the presence of NaH, followed by cyclization reaction of the phenylsulfanyl-3-phenylbenzo[1,2,4]triazines. The cyclization involves homolytic aromatic substitution (HAS) in the presence of tris(trimethylsilyl)silane (TMS₃SiH) and 2,2-azobisisobutyronitrile (AIBN), (Scheme 3.10). The [1,2,4]triazine **3.40** was prepared by cyclization of the benzhydrazide derivative under reductive conditions, which was prepared by N-arylation of 1,2-difluoro-3-nitrobenzene with benzhydrazide.¹

3.2.1. Synthesis of 8-phenylsulfanyl-3-phenylbenzo[1,2,4]triazines

The [1,2,4]triazine **3.40** was reacted with appropriate thiols **3.41-3.45** in the presence of NaH to obtain functionalized triazines **3.46-3.50** (Scheme 3.11).¹⁰ It was possible to obtain five derivatives of phenylsulfanyl-3-phenylbenzo[e][1,2,4]triazine. Unfortunately in the reaction of **3.40** with two thiols (**3.77**, and **3.78**, Scheme 3.10) byproducts were formed, which were purified to check by HRMS and NMR and indicated that the desired products were not formed.

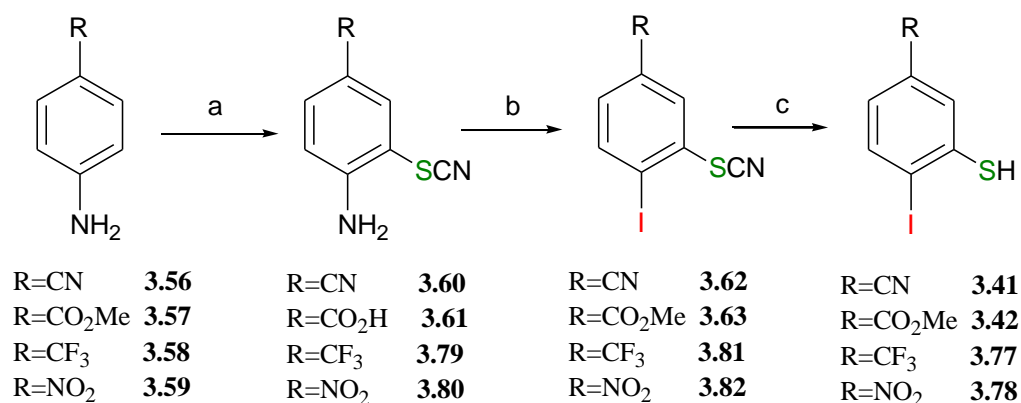


Scheme 3.11. Synthesis of derivatives of 8-phenylsulfanyl-3-phenylbenzo[e][1,2,4]triazine. Reagents and conditions: DMSO, NaH, 80 °C, 1-5 h

3.2.1.1. Synthesis of *ortho*-iodothiophenols

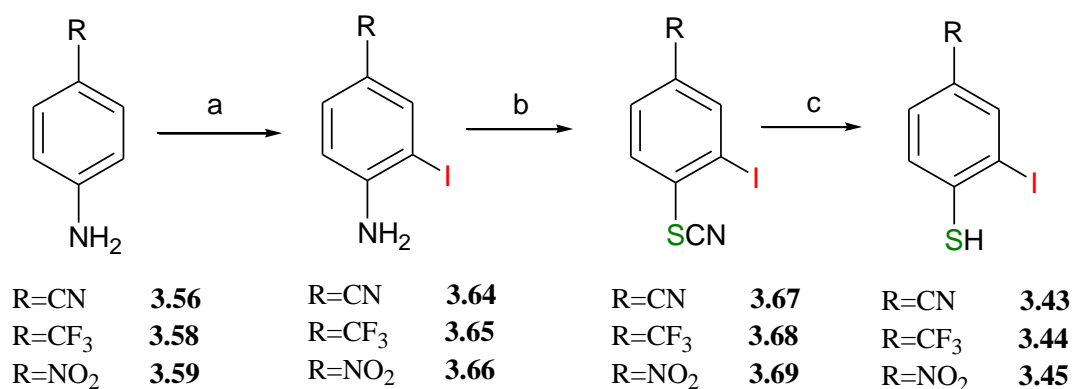
3.2.1.1.1. Synthesis of *ortho*-iodothiophenols through thiocyanate

Two different methods (A and B) were used to obtain *ortho*-iodothiophenols from the commercially available amines **3.56-3.59**. In method A (Scheme 3.12), *o*-iodothiophenols **3.41**, **3.42**, **3.77**, and **3.78** were synthesized by reducing the appropriate thiocyanate with sodium borohydride.²⁰ Thiocyanates **3.60**, **3.61**, **3.79**, and **3.80**, were synthesized by reacting the aryl amines with potassium thiocyanates in the presence of acetic acid and bromine using a general method.¹⁸ To obtain the **3.62**, **3.63**, **3.81**, and **3.82**, the amine was converted to iodo through the Sandmeyer reaction.¹⁹ Among these intermediates to the thiols, compounds **3.60**,¹⁸ **3.61**³⁴ and **3.80**³⁵ are known, and they have been synthesized and characterized before.



Scheme 3.12. Synthesis of *o*-iodothiophenols using method A. Reagents and conditions: (a) KSCN, AcOH, Br₂, (b) NaNO₂, H₂SO₄, CH₃CN, KI, (c) NaBH₄, MeOH.

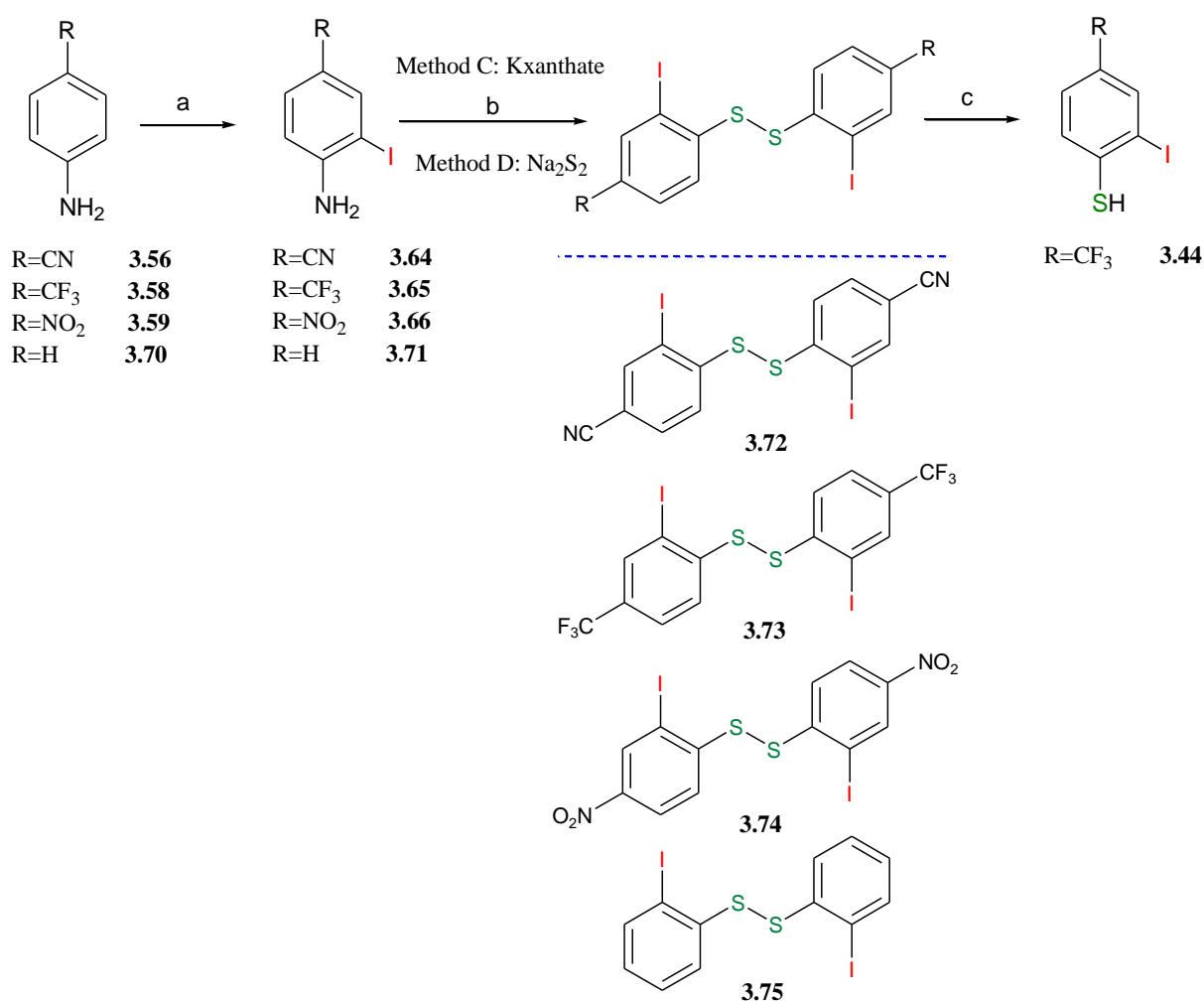
In method **B**, (Scheme 3.13), *o*-iodothiophenols **3.43-3.45** were obtained by reacting the commercially available amines with pyridiniumiodochloride in MeOH,²¹ followed by converting the amine group to thiocyanate through Sandmeyer reaction²² and then reducing the thiocyanate to thiol²⁰ with sodium borohydride. Among these intermediates to the thiols, compounds **3.64**,³⁶ **3.65**³⁷ and **3.66**³⁸ are known compounds, and they have been synthesized and characterized before.



Scheme 3.13. Synthesis of *o*-iodothiophenols through method **B**. Reagents and conditions: (a) pyridinium chloride, MeOH, (b) NaNO₂, H₂SO₄, CuSCN, KSCN, (c) NaBH₄, MeOH.

3.2.1.1.2. Synthesis of *ortho*-iodothiophenols through disulfides

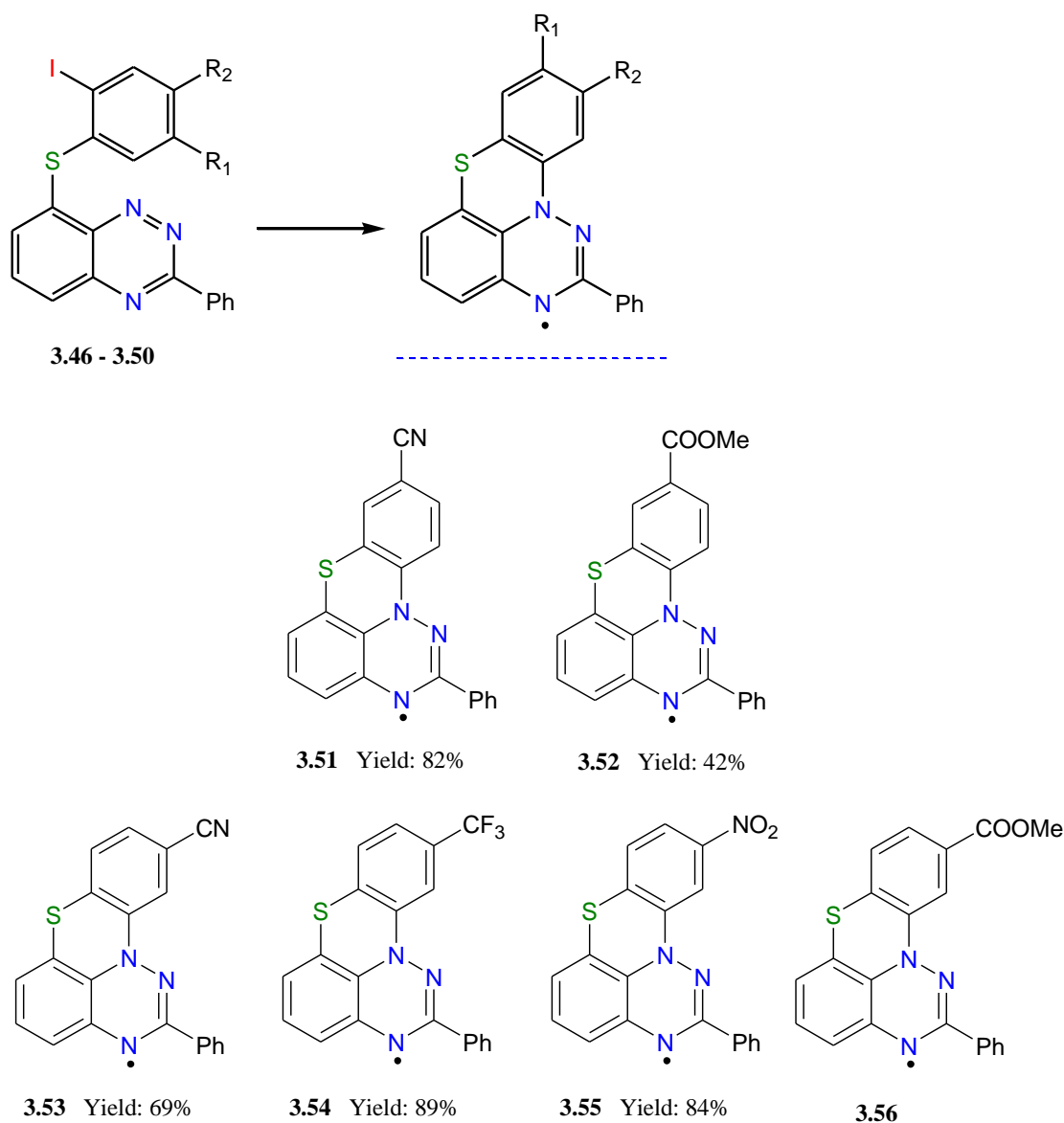
As it was mentioned in the Introduction, there are different methodologies for synthesis of thiols. Methods A and B are the best for the synthesis of *ortho*-iodothiophenols. Although, another method through disulfides was investigated. The disulfides were obtained using two different methods C and D. In method C disulfides were prepared through potassium xanthate and in method D, through sodium disulfide. Both of these methods gave the desired product in low yields (around 10%). The lower yield of the disulfides method was the reason that we preferred to use the thicyanate method even it had more steps for synthesis the thiols (Scheme 3.14).^{23,24}



Scheme 3.14. Synthesis of *o*-iodothiophenols through disulfides (method C and D). Reagents and conditions: (a) pyridinium chloride, MeOH, (b) potassium xanthate or Na₂S₂, (c) NaBH₄, THF.

3.2.2. Synthesis of 2-phenyl-3*H*-[1,2,4]triazino[5,6,1 *kl*]phenothiazin-3-yls

Radicals **3.51-3.55** were obtained by reacting the [1,2,4]triazine **3.40** with appropriate thiols **3.41-3.45** in the presence of NaH, followed by cyclization reaction of triazines **3.46-3.50**. Cyclization was performed through homolytic aromatic substitution (HAS) in the presence of tris(trimethylsilyl)silane (TMS₃SiH) and 2,2-azobisisobutyronitrile (AIBN)²⁵ (Scheme 3.15). The final radicals were characterized by spectroscopic (UV-vis, EPR), electrochemical, and high resolution mass spectrometry methods. Radical **3.56** was prepared by this method in another work in the Kaszynski's group²⁶ and in their work thiols were prepared through the disulfide method. In order to compare the electronic properties of this radical (**3.56**) with other radicals prepared in my project, I put the structure and data of this molecule in my Thesis.



Scheme 3.15. Synthesis of radicals. Reagents and conditions: TMS₃SiH, AIBN.

3.2.2.1. Characterisation of the electronic structure of the radicals

The influence of the substituents on the electronic characteristics was studied by spectroscopic (UV-vis and EPR) and electrochemical methods.

3.2.2.1.1. Electronic absorption spectroscopy (UV-vis)

The substituent effect on the electronic structure of the sulfur *peri*-annulated benzo[*e*][1,2,4]triazinyls was investigated by spectroscopic (UV-vis) method. A Jasco V770 spectrophotometer was used to record the UV-vis absorption spectra of radicals. Solutions were prepared in spectroscopic grade CH₂Cl₂ at concentrations ranging from 1.0 to 3.0×10⁻⁵ mol·L⁻¹ and the measurements were taken shortly after. The measured UV-vis spectra were fitted to the Beer-Lambert law ($A = \epsilon cl$), the molar absorption coefficient (ϵ) was derived from the linear plots. Results are shown in Table 3.8 and Figures 3.27–3.31.

Table 3.8. Absorption maximum wavelength of radicals

Compound	λ_{\max} (nm)
Blatter radical ^a	492
<i>S-peri</i> -annulated (H) ^b	688
3.51 (9-CN)	790
3.52 (9-CO₂Me)	787
3.53 (10-CN)	694
3.54 (10-CF₃)	761
3.55 (10-NO₂)	668
3.56 (10-CO₂Me) ^c	750

^a Ref. ⁶ ^b Ref ¹; ^c Ref. ²⁶

Similar to the *S-peri*-annulated benzo[*e*][1,2,4]triazinyl, radicals **3.51-3.55** exhibit significant bathochromic and hyperchromic shifts relative to the Blatter radical, particularly of the low-energy electronic absorption bands (Figures 3.27-3.31, Table 3.8). Analysis of the data reveals that substitution of the CN group at the C(9) position **3.51** shifts maximum of the lowest energy absorption band in the *S-peri*-annulated parent radical ($\lambda_{\max} = 688$ nm) to higher wavelengths ($\lambda_{\max} = 790$ nm) and leads to a bathochromic shift of the absorption maximum. However, this result was not observed by substitution of the cyano group at the C(10) position **3.53**.

By substitution of the COOMe group at the C(9) position (**3.52**), bathochromic shift of the absorption maximum ($\lambda_{\max} = 787 \text{ nm}$) was observed relative to that in the spectrum of the parent *S*-peri-annulated. Substitution at the C(10) position (CN, COOMe, CF₃, NO₂) shifts the maximum of the lowest energy absorption band in the *S*-periannulated to lower energies with the largest shift for the CF₃ derivative **3.54** ($\lambda_{\max} = 761 \text{ nm}$) and COOMe **3.56** ($\lambda_{\max} = 750 \text{ nm}$).²⁵ The bathochromic shift is progressively smaller for NO₂ **3.55** and CN **3.53** at the C(10) position and is the smallest for the 10-NO₂ derivative **3.55** ($\lambda_{\max} = 668 \text{ nm}$).

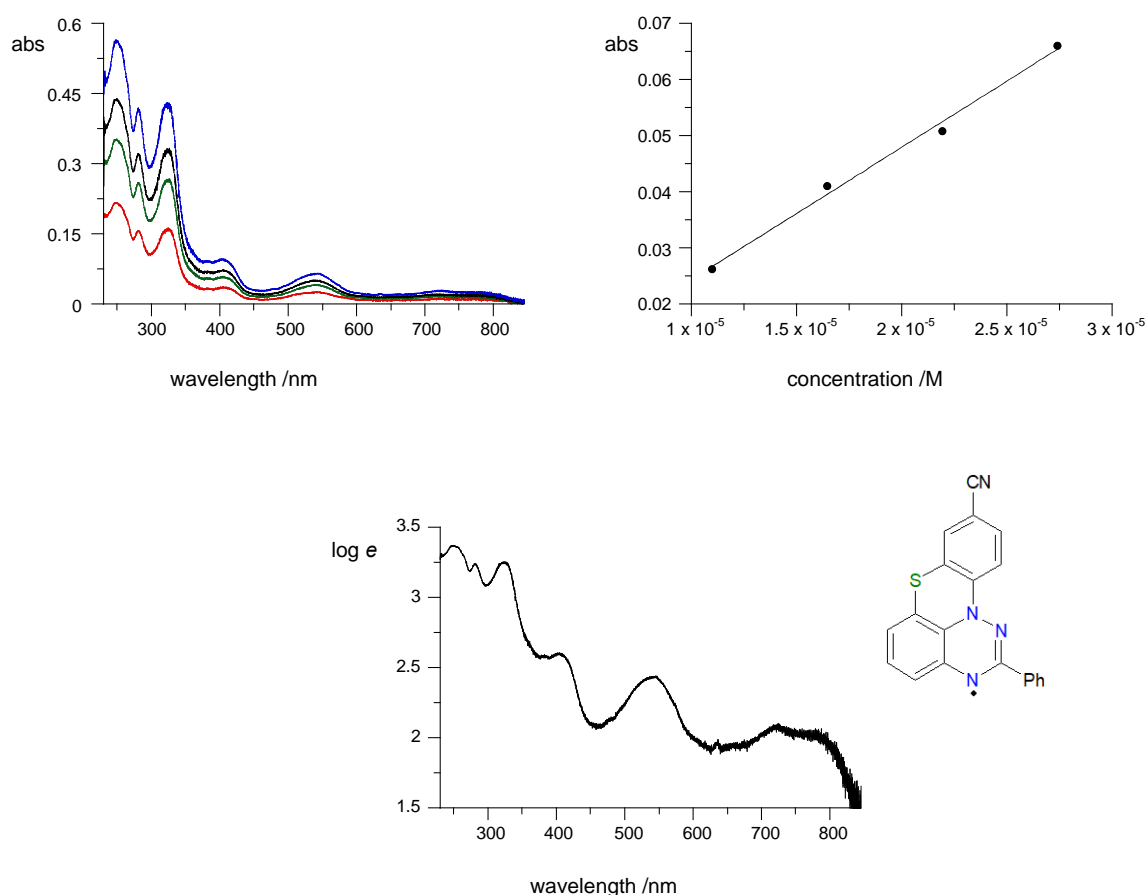


Figure 3.27. Clockwise: electronic absorption spectra for **3.51** in CH₂Cl₂ at four different concentrations (top left), determination of molar extinction coefficient ϵ at $\lambda = 545.9 \text{ nm}$ (top right, best fit function: $\epsilon = 2360 \times \text{conc}$, $r^2 = 0.9935$) and molar extinction $\log(\epsilon)$ plot (bottom).

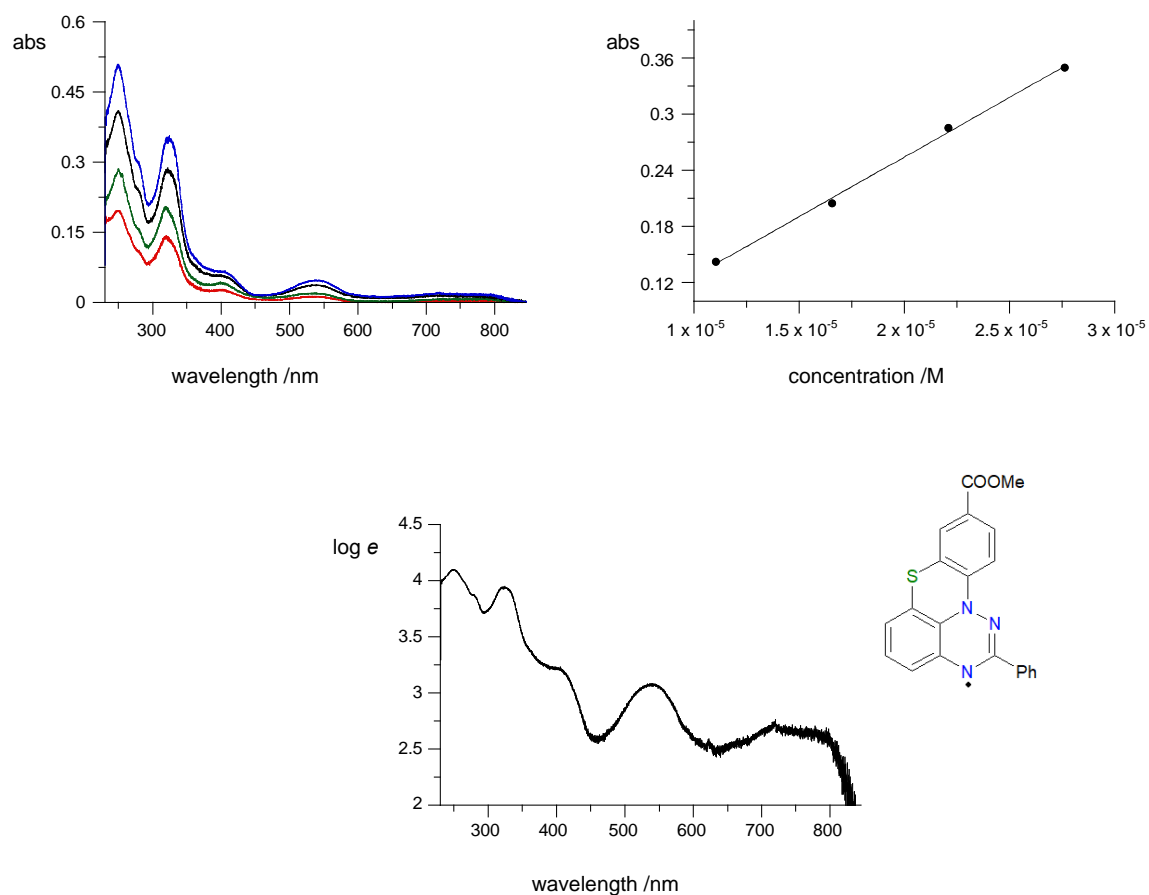


Figure 3.28. Clockwise: electronic absorption spectra for **3.52** in CH₂Cl₂ at four different concentrations (top left), determination of molar extinction coefficient ϵ at $\lambda = 318.6$ nm (top right, best fit function: $\epsilon = 12732 \times \text{conc}$, $r^2 = 0.9977$) and molar extinction $\log(\epsilon)$ plot (bottom).

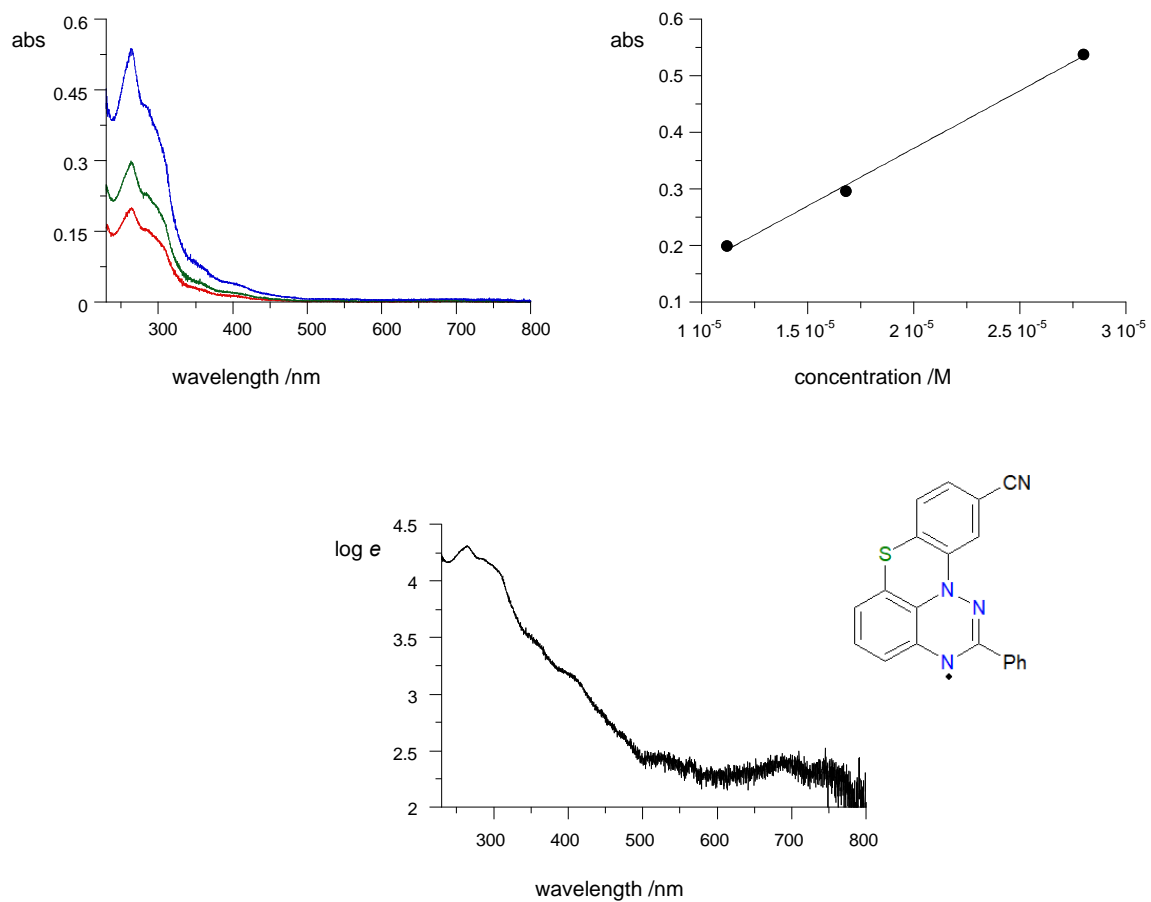


Figure 3.29. Clockwise: electronic absorption spectra for **3.53** in CH_2Cl_2 at three different concentrations (top left), determination of molar extinction coefficient ϵ at $\lambda = 264$ nm (top right, best fit function: $\epsilon = 20375 \times \text{conc}$, $r^2 = 0.9987$) and molar extinction $\log(\epsilon)$ plot (bottom).

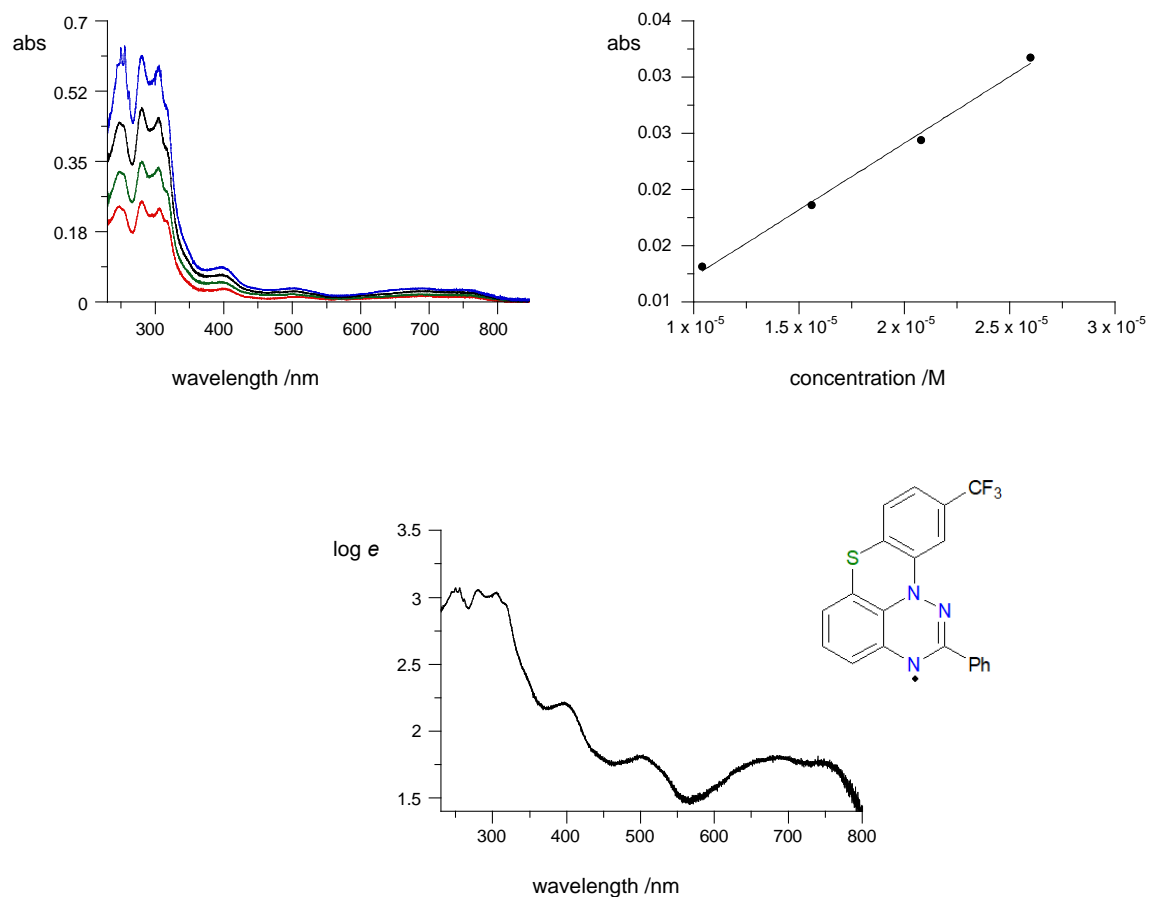


Figure 3.30. Clockwise: electronic absorption spectra for **3.54** in CH₂Cl₂ at four different concentrations (top left), determination of molar extinction coefficient ϵ at $\lambda = 750$ nm (top right, best fit function: $\epsilon = 1185 \times \text{conc}$, $r^2 = 0.9948$) and molar extinction $\log(\epsilon)$ plot (bottom).

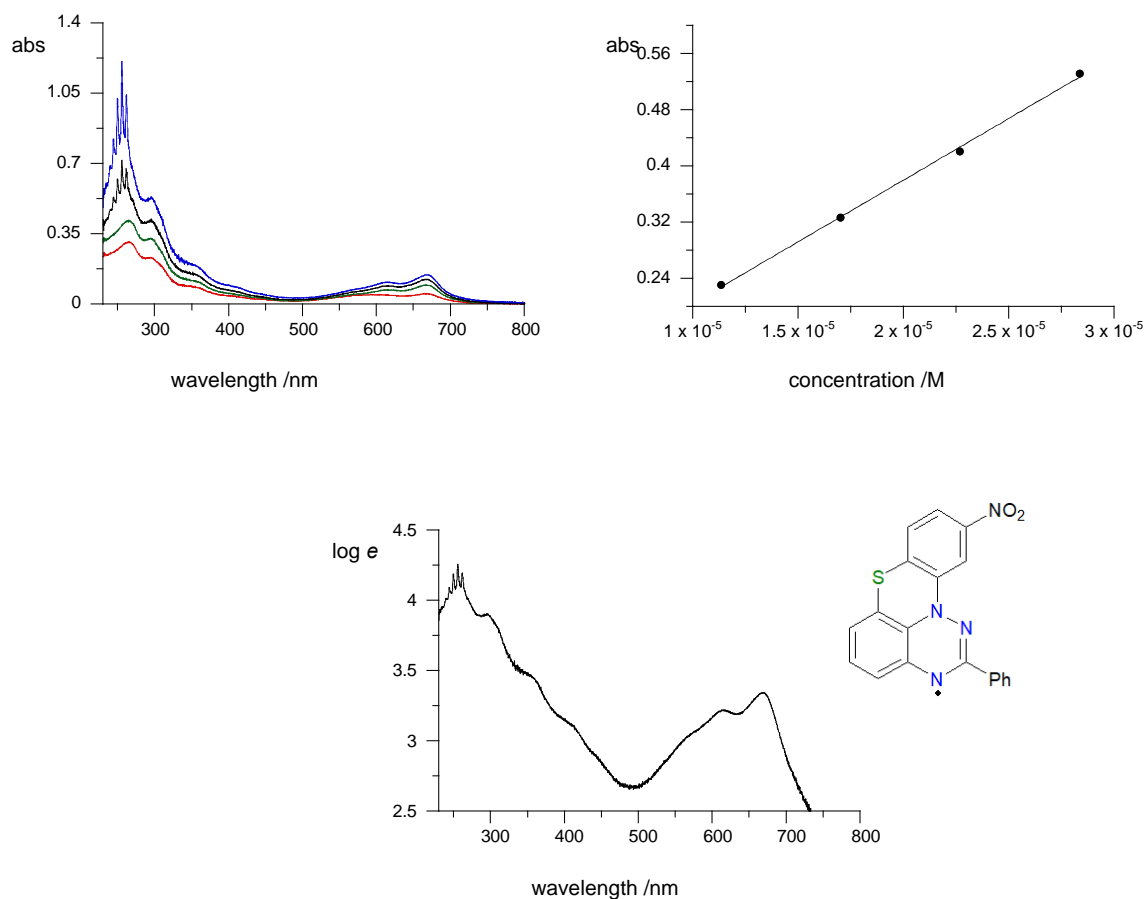


Figure 3.31. Clockwise: electronic absorption spectra for **3.55** in CH₂Cl₂ at four different concentrations (top left), determination of molar extinction coefficient ϵ at $\lambda = 294$ nm (top right, best fit function: $\epsilon = 17558 \times \text{conc}$, $r^2 = 0.9986$) and molar extinction $\log(\epsilon)$ plot (bottom).

3.2.2.1.2. Electrochemistry (cyclic voltammetry measurements)

A Metrohm Autolab PGSTAT 128N potentiostat/galvanostat equipment was used to perform electrochemical characterization of the radicals. The concentrations of the radicals were 0.5 mM in dry and degassed, spectroscopic grade CH₂Cl₂ (7 mL) containing [n-Bu₄N]⁺ [PF₆]⁻ (50 mM) as an electrolyte. A three-electrode electrochemical cell was employed with a glassy carbon disk as working electrode (ø 2 mm), Pt wire as the counter electrode and Ag/AgCl wire as the pseudoreference electrode. Temperature was around *ca.* 20 °C and scan rate was 50 mV·s⁻¹. All samples were measured twice, once without an internal reference and once with internal reference. The oxidation potential for the FcMe₁₀/ FcMe₁₀⁺ couple was established at -0.56 V *vs* the FcMe₁₀/ FcMe₁₀⁺ couple ($E_{\text{FcMe}_{10}/\text{FcMe}_{10}^+} = -0.10$ V *vs* SCE).⁸ Results are shown in Figures 3.32-3.36 and summarized in Table 3.9.

Table 3.9. Electrochemical properties of radicals^a

Compound	$E_{1/2}^{-1/0}$ (V)	$E_{1/2}^{0/+1}$ (V)	E_{HOMO}^b (eV)	E_{LUMO}^b (eV)	E_{cell} (V)
3.51 (9-CN)	-0.76	0.30	-5.06	-4.16	1.05
3.52 (9-CO₂Me)	-0.67	0.34	-5.10	-4.24	1.00
3.53 (10-CN)	-	0.37	-5.14	-	-
3.54 (10-CF₃)	-	0.18	-4.95	-	-
3.56 (10-CO₂Me)^c	-0.98	0.09	-4.85	-3.95	1.07

^a Potential *vs* SCE. ^b $E_{\text{HOMO/LUMO}} = -(E_{\text{onset ox/red vs Fc+/Fc}} + 5.1)$; ^c Ref.²⁶

Cyclic voltammetry measurements revealed that oxidation and reduction processes are reversible redox processes only for radicals **3.51** and **3.52**, while for **3.53** and **3.54** only the oxidation process is reversible (Figures 3.32-3.36, Table 3.9). This indicates that some of these radicals contain impurities such as decomposition products. No useful data was obtained for radical **3.55** (Figures 3.36), and for radicals **3.53** and **3.54** the reduction potential is not discussed due to the bad data achieved.

Data listed in the Table 3.9 suggests that, by increasing in the electron withdrawing character of the C(10) substituent, **3.56** (10-CO₂Me) → **3.54** (10-CF₃) → **3.53** (10-CN), the oxidation potential $E_{1/2}^{0/+1}$ systematically increases from 0.09 V in **3.56** to 0.37 V in **3.53**. However, for C(9) substituted radicals by increasing the electron withdrawing character, **3.52** (9-CO₂Me) → **3.51** (9-CN), both oxidation and reduction potential decrease from 0.34 V in **3.52** to 0.30 V in **3.51** for the oxidation potential $E_{1/2}^{0/+1}$ and from -0.67 V in **3.52** to -0.76 V in **3.51** for the reduction potential $E_{1/2}^{-1/0}$. By increasing the electron withdrawing character of the C(10) substituent, the α -HOMO decreases by 0.29 eV (from -4.85 eV for **3.56** to -5.14 eV for **3.53**) whereas it was increased in C(9) substituents by 0.04 eV (from -5.10 eV for **3.52** to -5.06 eV for **3.51**) and the β -LUMO follow the same trend and increased by 0.08 eV (from -4.24 eV for **3.52** to -4.16 eV for **3.51**).

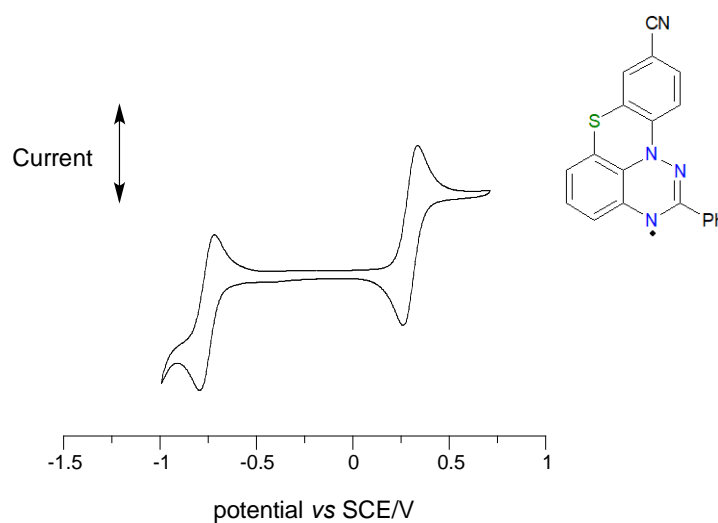


Figure 3.32. Cyclic voltammogram of **3.51** in CH₂Cl₂.

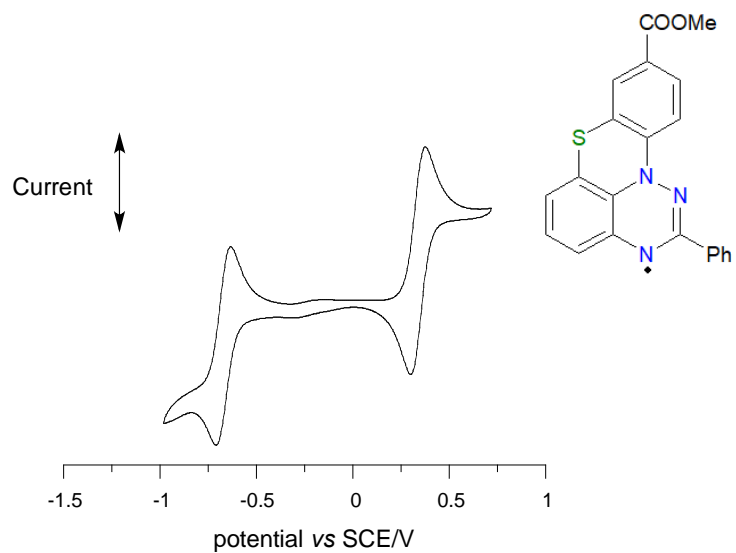


Figure 3.33. Cyclic voltammogram of **3.52** in CH_2Cl_2 .

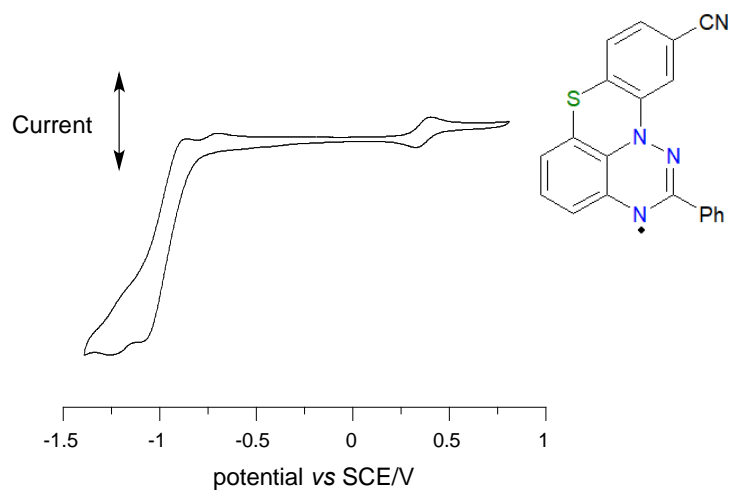


Figure 3.34. Cyclic voltammogram of **3.53** in CH_2Cl_2 .

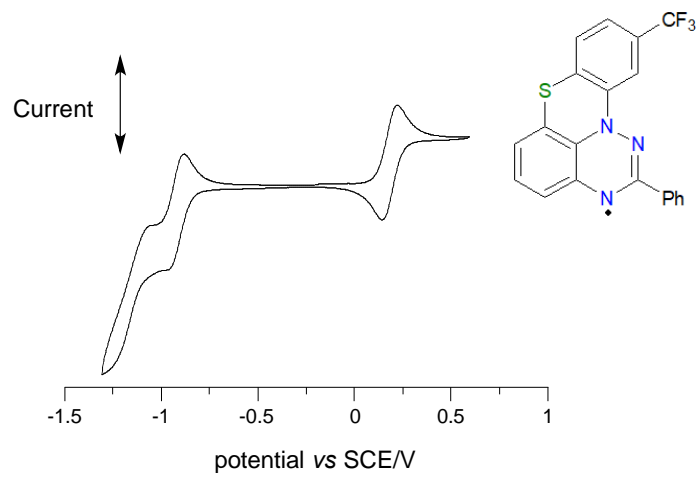


Figure 3.35. Cyclic voltammogram of **3.54** in CH_2Cl_2 .

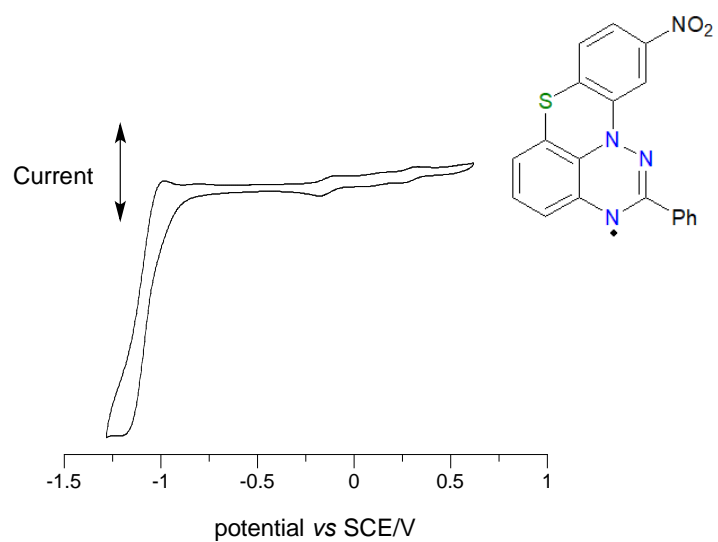
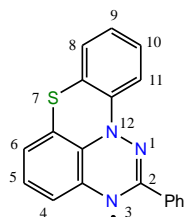


Figure 3.36. Cyclic voltammogram of **3.55** in CH_2Cl_2 .

3.2.2.1.3. Electron paramagnetic resonance spectroscopy (EPR)

The distribution of spin density in radicals was assessed with electron paramagnetic resonance spectroscopy. EPR spectra for radicals were recorded on an X-band EMX-Nano EPR spectrometer at ambient temperature on dilute and degassed solutions in distilled benzene in a concentration range of $2\text{-}5 \times 10^{-4}$ M. The microwave power was set with the Power Sweep program below the saturation of the signal, modulation frequency of 100 kHz, modulation amplitude of 0.5 G_{pp} and spectral width of 100 G. Accurate g -values were obtained using TEMPO as EMX-Nano internal standard. Simulations of the spectra were performed with the EMX-Nano software using DFT results (*vide infra*) as the starting point including all nitrogen and up to 4 hydrogen atoms. The resulting $hfcc$ values were perturbed several times until a global minimum for the fit was achieved. Experimental and simulated spectra are shown in Figures 3.37-3.41 and resulting $hfcc$ are listed in Table 3.10.

Table 3.10. Summary of hyperfine coupling constants (G) for radicals



Compound	a_{N12}^a	a_{N1}^a	a_{N3}^a	a_H	a_H	a_H	a_H	g^b
parent <i>S</i> - <i>peri</i> -annulated ^c	7.54	4.47	4.49	1.18	0.76	0.74	0.72	2.0039
3.51 (9-CN)	6.41	4.52	4.52	-1.40	1.40	1.40	1.40	2.0041
3.52 (9-CO₂Me)	6.62	4.47	4.47	-1.37	1.37	1.37	1.37	2.0041
3.53 (10-CN)	6.82	4.57	4.57	-0.76	1.40	1.70	1.70	2.0040
3.54 (10-CF₃)	6.93	4.54	4.54	-0.62	1.40	1.68	1.68	2.0040
3.55 (10-NO₂)	7.67	3.94	4.31	-1.66	0.97	1.23	0.70	2.0045
3.56 (10-CO₂Me)^d	7.08	4.44	4.52	1.78	1.47	1.36	0.74	2.0043

^aAssignments follow the previous EPR and ENDOR studies on ¹⁵N-labeled derivatives (ref⁹).

^bReferenced to TEMPO as the internal standard. ^{c,d}Ref²⁶

EPR spectra of radicals revealed a typical complex pattern of signals resulting from splitting with three ^{14}N nuclei modulated with additional smaller splitting by ^1H nuclei, as shown in Figures 3.37-3.41. The analysis of the a_{N} hyperfine coupling constant (hfcc) for the series is consistent with those for *S-peri*-annulated Blatter radical^{1,26} (Table 3.10) and are in the range of ~ 6.4 to 7.6 G for $a_{\text{N}(12)}$ and ~ 3.9 to 4.5 G for $a_{\text{N}(1)}$ and ~ 4.3 to 4.5 G for $a_{\text{N}(3)}$.

Analysis of the results indicates that by increasing of the electron withdrawing character of the C(10) substituent, *S-peri*-annulated (H) \rightarrow **3.56** (10-CO₂Me) \rightarrow **3.54** (10-CF₃) \rightarrow **3.53** (10-CN), the $a_{\text{N}(12)}$ value decreases from 7.54 to 6.82 G, while the sum of $a_{\text{N}(1)}$ and $a_{\text{N}(3)}$ increases. This is consistent with the instability of the dipolar resonance form in the triazine ring required for spin density delocalization onto the "upper" benzene ring. So, the C(10) substituted radicals exhibit slightly lower spin delocalization than the parent (*S-peri*-annulated), with least delocalization for **3.53** (10-CN).

The same results are obtained for the C(9) substituent and indicates that by increasing of the electron withdrawing character of the C(10) substituent, parent *S-peri*-annulated (H) \rightarrow **3.52** (9-CO₂Me) \rightarrow **3.51** (9-CN), the $a_{\text{N}(12)}$ value decreases from 7.54 to 6.41 G, while the sum of $a_{\text{N}(1)}$ and $a_{\text{N}(3)}$ increases.

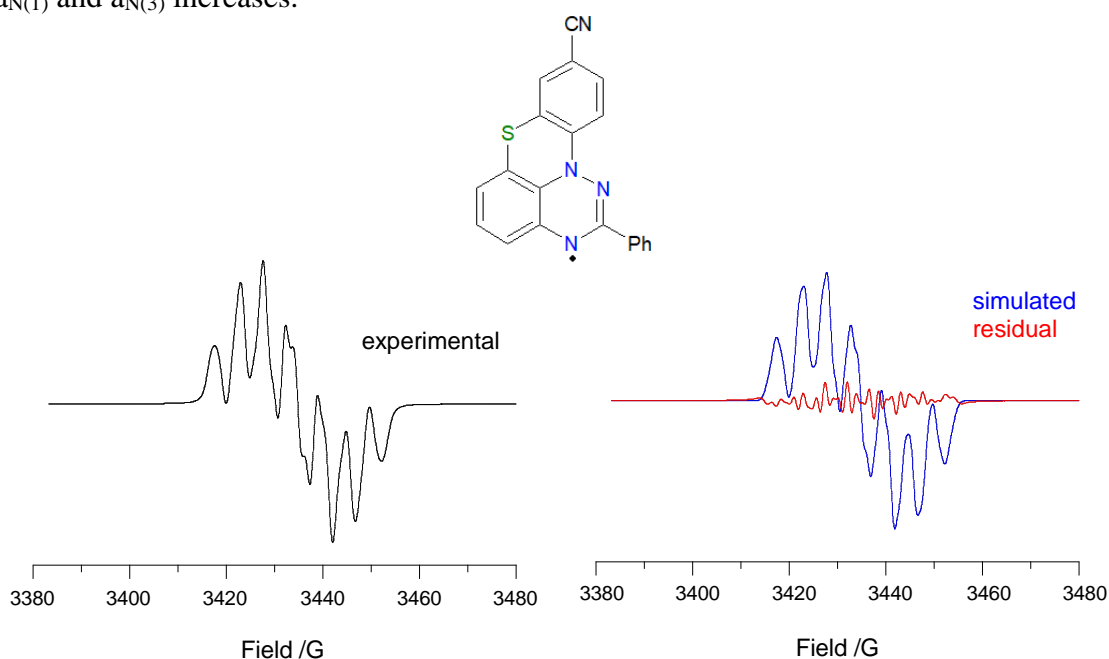


Figure 3.37. Experimental (black, left), simulated (blue, right) and difference (red, right) spectra for **3.51** recorded in benzene at *ca* 20 °C.

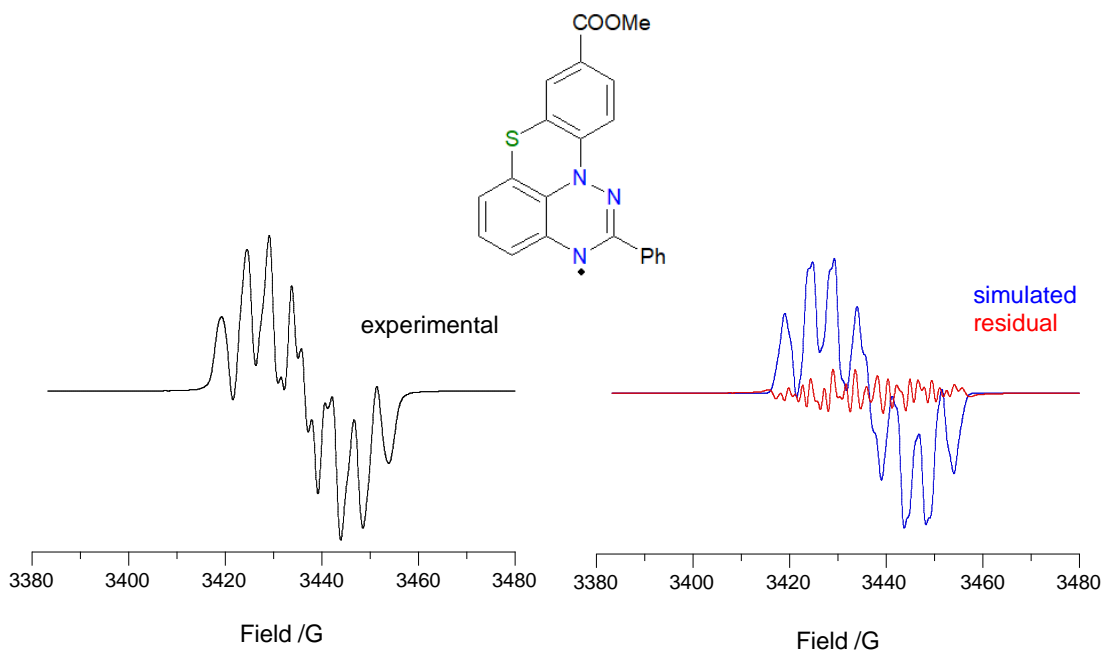


Figure 3.38. Experimental (black, left), simulated (blue, right) and difference (red, right) spectra for **3.52** recorded in benzene at *ca* 20 °C.

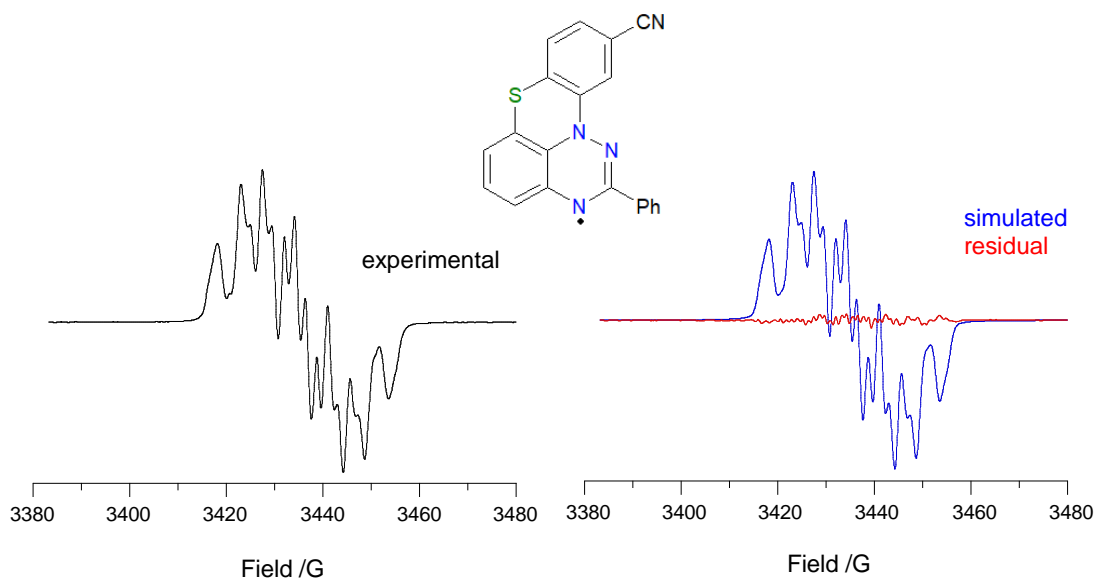


Figure 3.39. Experimental (black, left), simulated (blue, right) and difference (red, right) spectra for **3.53** recorded in benzene at *ca* 20 °C.

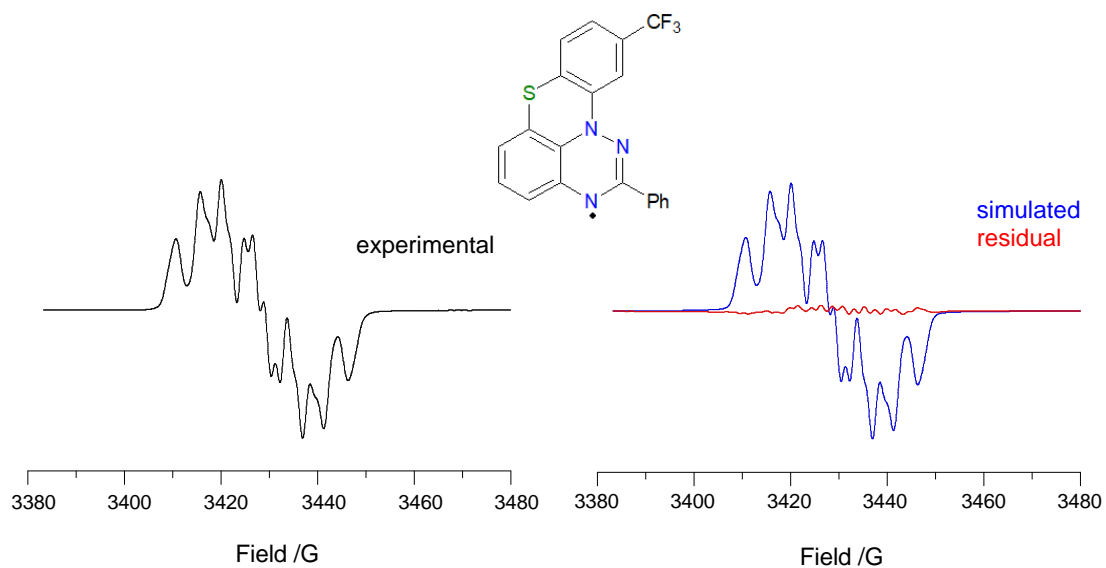


Figure 3.40. Experimental (black, left), simulated (blue, right) and difference (red, right) spectra for **3.54** recorded in benzene at *ca* 20 °C.

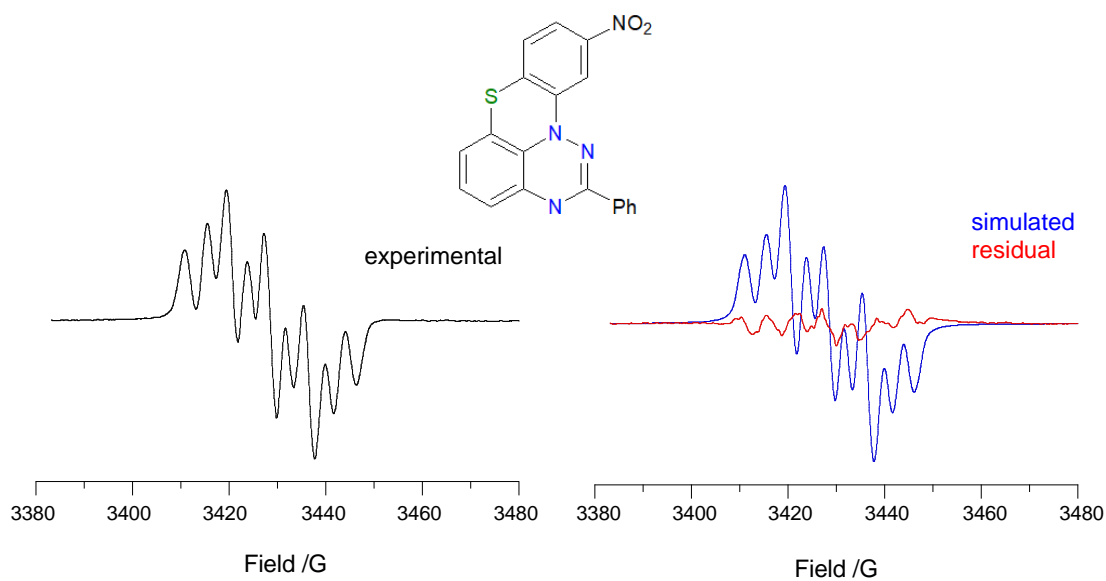


Figure 3.41. Experimental (black, left), simulated (blue, right) and difference (red, right) spectra for **3.55** recorded in benzene at *ca* 20 °C.

3.3. Summary and conclusions

Blatter radicals stand out for their exceptional stability, spin delocalization, low excitation energies and interesting electrochemical and photophysical properties, such as favorable redox behavior with a narrow electrochemical window (~1.2 V) and a broad absorption in the visible range.

In the first part of the Thesis, we described the development of a new class of paramagnetic nanographenes, in which the [1,2,4]triazinyl is docked to a polycyclic aromatic compounds to provide maximum spin delocalization, and to understand their structure-property relationships. We expected to have greater spin delocalization and greater control of the electronic properties of the [1,2,4]triazinyl-based radicals due to ring fusion at the *e* and *f* edges of [1,2,4]triazin-4-yl and planarization of the entire structure. We anticipated to observe bathochromic shift to the near-IR region of the electronic absorption spectra and anodic shift of the reduction potential in the synthesized derivatives of Blatter radicals.

Radicals in the first part of the project, undergo slow decomposition in solutions. Spectroscopic (UV-vis and EPR) and electrochemical methods and high-resolution mass spectrometry (HRMS) measurements for the final products indeed confirmed the formation of the radicals. However, for some radicals, it was not possible to obtain good quality data due to their low stability. Direct recrystallization of the reaction mixture also failed to give the pure product. Radical **3.21** was the most stable radical however it was not possible to keep it at room temperature and in the present of light.

As expected, analysis of data from electronic absorption spectroscopy (UV-vis) reveals that the size of the rings at the C(5)-C(7) positions of the Blatter radical, have some, albeit modest, effects on the electronic absorption energy of the molecules. Thus, fusing more aromatic rings at the *e* edge of [1,2,4]triazin-4-yl results in higher intensity of the absorption bands in the visible range, and a bathochromic shift of the absorption maximum. Among the radicals, **3.20** (the phenanthrene analogue) shows the most significant bathochromic shift.

Cyclic voltammetry measurements revealed that the oxidation and reduction are not reversible processes for the radicals, which indicates that they contained impurities such as decomposition products. Results show that, the extension of the π system in the radicals **3.18** (naphthalene analogue) \rightarrow **3.20** (phenanthrene analogue) \rightarrow **3.21** (pyrene analogue), does not have effect on the oxidation potential and HOMO.

As predicted, EPR spectra of the radicals show the value for $a_{N(4)}$ for all radicals slightly decreases relative to the Blatter radical especially in **3.20** (phenanthrene analogue), reflecting the increasing delocalization of the spin from the [1,2,4]triazinyl ring.

In the part of synthesis of ring expanded planar Blatter radicals through cyclization, electron paramagnetic resonance spectroscopy (EPR) was done, and analysis of the results indicates that by connecting of two aromatic parts of the structure and planarize the structure of the molecule, the spin is delocalized.

The second part of this Thesis, presents preparative routes to five new derivatives of functionalized *S-peri*-annulated benzo[*e*][1,2,4]triazinyl containing CO₂Me, CN, CF₃ and NO₂ groups at the C(10) or C(9) positions through the TMS₃SiH-assisted cyclization of aryl iodides.

Analysis of data from electronic absorption spectroscopy (UV-vis) reveals that, substitution at the C(10) position (CN, CO₂Me, CF₃, NO₂) shifts the maximum of the lowest energy absorption band in the *S-peri*-annulated radicals to lower energies or higher wavelengths and leads to more bathochromic shift of the absorption maximum as we expected with the largest shift for the CF₃ derivative **3.54**.

Cyclic voltammetry measurements revealed that oxidation and reduction processes are reversible redox processes only for radicals **3.51** and **3.52**, which indicate that they were not pure during measurements. Most likely they are contaminated with decomposition products. Cyclic voltammetry measurements showed that by increasing the electron withdrawing character of the C(10) substituent, the oxidation potentials systematically increase. However, for C(9) substituted radicals both oxidation and reduction potential decrease.

EPR spectra of radicals in benzene solutions revealed that C(10) substituted radicals exhibit slightly lower spin delocalization than the parent (*S-peri*-annulated), with least delocalization for **3.53** (10-CN). This is consistent with the instability of the dipolar resonance form in the triazine ring required for spin density delocalization onto the "upper" benzene ring.

3.4. References

- (1) Kaszyński, P.; Constantinides, C. P.; Young Jr, V. G. *Angewandte Chemie International Edition*. **2016**, 55(37), 11149-11152.
- (2) Nagy, J.; Nyitrai, J.; Kolonits, P.; Lempert, K.; Gergely, A.; Párkányi, L.; Kálmán, A. *Journal of the Chemical Society, Perkin Transactions 1*. **1988**, (12), 3267-3274.
- (3) Liu, M.; Li, X. L.; Chen, D. C.; Xie, Z.; Cai, X.; Xie, G.; Cao, Y. *Advanced Functional Materials*. **2015**, 25(32), 5190-5198.
- (4) Bachman, G. B.; Welton, D. E.; Jenkins, G. L.; Christian, J. E. *Journal of the American Chemical Society*. **1947**, 69(2), 365-371.
- (5) Van Galen, P. J.; Nissen, P.; Van Wijngaarden, I.; Ijzerman, A. P.; Soudijn, W. *Journal of Medicinal Chemistry*. **1991**, 34(3), 1202-1206.
- (6) Constantinides, C. P.; Obijalska, E.; Kaszynski, P. *Organic Letters*. **2016**, 18(5), 916-919.
- (7) Gardias, A.; Kaszyński, P.; Obijalska, E.; Trzybiński, D.; Domagała, S.; Woźniak, K.; Szczytko, J. *Chemistry—A European Journal*. **2018**, 24(6), 1317-1329.
- (8) Connelly, N. G.; Geiger, W. E. *Chem. Rev.* **1996**, 96, 877–910.
- (9) Neugebauer, F. A.; Rimmler, G. *Magnetic Resonance in Chemistry*. **1988**, 26(7), 595-600.
- (10) Bartos, P.; Young Jr, V. G.; Kaszynski, P. *Organic Letters*. **2020**, 22(10), 3835-3840.
- (11) Liu, M.; Li, X. L.; Chen, D. C.; Xie, Z.; Cai, X.; Xie, G.; Cao, Y. *Advanced Functional Materials*. **2015**, 25(32), 5190-5198.
- (12) Zhao, K.; Long, G.; Liu, W.; Li, D. S.; Gao, W.; Zhang, Q. *The Journal of Organic Chemistry*. **2019**, 85(1), 291-295.
- (13) Fell, J. B.; Fischer, J. P.; Baer, B. R.; Blake, J. F.; Bouhana, K.; Briere, D. M.; Marx, M. A. *Journal of Medicinal Chemistry*. **2020**, 63(13), 6679-6693.
- (14) Anuradha, V.; Srinivas, P. V.; Aparna, P.; Rao, J. M. *Tetrahedron Letters*. **2006**, 47(28), 4933-4935.
- (15) Hellwinkel, D.; Krapp, W. *Chemische Berichte*. **1977**, 110(2), 693-702.

- (16) Ganguly, N. C.; Dutta, S.; Datta, M.; De, P. *Journal of Chemical Research*. **2005**, 2005(11), 733-735.
- (17) Jasinski, M.; Szczytko, J.; Pocięcha, D.; Monobe, H.; Kaszynski, P. *Journal of the American Chemical Society*. **2016**, 138(30), 9421-9424.
- (18) Sawhney, S. N.; & Boykin, D. W. *The Journal of Organic Chemistry*. **1979**, 44(7), 1136-1142.
- (19) Gong, S.; Chang, Y. L.; Wu, K.; White, R.; Lu, Z. H.; Song, D.; Yang. *Chemistry of Materials*. **2014**, 26(3), 1463-1470.
- (20) Okamoto, H.; Wu, J.; Morita, Y.; Takenaka, S. *Bulletin of the Chemical Society of Japan*. **2002**, 75(1), 175-179.
- (21) Khansole, S. V.; Mokle, S. S.; Sayyed, M. A.; Vibhute, Y. B. *Journal of the Chinese Chemical Society*. **2008**, 55(4), 871-874.
- (22) Still, I. W.; Sayeed, V. A. *Synthetic Communications*. **1983**, 13(14), 1181-1192.
- (23) Xing, B.; Ni, C.; Hu, J. *Angewandte Chemie International Edition*. **2018**, 57(31), 9896-9900.
- (24) Allen, C. F. H.; MacKay, D. D. *Organic Syntheses*. **1943**, 2, 580.
- (25) Zhao, K.; Long, G.; Liu, W.; Li, D. S.; Gao, W.; Zhang, Q. *The Journal of Organic Chemistry*. **2019**, 85(1), 291-295.
- (26) Bartos, P.; Celeda, M.; Pietrzak, A.; Kaszyński, P. *Organic Chemistry Frontiers*. **2022**, 9(4), 929-938.
- (27) Bartos, P.; Anand, B.; Pietrzak, A.; Kaszynski, P. *Organic Letters*. **2019**, 22(1), 180-184.
- (28) Bartos, P.; Hande, A. A.; Pietrzak, A.; Chrostowska, A.; Kaszyński, P. *New Journal of Chemistry*. **2021**, 45(48), 22876-22887.
- (29) Zissimou, G. A.; Bartos, P.; Pietrzak, A.; Kaszyński, P. *The Journal of Organic Chemistry*. **2022**, 87(7), 4829-4837.
- (30) Shivakumar, K. I.; Pocięcha, D.; Szczytko, J.; Kapuściński, S.; Monobe, H.; Kaszyński, P. *Journal of Materials Chemistry C*. **2020**, 8(3), 1083-1088.
- (31) Noland, W. E.; Narina, V. S.; Britton, D. *Journal of Chemical Research*. **2011**, 35(12), 694-697.

- (32) Fujita, H.; Jing, H.; Kraymer, M.; Allu, S.; Veeraraghavaiah, G.; Wu, Z.; Lindsey, J. S. *New Journal of Chemistry*. **2019**, 43(19), 7209-7232.
- (33) Gupta, S.; Chaudhary, P.; Seva, L.; Sabiah, S.; Kandasamy, J. *RSC Advances*. **2015**, 5(108), 89133-89138.
- (34) Lang, R. C.; Williams, C. M.; & Garson, M. J. *Organic Preparations and Procedures International*. **2003**, 35(5), 520-524.
- (35) Malik, J. K.; Noolvi, M. N.; Manvi, F. V.; Nanjwade, B. K.; Patel, H. M.; Manjula, S. N.; & Barve, A. *Letters in Drug Design and Discovery*. **2011**, 8(8), 717-724.
- (36) Vaidyanathan, G.; Affleck, D. J.; & Zalutsky, M. R. *Journal of Medicinal Chemistry*. **1994**, 37(21), 3655-3662.
- (37) Drennhaus, T.; Leifert, D.; Lammert, J.; Drennhaus, J. P.; Bergander, K.; Daniliuc, C. G.; & Studer, A. *Journal of the American Chemical Society*. **2023**, 145(15), 8665-8676.
- (38) Wescott, L. D.; & Mattern, D. L. *The Journal of Organic Chemistry*. **2003**, 68(26), 10058-10066.

4. Experimental part

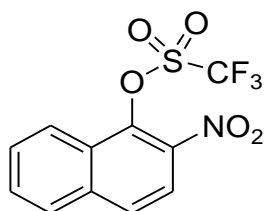
4.1. General information

Commercially available reagents and solvents were used. NMR spectra were obtained at 600 MHz (^1H), 151 MHz (^{13}C) in CDCl_3 and referenced to the solvent ($\delta = 7.26$ ppm for ^1H and $\delta = 77.16$ ppm for ^{13}C) or in $\text{DMSO}-d_6$ and referenced to the solvent ($\delta = 2.50$ ppm for ^1H and $\delta = 39.52$ ppm for ^{13}C). Nexus FT-IR Thermo Nicolet IR spectrometer in KBr tablets and on a Bruker Alpha ATR spectrophotometer (neat) were used to record the IR spectra. PerkinElmer Lambda 45 spectrophotometer was used to detect UV spectra in CH_2Cl_2 . The uncorrected melting points were established using a Stuart SMP30 Advanced Digital Melting Point Apparatus. High-resolution mass spectrometry (HRMS) measurements were carried out utilizing a SYNAPT G2-Si High-Definition Mass Spectrometry equipped with an ESI or APCI source and Quantitative Time-of-Flight (QuanTof) mass analyzer. A 300 W halogen lamp (“Portable halogen Work Lamp” without the protecting front glass window) fitted with a T3 double-ended RSC base J118 light bulb was used for irradiations. An inert atmosphere (Ar gas) was used for the reactions, while reaction workups were conducted in air. Oil baths were used to provide heat for the processes that required high temperatures. Volatiles were evaporated under reduced pressure. Progress of the reaction mixtures and column eluents were monitored by TLC using aluminum-backed thin layer chromatography (TLC) plates (Merck Kieselgel 60 F254 or, where stated, Merck Al_2O_3 F254 neutral). For the chromatographic separation, silica gel 60 (70–230 μm) or, in the case of radicals, passivated silica gel 60 (35–70 μm) was used in column chromatography. Details of measuring electronic absorption spectra, EPR spectra and electrochemical redox potentials of radicals are listed in the discussion part.

4.2. Post-radical-generation ring-extended planar Blatter radicals

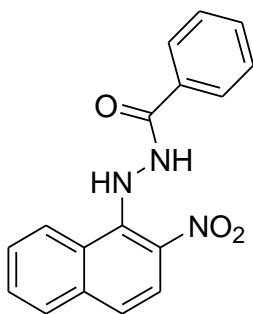
4.2.1. Synthesis of ring-fused [1,2,4]triazines

4.2.1.1. Preparation of 3-phenylnaphtho[2,1-*e*][1,2,4]triazine



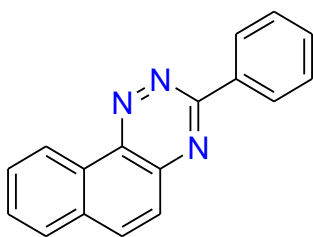
Trifluoromethanesulfonic acid 2-nitronaphthalen-1-yl ester (3.2).¹

To a solution of commercially available 2-nitro-1-naphthol (2.0 g, 10.30 mmol) and dry DCM, triethylamine (3 eq, 4.35 mL) was added and trifluoromethanesulfonic anhydride (1.5 eq, 2.6 mmol) was dropped into the reaction mixture at 0 °C. The mixture was stirred overnight at room temperature then poured into ice-water and organic phase was extracted by DCM two times. The combined organic phases were washed with brine and dried over anhydrous sodium sulfate. After the solvent was removal, the product was further purified by silica column using DCM as eluent to obtain product. 3.0 g (91% yield). Brown solid: mp 65-70 °C; ¹H NMR (600 MHz, CDCl₃) δ 8.27 (d, *J* = 8.1 Hz, 1H), 8.07 (d, *J* = 9.0 Hz, 1H), 7.99 (d, *J* = 8.7 Hz, 2H), 7.79 (p, *J* = 7.0 Hz, 2H); ¹³C{¹H} NMR (151 MHz, CDCl₃) δ 139.2, 138.1, 136.5, 130.6, 129.6, 129.3, 128.4, 126.7, 123.2, 121.8, 120.8, 119.6, 117.5, 115.4; IR (KBr) ν 1599, 1532, 1428, 1349, 1207, 1144, 1054, 958, 897, 810, 761, 614, 502, 420 cm⁻¹; HRMS (APCI) [M-H]⁻ *m/z* calcd for C₁₁H₅F₃NO₅S: 319.9841; found: 319.9835. Anal. Calcd for C₁₁H₆F₃NO₅S: C, 41.13; H, 1.88; N, 4.36; S, 9.98. Found: C, 41.16; H, 1.96; N, 4.61; S, 9.83.



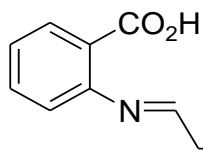
Benzoic acid *N'*-(2-nitronaphthalen-1-yl)-hydrazide (3.3).²

A mixture of compound **3.2** (50.0 mg, 0.155 mmol) and benzhydrazide (1 eq, 21.08 mg, 0.155 mmol) in DMSO (2 mL) stirred at room temperature under argon overnight. After completion of the reaction, the reaction mixture extracted with DCM and purified by 50% DCM/pet. ether on silica column to give pure product. Analytically pure samples were obtained by recrystallization typically from ethanol. 43.0 mg (90% yield). Yellow solid: mp 195-200 °C; ¹H NMR (600 MHz, DMSO-*d*₆) δ 11.03 (s, 1H), 9.32 (s, 1H), 8.74 (d, *J* = 8.5 Hz, 1H), 7.97 (d, *J* = 8.1 Hz, 1H), 7.88 (d, *J* = 9.1 Hz, 1H), 7.76 (d, *J* = 7.4 Hz, 2H), 7.69 (t, *J* = 7.4 Hz, 1H), 7.63 (t, *J* = 7.5 Hz, 1H), 7.55 (t, *J* = 9.1 Hz, 2H), 7.46 (t, *J* = 7.6 Hz, 2H); ¹³C{¹H} NMR (151 MHz, DMSO-*d*₆) δ 166.7, 142.8, 135.8, 134.7, 132.0, 131.9, 129.5, 128.5, 127.3, 126.5, 125.8, 125.0, 121.4, 120.6; IR (KBr) ν 3260, 1648, 1578, 1515, 1457, 1393, 1303, 1211, 1140, 1092, 1025, 903, 812, 761, 689 cm⁻¹; HRMS (ESI) [M-H]⁻ *m/z* calcd for C₁₇H₁₂N₃O₃: 306.0879; found: 306.0884. Anal. Calcd for C₁₇H₁₃N₃O₃: C, 66.44; H, 4.26; N, 13.67. Found: C, 66.30; H, 4.42; N, 13.52.

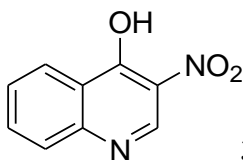


3-Phenylnaphtho[2,1-*e*][1,2,4]triazine (3.4).² To the solution of compound **3.3** (533.0 mg, 1.73 mmol) in warm acetic acid (10 mL), Tin powder (4.0 eq, 812 mg, 6.924 mmol) was added in one portion and the mixture was stirred at room temperature for 1 hour and then for 30 minutes at 65 °C. After cooling, it was poured into water, filtered through Cellite to remove tin, and washed well by AcOEt and organic phase was extracted with AcOEt. For neutralization of AcOH, water was added to the combined extracts and while stirring solid NaHCO₃ was added in portions. The organic layer was separated, and after drying over Na₂SO₄ and solvent removal a yellow solid was obtained which was dissolved in a DCM / MeOH mixture (1:1, 10 mL). NaIO₄ was added in one portion. The mixture was stirred for 30 minutes and then filtered and washed with DCM and the filtrate was evaporated. For purification, the resulting residue was passed through a SiO₂ plug by 20 % DCM in pet. ether and after removing the solvent, pure product formed and it was recrystallized by ethanol to give pure product. 295.0 mg (66% yield). Yellow solid: mp 135-140 °C; ¹H NMR (600 MHz, CDCl₃) δ 9.50 (d, *J* = 8.1 Hz, 1H), 8.77 (dt, *J*₁ = 8.4 Hz, *J*₂ = 2.3 Hz, 2H), 8.19 (d, *J* = 9.1 Hz, 1H), 7.93 (d, *J* = 7.8 Hz, 1H), 7.89 – 7.83 (m, 2H), 7.83 – 7.78 (m, 1H), 7.65 – 7.51 (m, 3H); ¹³C{¹H} NMR (151 MHz, CDCl₃) δ 161.4, 144.9, 143.1, 138.3, 135.7, 132.8, 131.5, 130.2, 129.4, 129.4, 129.0, 128.6, 125.8, 124.0; IR (KBr) ν 1599, 1518, 1434, 1384, 1276, 1219, 1160, 1048, 927, 849, 738, 689, 544 cm⁻¹; UV (CH₂Cl₂) λ_{max} (log ε) 226 (4.39), 294 (4.71), 361 (3.87), 378 (3.92), 430 (2.73) nm; HRMS (ESI) [M+H]⁺ *m/z* calcd for C₁₇H₁₂N₃: 258.1031; found: 258.1029. Anal. Calcd for C₁₇H₁₁N₃: C, 79.36; H, 4.31; N, 16.33. Found: C, 79.15; H, 4.27; N, 16.44.

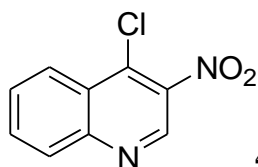
4.2.1.2. Synthesis of 3,5-diphenyl-[1,2,4]triazino[5,6-*c*]quinoline



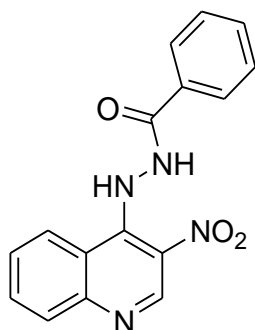
(E)-2-((2-Nitroethylidene)amino)benzoic acid (3.6).³ To a fresh solution of sodium hydroxide (30.0 g) in 60 mL of water, which had cooled to 47 °C, nitromethane (30.0 g, 492.0 mmol) was added dropwise at 25-45 °C. the color turned orange. The mixture was then warmed to 57 °C and then cooled to 5 °C. the mixture was nutralized with concentrated hydrochloric acid at 5-10 °C and then the resultant solution of methazonic acid filtered and dried by suction and immediately added to a filtered solution of commercially available anthranilic acid (30.671 g, 223.0 mmol) and 20 mL of concentrated hydrochloric acid in 500 mL of water and after 10 min, put it in refrigerator overnight. The solution filtered and washed with water repeatedly until filtered was nutral. The solid was allowed to dry at room temperature in vacum until to be a dry powder. 20.0 g (43% yield) from 30.67 g of substrate (anthranilic acid). Bright yellow microneedles: mp 185-186 °C; ¹H NMR (600 MHz, DMSO-*d*₆) δ 13.04 (d, *J* = 13.6 Hz, 1H), 8.07 – 7.99 (m, 2H), 7.72 (d, *J* = 8.3 Hz, 1H), 7.69 – 7.64 (m, 1H), 7.27 – 7.20 (m, 1H), 6.75 (d, *J* = 6.2 Hz, 1H); ¹³C{¹H} NMR (151 MHz, DMSO-*d*₆) δ 168.5, 140.8, 137.7, 134.5, 131.7, 123.5, 116.7, 115.3, 113.5; IR (KBr) ν 2833, 1634, 1474, 1371, 1262, 1205, 1155, 962, 919, 756, 696, 528 cm⁻¹; HRMS (ESI) [M+H]⁺ *m/z* calcd for C₉H₉N₂O₄: 209.0562; found: 209.0564. Anal. Calcd for C₉H₈N₂O₄: C, 52.69; H, 2.46; N, 13.66. Found: C, 52.39; H, 4.04; N, 12.73.



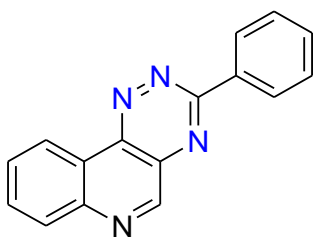
3-Nitroquinolin-4-ol (3.7).³ A mixture of compound **3.6** (19.5 g, 93.75 mmol) and technical acetic anhydride (93.6 mL) stirred and heated to 100-105 °C in a 3-necked flask with thermometer and reflux condenser until a clear solution was obtained. After stopping the heating, sodium acetate (7.68 g, 658.28 mmol) was added rapidly with stirring. The temperature rose to 134-138 °C and after five to ten min it began to fall and at this time external heat was applied at 140 °C and the mixture was refluxed overnight. After cooling to room temperature the mixture was filtered off and washed with glacial acetic acid until the washings were colorless, then water was added, filtered again and washed repeatedly with water and dried. 4.35 g (24% yield). Tan needles: mp 348-350 °C; ¹H NMR (600 MHz, DMSO-*d*₆) δ 13.01 (s, 1H), 9.19 (s, 1H), 8.25 (d, *J* = 8.0 Hz, 1H), 7.79 (t, *J* = 7.5 Hz, 1H), 7.72 (d, *J* = 8.2 Hz, 1H), 7.51 (t, *J* = 7.5 Hz, 1H); ¹³C{¹H} NMR (151 MHz, DMSO-*d*₆) δ 167.7, 142.4, 138.3, 133.2, 130.9, 128.1, 126.0, 125.8, 119.5; IR (KBr) ν 2900, 2842, 1952, 1630, 1542, 1493, 1343, 1204, 860, 758, 678, 608, 498, 415 cm⁻¹; HRMS (ESI) [M+H]⁺ *m/z* calcd for C₉H₇N₂O₃: 191.0457; found: 191.0457; Anal. Calcd for C₉H₆N₂O₃: C, 56.84; H, 3.18; N, 14.73. Found: C, 57.02; H, 3.12; N, 14.94.



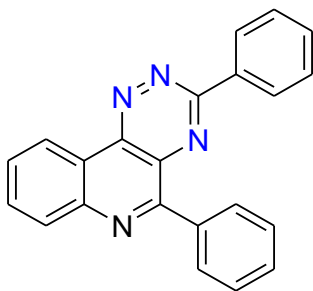
4-Chloro-3-nitroquinoline (3.8).⁴ A mixture of compound **3.7** (4.35 g, 31.861 mmol) and phosphorus oxychloride (12 mL, 130.0 mmol) was treated with PCl₅ (4.816 g, 20.0 mmol) with gradually stirring and heating during 40 min to 90 °C then refluxed at 110-112 °C for overnight. After cooling in an ice bath, volatiles were removed in vacuo and the residue which was dark yellow was taken up in DCM. This solution was slowly poured into mixture of ice and NH₄OH and then filtered to remove insoluble substrate. The organic layer was removed and combined with two additional DCM extracts of the aqueous layer and after drying over Na₂SO₄ and solvent removal, pure product formed. 3.88 g (58 % yield). Light yellow crystals: mp 328-330 °C; ¹H NMR (600 MHz, CDCl₃) δ 9.26 (s, 1H), 8.48 – 8.40 (m, 1H), 8.22 (d, *J* = 8.4 Hz, 1H), 8.01 – 7.91 (m, 1H), 7.83 (dd, *J*₁ = 11.4 Hz, *J*₂ = 4.0 Hz, 1H); ¹³C{¹H} NMR (151 MHz, DMSO-*d*₆) δ 167.7, 142.2, 138.3, 133.2, 130.9, 128.0, 126.0, 125.9, 119.5; IR (KBr) ν 2850, 1975, 1627, 1540, 1493, 1355, 1203, 1016, 879, 758, 678, 605, 496, 413 cm⁻¹; HRMS (ESI) [M+H]⁺ *m/z* calcd for C₉H₆ClN₂O₂: 209.0118; found: 209.0122. Anal. Calcd for C₉H₅ClN₂O₂: C, 51.82; H, 2.42; N, 13.43. Found: C, 50.33; H, 2.61; N, 12.83.



N'-(3-Nitroquinolin-4-yl)benzohydrazide (3.9).² It was obtained from compound **3.8** as the same as procedure for synthesis the compound **3.3**. 4.342 g (93% yield) from 3.0 g of substrate (4-chloro-3-nitroquinoline). Yellow solid: mp 228-229 °C; ¹H NMR (600 MHz, DMSO-*d*₆) δ 9.29 (s, 1H), 8.86 (s, 1H), 8.06 – 7.97 (m, 2H), 7.84 (d, *J* = 7.6 Hz, 2H), 7.78 (t, *J* = 7.6 Hz, 1H), 7.62 (t, *J* = 7.4 Hz, 1H), 7.54 (t, *J* = 7.6 Hz, 2H); ¹³C{¹H} NMR (151 MHz, DMSO-*d*₆) δ 168.0, 166.2, 142.4, 138.4, 133.5, 133.1, 131.0, 130.5, 129.0, 128.9, 128.2, 127.9, 127.7, 126.1, 119.7; IR (KBr) ν 3100, 3007, 2944, 2796, 1987, 1687, 1595, 1526, 1348, 1265, 1077, 1023, 880, 840, 754, 690, 608, 532, 445 cm⁻¹; HRMS (ESI) [M+H]⁺ *m/z* calcd for C₁₆H₁₃N₄O₃: 309.0988; found: 309.0991. Anal. Calcd for C₁₆H₁₂N₄O₃: C, 62.33; H, 3.92; N, 18.17. Found: C, 56.69; H, 3.88; N, 16.60.



3-Phenyl-[1,2,4]triazino[5,6-*c*]quinoline (3.10).² It was obtained from compound **3.9** like the procedure for synthesis the triazine **3.4**. 1.027 g (30% yield) from 4.22 g of substrate (*N'*-(3-nitroquinolin-4-yl)benzohydrazide). Orange needles: mp 204-205 °C; ¹H NMR (600 MHz, CDCl₃) δ 9.56 (s, 1H), 9.36 (dd, *J*₁ = 8.0 Hz, *J*₂ = 1.3 Hz, 1H), 8.74 (dd, *J*₁ = 6.7 Hz, *J*₂ = 3.0 Hz, 2H), 8.26 (d, *J* = 8.1 Hz, 1H), 7.97 – 7.93 (m, 1H), 7.92 – 7.87 (m, 1H), 7.63 – 7.53 (m, 3H); ¹³C{¹H} NMR (151 MHz, CDCl₃) δ 162.7, 154.8, 145.8, 144.6, 134.8, 134.6, 132.2, 132.0, 130.3, 129.9, 129.2, 128.7, 123.2, 121.7; IR (KBr) ν 1607, 1509, 1419, 1376, 1271, 1120, 1004, 931, 853, 766, 688, 563 cm⁻¹; UV (CH₂Cl₂) λ_{max} (log ε) 228 (4.37), 255 (4.09), 295 (4.67), 372 (3.71), 469 (2.49) nm; HRMS (ESI) [M+H]⁺ *m/z* calcd for C₁₆H₁₁N₄: 259.0984; found: 259.0988. Anal. Calcd for C₁₆H₁₀N₄: C, 74.40; H, 3.90; N, 21.69. Found: C, 74.53; H, 3.92; N, 21.80.

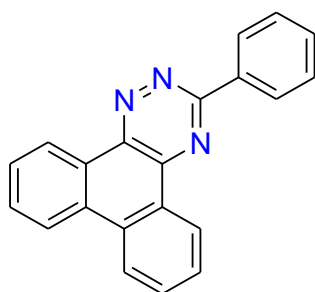


3,5-Diphenyl-[1,2,4]triazino[5,6-*c*]quinoline (3.11).⁵ It was obtained from triazine **3.10** as the same as procedure for synthesis the radicals. Analytically pure samples were obtained by recrystallization typically from MeCN. 35 mg (27% yield) from 100 mg of substrate (3-phenyl-[1,2,4]triazino[5,6-*c*]quinoline). Orange needles: mp 195-200 °C; ¹H NMR (600 MHz, CDCl₃) δ 9.40 (dd, *J*₁ = 8.0 Hz, *J*₂ = 1.0 Hz, 1H), 8.77 – 8.64 (m, 2H), 8.40 – 8.29 (m, 3H), 8.02 – 7.93 (m, 1H), 7.93 – 7.84 (m, 1H), 7.67 – 7.61 (m, 3H), 7.59 (dd, *J*₁ = 6.5 Hz, *J*₂ = 3.4 Hz, 3H); ¹³C{¹H} NMR (151 MHz, CDCl₃) δ 161.8, 160.0, 145.4, 145.2, 136.4, 135.0, 134.2, 132.2, 132.1, 131.2, 130.4, 130.3, 129.4, 129.2, 128.8, 128.4, 123.1, 121.6; IR (KBr) ν 2918, 2851, 2094, 1736, 1606, 1558, 1502, 1457, 1408, 1304, 1326, 1267, 1222, 1159, 1114, 1073, 1039, 976, 928, 767, 711, 682 cm⁻¹; UV (CH₂Cl₂) λ_{max} (log ε) 255 (3.75), 303 (3.81), 379 (3.14), 437 (1.73) nm; HRMS (ESI) [M+H]⁺ *m/z* calcd for C₂₂H₁₅N₄: 335.1297; found: 335.1299. Anal. Calcd for C₂₂H₁₄N₄: C, 79.02; H, 4.22; N, 16.76. Found: C, 79.01; H, 4.43; N, 16.89.

4.2.1.3. Synthesis of ring-fused [1,2,4]triazines through the diketones

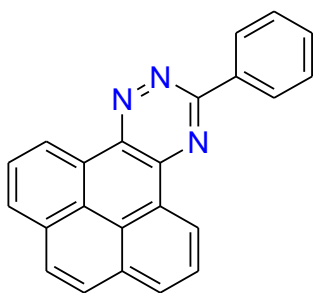
General procedure for synthesis of the [1,2,4]triazines (3.13, 3.15, 3.17)⁶

To ice-cooled solution of stirred benzonitrile (0.1 mol, 10.3 g) in dry MeOH (5.0 g), dry gaseous HCl was bubbled until the substrate was finished. The mixture was left at fridge overnight and then poured into Et₂O (100 mL). Colorless crystals were collected and washed with two Et₂O (30 mL) portions. Saturated aqueous NaHCO₃ was added to the solution of obtained crystals in DCM (20 mL) until to be neutralized. The organic layer was separated and aqueous phase was extracted with DCM (50 mL). The combined organic phases were dried over Na₂SO₄ and evaporated to dryness and hydrazine hydrate (1.04 mL, 20.98 mol) was added dropwisely to an ice-cooled stirred solution of the product (3.086 g, 22.83 mmol) in iPrOH (30 mL). The mixture was stirred for 1 hour under gradual cooling to room temperature and then at room temperature overnight. The residue after evaporation of volatiles was treated with Et₂O (50 mL) and cooled in ice. Crystals were filtered off and dried in vacuo and immediately used for the next step. A suspension of diketones (1 mmol) in dry methanol (5 mL) was added to a solution of benzamidrazone (1.5 mmol) in dry methanol under argon and stirred at room temperature. After 30 minutes the reaction mixture was precipitated and was filtered off, and washed with methanol to give the pure product.

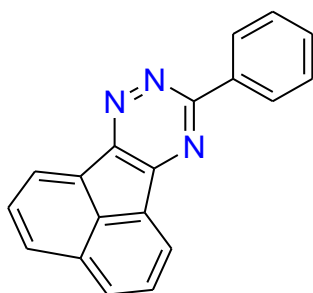


3-Phenylphenanthro[9,10-*e*][1,2,4]triazine (3.13).

1.150 g (86 % yield) from 905.7 mg of phenanthrene-9,10-dione (3.12). Yellow powder: mp 175-180 °C; ¹H NMR (600 MHz, CDCl₃) δ 9.41 (d, *J* = 7.8 Hz, 1H), 9.29 (d, *J* = 7.9 Hz, 1H), 8.87 – 8.79 (m, 2H), 8.48 (d, *J* = 8.0 Hz, 2H), 7.85 – 7.73 (m, 3H), 7.70 (t, *J* = 7.5 Hz, 1H), 7.66 – 7.57 (m, 3H); ¹³C{¹H} NMR (151 MHz, CDCl₃) δ 161.3, 144.8, 143.0, 135.8, 133.9, 132.4, 131.5, 131.0, 130.7, 129.0, 128.7, 128.5, 128.2, 128.1, 127.7, 126.6, 124.9, 123.1, 123.1; IR (KBr) ν 1607, 1508, 1448, 1408, 1369, 1279, 1167, 1080, 960, 870, 758, 690, 541, 431 cm⁻¹; UV (CH₂Cl₂) λ_{max} (log ε) 260 (3.95), 303 (3.66), 358 (3.16), 425 (1.98) nm; HRMS (ESI) [M+H]⁺ *m/z* calcd for C₂₁H₁₄N₃: 308.1188; found: 308.1191. Anal. Calcd for C₂₁H₁₃N₃: C, 82.06; H, 4.26; N, 13.67. Found: C, 82.16; H, 4.26; N, 13.49.



3-Phenylpyreno[9,10-*e*][1,2,4]triazine (3.15). 800.0 mg (73 % yield) from 760.0 mg of pyrene-4,5-dione (**3.14**). Yellow solid: mp 246-247 °C; ¹H NMR (600 MHz, CDCl₃) δ 9.58 (dd, *J*₁ = 7.6 Hz, *J*₂ = 0.9 Hz, 1H), 9.48 (dd, *J*₁ = 7.6 Hz, *J*₂ = 0.9 Hz, 1H), 8.89 (dt, *J*₁ = 8.4 Hz, *J*₂ = 2.1 Hz, 2H), 8.28 (dd, *J*₁ = 19.3 Hz, *J*₂ = 7.6 Hz, 2H), 8.10 (t, *J* = 7.7 Hz, 1H), 8.04 (t, *J* = 7.6 Hz, 1H), 7.98 (q, *J* = 8.9 Hz, 2H), 7.70 – 7.58 (m, 3H); ¹³C{¹H} NMR (151 MHz, CDCl₃) δ 161.6, 145.7, 144.0, 135.8, 131.6, 131.4, 131.3, 131.1, 129.4, 129.1, 128.6, 127.7, 127.5, 127.3, 127.3, 127.2, 126.9, 126.8, 125.2, 124.6, 122.6; IR (KBr) ν 3049, 1625, 1492, 1444, 1364, 1294, 1228, 1175, 1053, 928, 831, 769, 697 cm⁻¹; UV (CH₂Cl₂) λ_{max} (log ε) 239 (3.71), 287 (3.51), 333 (3.26), 348 (3.27), 408 (2.66), 426 (2.64) nm; HRMS (ESI) [M+H]⁺ *m/z* calcd for C₂₃H₁₄N₃: 332.1188; found: 332.1186. Anal. Calcd for C₂₃H₁₃N₃: C, 82.86; H, 4.54; N, 12.60. Found: C, 82.82; H, 4.27; N, 12.85.



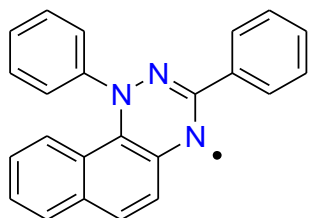
9-Phenylacenaphtho[1,2-*e*][1,2,4]triazine (3.17). 650 mg (42 % yield) from 1.0 g of acenaphthylene-1,2-dione (**3.16**). Yellow solid: mp 187-188 °C; ¹H NMR (600 MHz, CDCl₃) δ 8.74 – 8.68 (m, 2H), 8.50 (dd, *J*₁ = 6.8 Hz, *J*₂ = 5.2 Hz, 2H), 8.22 (d, *J* = 8.1 Hz, 1H), 8.13 (d, *J* = 8.2 Hz, 1H), 7.87 (dd, *J*₁ = 15.3 Hz, *J*₂ = 7.3 Hz, 2H), 7.63 – 7.54 (m, 3H); ¹³C{¹H} NMR (151 MHz, CDCl₃) δ 161.4, 157.6, 155.1, 136.0, 134.3, 132.2, 131.3, 130.1, 130.1, 130.0, 129.5, 129.1, 128.9, 128.8, 128.5, 125.1, 123.6; IR (KBr) ν 1617, 1565, 1479, 1428, 1382, 1353, 1315, 1207, 1159, 1110, 1028, 931, 831, 775, 704 cm⁻¹; UV (CH₂Cl₂) λ_{max} (log ε) 236 (4.69), 255 (4.31), 261 (4.32), 317 (4.76) nm; HRMS (ESI) [M+H]⁺ *m/z* calcd for C₁₉H₁₂N₃: 282.1031; found: 282.1033. Anal. Calcd for C₁₉H₁₁N₃: C, 81.12; H, 3.94; N, 14.94. Found: C, 81.06; H, 3.88; N, 14.97.

4.2.2. General procedure for synthesis of radicals⁵

To a stirred solution of appropriate [1,2,4]triazines (1.0 mmol) in dry THF (3 mL) under argon atmosphere, a 1.9 M solution of phenyllithium in n-butyl ether (0.68 mL, 1.30 mmol) was added dropwise at $-78\text{ }^{\circ}\text{C}$. The resulting mixture was stirred for 1 hr at $-78\text{ }^{\circ}\text{C}$ and then at room temperature overnight under argon atmosphere. The reaction mixture was saturated with air for 30 min. The resulting residue was diluted with H_2O and DCM, the organic phase was separated, washed with water (3 x 40 mL), and dried over Na_2SO_4 and the filtrate was evaporated. For purification, the resulting residue was passed through a column (SiO_2 passivated with 3% Et_3N in n-pentane/AcOEt) to afford radical which was washed three times by hot n-pentane to have totally pure product.

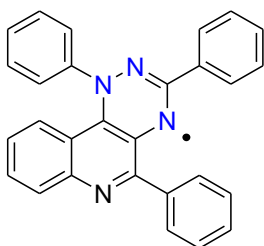
Et_3N -Passivated SiO_2 gel and chromatographic separation of radicals

Solid support was combined with 2% Et_3N in CH_2Cl_2 for the chromatographic separation of radicals, and the solvent was then evaporated using a rotovap until it was completely dry. The reaction mixture was mixed with dry passivated SiO_2 , which was then evaporated to dryness and placed on top of a passivated SiO_2 plug or column. Pet. ether was used as the eluting agent for purifying the product.



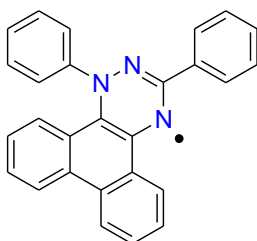
1,3-Diphenyl-1,4-dihydro-2,1-e-naphtho[1,2,4]triazin-3-yl (3.18).

64 mg (42% yield) from 100.0 mg of substrate (3-phenylnaphtho[2,1-e][1,2,4]triazine); Dark brown solid: mp $80\text{--}85\text{ }^{\circ}\text{C}$; IR (KBr) ν 1595, 1490, 1364, 1189, 1080, 1025, 961, 853, 820, 749, 689 cm^{-1} ; UV (CH_2Cl_2) λ_{max} (log ϵ) 254 (4.06), 305 (3.84), 348 (3.41), 398 (3.08), 462 (2.84), 491 (2.72) nm; HRMS (ESI) $[\text{M}]^+$ m/z calcd for $\text{C}_{23}\text{H}_{16}\text{N}_3$: 334.1344; found: 334.1340. Anal. Calcd for $\text{C}_{23}\text{H}_{16}\text{N}_3$: C, 82.61; H, 4.82; N, 12.57. Found: C, 78.17; H, 5.30; N, 10.28.



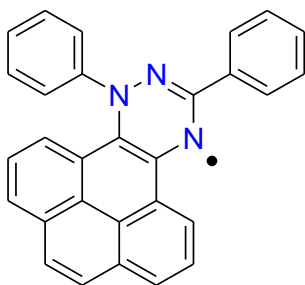
1,3,5-Triphenyl-1,4-dihydro-[1,2,4]triazino[5,6-c]quinolin-3-yl (3.19).

53.0 mg (22% yield) from 200.0 mg of substrate (**3.11**, 3,5-diphenyl-[1,2,4]triazino[5,6-c]quinoline); Dark brown solid: mp: 98-99 °C; IR (KBr) ν 3384, 3056, 3026, 2974, 2926, 2105, 1684, 1599, 1490, 1446, 1364, 1326, 1181, 1121, 1066, 1028, 976, 909, 842 cm^{-1} ; UV (CH_2Cl_2) λ_{max} (log ϵ) 229 (3.19), 252 (3.14), 304 (2.90), 372 (2.39) nm; HRMS (ESI) $[\text{M}]^+$ m/z calcd for $\text{C}_{28}\text{H}_{19}\text{N}_4$: 411.1610; found: 411.1617.



1,3-Diphenyl-1,4-dihydrophenanthro[9,10-e][1,2,4]triazin-3-yl (3.20).

75 mg (60% yield) from 100 mg of substrate (**3.13**, 3-phenylphenanthro[9,10-e][1,2,4]triazine). Brown crystals: mp 194-195 °C; IR (KBr) ν 1587, 1483, 1390, 1356, 1319, 1271, 1237, 1174, 1073, 1021, 976, 924, 868, 749 cm^{-1} ; UV (CH_2Cl_2) λ_{max} (log ϵ) 259 (4.29), 315 (3.93), 410 (3.31), 464 (3.17), 762 (2.26) nm; HRMS (ESI) $[\text{M}]^+$ m/z calcd for $\text{C}_{27}\text{H}_{18}\text{N}_3$: 384.1501; found: 384.1498. Anal. Calcd for $\text{C}_{27}\text{H}_{18}\text{N}_3$: C, 84.35; H, 4.72; N, 10.93. Found: C, 82.56; H, 4.73; N, 9.97.

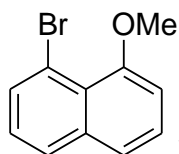


1,3-Diphenyl-1,4-dihydropyreno[9,10-e][1,2,4]triazin-3-yl (3.21).

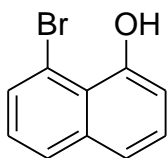
40 mg (33% yield) from 100 mg of substrate (**3.15**, 3-phenylpyreno[9,10-e][1,2,4]triazine). Dark red solid: mp 206-207 °C; IR (KBr) ν 1736, 1584, 1479, 1420, 1382, 1315, 1263, 1200, 1174, 1125, 1069, 1025, 972, 823, 760, 715, 693 cm^{-1} ; UV (CH_2Cl_2) λ_{max} (log ϵ) 240 (3.46), 288 (3.30), 342 (3.11), 465 (2.27), 545 (2.22) nm; HRMS (ESI) $[\text{M}]^+$ m/z calcd for $\text{C}_{29}\text{H}_{18}\text{N}_3$: 408.1501; found: 408.1498. Anal. Calcd for $\text{C}_{29}\text{H}_{18}\text{N}_3$: C, 85.27; H, 4.44; N, 10.29. Found: C, 84.69; H, 5.04; N, 10.25.

4.3. Synthesis of ring expanded planar Blatter radicals through cyclization

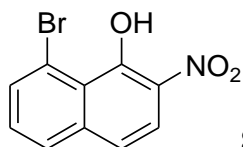
4.3.1. Synthesis of 10-bromo-3-phenyl-naphtho[2,1-*e*][1,2,4]triazine



1-Bromo-8-methoxynaphthalene (3.25).⁷ To a solution of 1,8-dibromonaphthalene (1 eq, 5.25 mmol, 1.50 g) in MeOH (50 mL), CuI (1 eq, 5.25 mmol, 1.50 g) and NaOMe (1eq, 5.25 mmol, 285.0 mg) were added. The mixture was stirred at reflux overnight then cooled to room temperature and concentrated under reduced pressure to provide a crude residue. The residue was purified by column chromatography (SiO₂, pet. ether) to afford pure product; 400.0 mg (32% yield) from 1.50 g of substrate. 870.0 mg of the substrate recovered. white solid. mp 52-53 °C; ¹H NMR (600 MHz, CDCl₃) δ 7.77 (dd, *J*₁ = 7.4 Hz, *J*₂ = 1.2 Hz, 1H), 7.73 (dd, *J*₁ = 8.1 Hz, *J*₂ = 0.9 Hz, 1H), 7.45 – 7.37 (m, 2H), 7.22 (dd, *J*₁ = 8.0 Hz, *J*₂ = 7.5 Hz, 1H), 6.92 (dd, *J*₁ = 7.5 Hz, *J*₂ = 1.3 Hz, 1H), 3.97 (s, 3H); ¹³C{¹H} NMR (151 MHz, CDCl₃) δ 167.2, 155.8, 137.1, 133.0, 128.0, 126.6, 126.4, 123.8, 121.5, 116.7, 107.2, 55.8; IR (KBr) ν 1561, 1456, 1366, 1262. 1196, 1108, 1048, 985, 897, 810, 746, 624 cm⁻¹; HRMS (APCI) [M+H]⁺ *m/z* calcd for C₁₁H₁₀BrO: 236.9915; found: 236.9917. Anal. Calcd for C₁₁H₉BrO: C, 55.72; H, 3.83. Found: C, 55.42; H, 3.92.

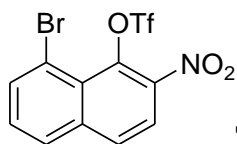


8-Bromo-1-naphthol (3.26).⁸ 1-Bromo-8-methoxynaphthalene (3.628 mmol, 860.0 mg) was dissolved in dry DCM (10 mL) and was cooled to 0 °C using an ice/water bath, followed by the dropwise addition of BBr₃ (1 eq, 3.628 mmol, 3.628 mL of 1M solution in DCM) under Ar. Then the cooling bath was removed, and the mixture was heated to reflux in an oil bath for 3 hours. After finishing the reaction (monitored by TLC) the reaction mixture was cooled again to 0 °C, ice-cold water was carefully added to the mixture to quench the unreacted BBr₃. The resulting mixture was extracted with EtOAc (3 × 50 mL), and the organic phase was combined and dried by sodium sulfate. The removal of solvent under reduced pressure and purification by column chromatography on silica gel with pet. ether gave pure product. 690.0 mg (85 % yield) from 860.0 mg of substrate. white solid: mp 45-50 °C; ¹H NMR (600 MHz, CDCl₃) δ 8.07 (s, 1H), 7.78 (dd, *J*₁ = 8.2 Hz, *J*₂ = 0.7 Hz, 1H), 7.63 (dd, *J*₁ = 7.4 Hz, *J*₂ = 1.1 Hz, 1H), 7.47 – 7.33 (m, 2H), 7.25 – 7.14 (m, 1H), 7.08 (dd, *J*₁ = 7.4 Hz, *J*₂ = 1.4 Hz, 1H); ¹³C{¹H} NMR (151 MHz, CDCl₃) δ 152.5, 137.0, 131.5, 129.3, 127.5, 125.9, 121.2, 120.5, 115.1, 113.2; IR (KBr) ν 3475, 1595, 1446, 1351, 1142, 1096, 1074, 881, 450, 439, 435, 431, 427, 423 cm⁻¹; HRMS (ESI) [M-H]⁻ *m/z* calcd for C₁₀H₆BrO: 220.9602; found: 220.9611. Anal. Calcd for C₁₀H₇BrO: C, 53.84; H, 3.16. Found: C, 53.87; H, 3.29.



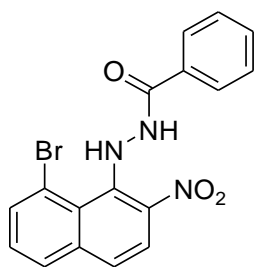
8-Bromo-2-nitronaphthol (3.27).⁹

To a stirred solution of 8-bromonaphthol (0.223 mmol, 50 mg) in acetonitrile (2 mL), KHSO₄ (0.012 eq) was added as a catalyst and the mixture was heated to boil and then stopped heating and Ni(NO₃)₂·6H₂O (1.0 eq, 0.223 mmol, 64.65 mg) was added immediately without extra heating. The color of the reaction mixture changed from light green to dark brown and it was stirred at room temperature for 10 minutes. Then the catalyst was filtered and it was washed with DCM and then the solvent was evaporated. For purification, the resulting residue was set up on silica gel column without any extraction and eluted with petroleum ether. After removing the solvent, an orange solid formed. 10.0 mg (17 % yield) from 50.0 mg of substrate. orange needles: mp 140-145 °C; ¹H NMR (600 MHz, CDCl₃) δ 13.12 (s, 1H), 8.06 (d, *J* = 9.4 Hz, 1H), 7.91 (dd, *J*₁ = 7.6 Hz, *J*₂ = 1.1 Hz, 1H), 7.74 (dd, *J*₁ = 8.1 Hz, *J*₂ = 0.8 Hz, 1H), 7.46 (t, *J* = 7.8 Hz, 1H), 7.31 (d, *J* = 9.4 Hz, 1H); IR (KBr) ν 3481, 2926, 2853, 1618, 1571, 1449, 1379, 1287, 1236, 1183, 1024, 914, 812, 749 cm⁻¹; HRMS (ESI) [M-H]⁻ *m/z* calcd for C₁₀H₅BrNO₃: 265.9453; found: 265.9461. Anal. Calcd for C₁₀H₆BrNO₃: C, 44.81; H, 2.26; N, 5.23. Found: C, 44.95; H, 2.52; N, 5.11.



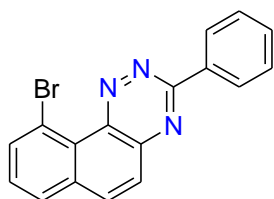
Trifluoromethanesulfonic acid 8-bromo-2-nitronaphthalen-1-yl ester

(3.28).¹ Triethylamine (3 eq, 1.11 mmol, 0.2 mL) was added into a solution of 8-bromo-2-nitronaphthalen-1-ol (0.37 mmol, 100 mg) and dry DCM (2 mL). Trifluoromethanesulfonic anhydride (1.5 eq, 0.55 mmol, 0.1 mL) was then dropped into the mixture at 0 °C. The mixture was stirred overnight at room temperature then poured into ice-water and extracted by DCM (3 × 50 mL). The combined organic phases were washed with brine and dried over anhydrous sodium sulfate. After the solvent was removed, the product was further purified by column chromatography on silica gel to obtain a brown product. 197.0 mg (44 % yield) from 300.0 mg of substrate. ¹H NMR (600 MHz, CDCl₃) δ 8.08 (t, *J* = 9.2 Hz, 2H), 8.02 (d, *J* = 8.9 Hz, 1H), 7.94 (d, *J* = 8.2 Hz, 1H), 7.55 (t, *J* = 7.9 Hz, 1H); ¹³C{¹H} NMR (151 MHz, CDCl₃) δ 142.5, 138.3, 137.0, 136.1, 130.1, 130.1, 128.3, 125.6, 121.4, 119.4, 117.3; IR (KBr) ν 1432, 1334, 1320, 1162, 1154, 1077, 772, 537, 439, 436, 430, 423 cm⁻¹.



Benzoic acid *N'*-(8-bromo-2-nitronaphthalen-1-yl)-hydrazide (3.29).²

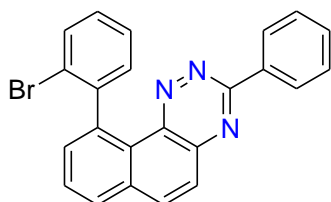
A mixture of trifluoromethanesulfonic acid 8-bromo-2-nitronaphthalen-1-yl ester (0.348 mmol, 142 mg) and benzhydrazide (5 eq, 1.744 mmol, 240.5 mg) in DMSO (2 mL) stirred at room temperature overnight. The reaction mixture extracted with DCM and purified by column chromatography (SiO₂, 50 % DCM/pet. ether). 115.0 mg (84 % yield) from 142 mg of substrate. Yellow powder: mp 150-155 °C; ¹H NMR (600 MHz, CDCl₃) δ 9.47 (d, *J* = 2.7 Hz, 1H), 8.61 (d, *J* = 1.8 Hz, 1H), 8.05 (d, *J* = 9.0 Hz, 1H), 7.93 (dd, *J*₁ = 7.5 Hz, *J*₂ = 0.6 Hz, 1H), 7.78 (d, *J* = 8.0 Hz, 1H), 7.63 (d, *J* = 7.5 Hz, 2H), 7.49 (t, *J* = 7.7 Hz, 2H), 7.39 (q, *J* = 7.5 Hz, 3H); ¹³C{¹H} NMR (151 MHz, CDCl₃) δ 167.2, 143.0, 139.1, 139.1, 134.8, 132.4, 131.5, 129.3, 129.1, 128.8, 127.0, 124.9, 123.7, 121.5, 119.2; IR (KBr) ν 3411, 3366, 3320, 1685, 1609, 1562, 1457, 1342, 1301, 1221, 1061, 960, 886, 826, 769, 693, 600 cm⁻¹; HRMS (ESI) [M+H]⁺ *m/z* calcd for C₁₇H₁₃BrN₃O₃: 386.0140; found: 386.0144. Anal. Calcd for C₁₇H₁₂BrN₃O₃: C, 52.87; H, 3.13; N, 10.88. Found: C, 52.60; H, 3.27; N, 10.98.



10-Bromo-3-phenyl-naphtho[2,1-*e*][1,2,4]triazine (3.30).² Tin powder (4 eq, 0.7 mmol, 84 mg) was added in one portion to the solution of Benzoic acid N'-(8-bromo-2-nitronaphthalen-1-yl)-hydrazide (0.175 mmol, 70 mg) in AcOH (4 mL) and the mixture was stirred at room temperature overnight. After cooling, it was poured into water, filtered through Cellite to remove tin, and extracted with AcOEt. For neutralization of AcOH, saturated water solution of NaHCO₃ was added. The organic layer was separated, and after drying over Na₂SO₄ and solvent removal a yellow-orange solid was obtained which was dissolved in a CH₂Cl₂ / MeOH mixture (1:1, 10 mL) and solid NaIO₄ (3.96 g) was added in one portion. The mixture was stirred for 30 minutes at room temperature and then filtered and washed with CH₂Cl₂ and the filtrate was evaporated. For purification, the resulting residue was passed through a SiO₂ plug by 10% AcOEt/pet. ether and after removing the solvent, pure product formed. 30.0 mg (51 % yield) from 70 mg of substrate. Orange powder: mp 175-176 °C; ¹H NMR (600 MHz, CDCl₃) δ 8.85 – 8.77 (m, 2H), 8.23 (dd, *J*₁ = 7.7 Hz, *J*₂ = 0.9 Hz, 1H), 8.16 (d, *J* = 9.1 Hz, 1H), 7.94 (d, *J* = 7.7 Hz, 1H), 7.90 (d, *J* = 9.0 Hz, 1H), 7.64 – 7.56 (m, 4H); ¹³C{¹H} NMR (151 MHz, CDCl₃) δ 160.2, 145.2, 143.1, 138.2, 137.0, 135.2, 131.6, 129.6, 128.9, 128.7, 127.1, 126.6, 119.6; HRMS (ESI) [M+H]⁺ *m/z* calcd for C₁₇H₁₁BrN₃: 336.0136; found: 336.0142. Anal. Calcd for C₁₇H₁₀BrN₃: C, 60.73; H, 3.00; N, 12.50. Found: C, 60.70; H, 3.21; N, 12.43.

4.3.2. General procedure for Suzuki-Miyaura coupling¹¹

A solution of 10-bromo-3-phenylnaphtho[2,1-*e*][1,2,4]triazine (**3.30**, 0.237 mmol, 80.0 mg), K₂CO₃ (3.0 eq, 0.711 mmol, 98.52 mg), and 2-bromophenylboronic acid (1.5 eq, 0.356 mmol) in THF/H₂O (5:2 mixture, 7 mL) was degassed. Pd(PPh₃)₄ (10 mol% with respect to the boronic acid, 0.0356 mmol) was added. The mixture was refluxed overnight under argon atmosphere. After completion, the reaction mixture poured into water (40 mL) and extracted with CH₂Cl₂ (3×25 mL). Combined organic extracts were dried by Na₂SO₄ and the solvents were removed in *vacuo*. The resulting solid was chromatographed (SiO₂, pet. ether) to give pure product.

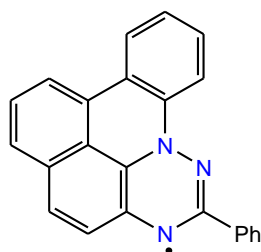


10-(2-Bromo-phenyl)-3-phenylnaphtho[2,1-*e*][1,2,4]triazine

(3.36). 33 mg (34 % yield) from 80.0 mg of substrate. Yellow solid; ¹H NMR (600 MHz, CDCl₃) δ 8.67 – 8.63 (m, 2H), 8.28 (d, *J* = 9.1 Hz, 1H), 8.05 (dd, *J*₁ = 7.9 Hz, *J*₂ = 1.1 Hz, 1H), 7.92 (d, *J* = 9.0 Hz, 1H), 7.87 (t, *J* = 7.6 Hz, 1H), 7.72 (dd, *J*₁ = 8.1 Hz, *J*₂ = 1.1 Hz, 1H), 7.65 (dd, *J*₁ = 7.3 Hz, *J*₂ = 1.2 Hz, 1H), 7.56 – 7.50 (m, 3H), 7.47 (td, *J*₁ = 7.5 Hz, *J*₂ = 1.2 Hz, 1H), 7.38 (dd, *J*₁ = 7.5 Hz, *J*₂ = 1.7 Hz, 1H), 7.36 – 7.30 (m, 1H); ¹³C{¹H} NMR (151 MHz, CDCl₃) δ 160.2, 145.7, 145.0, 142.9, 140.2, 138.6, 135.7, 133.7, 132.8, 132.5, 131.3, 129.9, 129.3, 129.1, 128.8, 128.8, 128.6, 127.6, 127.1, 126.7, 123.3; IR (KBr) ν 3046, 2917, 2850, 1734, 1591, 1511, 1434, 1349, 1336, 1271, 1151, 1110, 1024, 928, 833, 755, 692, 602, 509, 447 cm⁻¹; HRMS (APCI) [M+H]⁺ *m/z* calcd for C₂₃H₁₅BrN₃: 412.0449; found: 412.0461.

4.3.3. General procedure for synthesis of radicals¹¹

A 250 mL borosilicate RB flask was filled with triazines (0.10 mmol) that had been dissolved in 100 mL of dry CH₂Cl₂. The mixture was stirred at reflux under an Ar atmosphere, while being exposed to radiation from a 300 W halogen lamp (see above). The lamp was positioned around 30 cm from the flask. During irradiation, the reaction mixture warmed to 30-35 °C. The reaction was tracked using TLC (20% AcOEt/pet. ether), and the irradiation was stopped after 24 hours. The residue was adsorbed onto passivated silica gel after evaporation the solvent. A short column with Et₃N-passivated silica was used for purification the product from unreacted starting materials (if any were present). The resultant radical was carefully washed with hot n-pentane three times.



2-Phenylbenzo[m,n][1,2,4]triazino[5,6,1-de]acidin-3-yl (3.38).

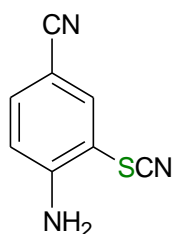
light pink solid: HRMS (ESI) [M]⁺ *m/z* calcd for C₂₃H₁₄N₃: 332.1188; found: 332.1192.

4.4. Functionalization of the *S-peri*-annulated benzo[*e*][1,2,4]triazinyl

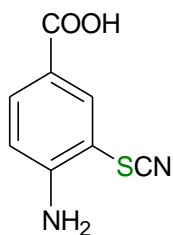
4.4.1. Synthesis of *ortho*-iodothiophenols

4.4.1.1. General procedure for synthesis of thiocyanates through method A¹²

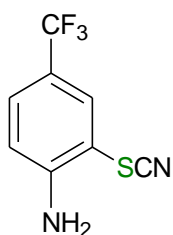
A mixture of 4-substituted aniline (10.0 mmol) and potassium thiocyanate (KSCN, 4 eq, 40 mmol, 4.0 g) was dissolved totally in glacial acetic acid (AcOH, 50 mL) with 5 minutes of sonication then the reaction mixture was cooled in an ice bath and stirred for 10-20 min. A solution of bromine (Br₂, 1.5 eq, 15 mmol, 0.75 mL) in glacial acetic acid was added dropwise at such a rate to keep the temperature below 10 °C throughout the addition. The reaction mixture was stirred at room temperature for 2-10 hours. The progress of the reaction was monitored by TLC analysis and after completion of the reaction, the reaction mixture was poured into the cold water to form the precipitate which was filtered and washed with water and dried. For purification 20-30% EtOAc/pet. ether on silica column was used and crystalized from DCM/cyclohexane to give the pure product. Compounds **3.60**,¹² **3.61**²² and **3.80**²³ are known compounds, and they have been synthesized and identified before through known procedures.



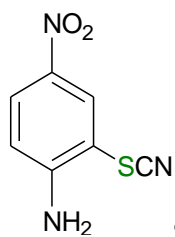
4-Amino-3-thiocyanatobenzonitrile (3.60).¹² Starting from 4-amino-benzonitrile and using method A (reaction time: 4 hours). 1.137 g (65 % yield) from 1.20 g of substrate. Light yellow crystals: mp 179-180 °C (lit¹² mp 184 °C); ¹H NMR (600 MHz, DMSO-*d*₆) δ 7.95 (d, *J* = 2.0 Hz, 1H), 7.57 (dd, *J*₁ = 8.7 Hz, *J*₂ = 2.0 Hz, 1H), 6.94 (s, 2H), 6.87 (d, *J* = 8.7 Hz, 1H); ¹³C{¹H} NMR (151 MHz, DMSO-*d*₆) δ 153.5, 140.8, 135.6, 118.9, 115.6, 110.9, 103.7, 97.2; IR (neat) ν 3444, 3347, 3220, 2221, 2154, 1632, 1599, 1505, 1416, 1345, 1319, 1271, 1200, 1170, 905, 834, 752, 726, 674 cm⁻¹; HRMS (ESI) [M-H]⁻ *m/z* calcd for C₈H₄N₃S: 174.0125; found: 174.0137. Anal. Calcd for C₈H₅N₃S: C, 54.84; H, 2.88; N, 23.98; S, 18.30. Found: C, 54.73; H, 2.88; N, 23.77; S, 18.43.



4-Amino-3-thiocyanatobenzoic acid (3.61).^{12,22} Starting from 4-aminobenzoic acid using method A (reaction time: 2 hours). 870.0 mg (45 % yield) from 1.94 g of substrate. Light yellow crystals: mp 317-320 °C; ¹H NMR (600 MHz, DMSO-*d*₆) δ 12.54 (s, 1H), 7.96 (d, *J* = 1.9 Hz, 1H), 7.75 (dd, *J*₁ = 8.6, *J*₂ = 1.9 Hz, 1H), 6.84 (d, *J* = 8.7 Hz, 1H), 6.69 (s, 2H); ¹³C{¹H} NMR (151 MHz, DMSO-*d*₆) δ 166.2, 153.6, 138.0, 133.5, 118.5, 114.9, 111.3, 102.7; IR (neat) ν 3466, 3362, 2146, 1654, 1606, 1591, 1546, 1408, 1289, 1252, 1151, 916, 834, 767, 730, 700, 670 cm⁻¹; HRMS (ESI) [M+H]⁺ *m/z* calcd for C₈H₇N₂O₂S: 195.0228; found: 195.0220.



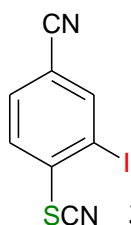
2-Thiocyanato-4-trifluoromethylaniline (3.79).¹² Starting from 4-trifluoromethylaniline (**3.58**) using method A (reaction time: 10 hours). 2.10 g (96 % yield) from 1.61 g of substrate. Light yellow crystals: mp 119-121 °C; ¹H NMR (600 MHz, DMSO-*d*₆) δ 8.10 (s, 1H), 7.88 (s, 2H), 7.50 (dd, *J*₁ = 8.4, *J*₂ = 1.2 Hz, 1H), 7.44 (d, *J* = 8.4 Hz, 1H); ¹³C{¹H} NMR (151 MHz, DMSO-*d*₆) δ 169.3, 155.8, 131.5, 127.5, 125.7, 123.9, 122.5, 122.5, 122.5, 122.5, 122.1, 121.2, 121.0, 120.8, 120.6, 118.5, 118.5, 118.5, 118.4, 117.4; IR (KBr) ν 3492, 3295, 3071, 2940, 2732, 2117, 1640, 1606, 1528, 1472, 1416, 1315, 1282, 1248, 1170, 1110, 1077, 1047, 883, 823, 745, 715, 689 cm⁻¹; HRMS (ESI) [M+H]⁺ *m/z* calcd for C₈H₆F₃N₂S: 219.0203; found: 219.0211. Anal. Calcd for C₈H₅F₃N₂S: C, 44.04; H, 2.31; N, 12.84; S, 14.70. Found: C, 44.10; H, 2.36; N, 12.52; S, 14.94.



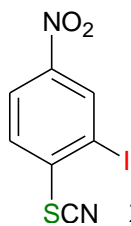
4-Nitro-2-thiocyanatoaniline (3.80).¹² Starting from 4-nitroaniline (**3.59**) using method A (reaction time: 6 hours). 1.100 g (56 % yield) from 1.381 g of substrate. Yellow crystals: mp 137-138 °C; ¹H NMR (600 MHz, DMSO-*d*₆) δ 8.34 (d, *J* = 2.7 Hz, 1H), 8.07 (dd, *J*₁ = 9.2 Hz, *J*₂ = 2.7 Hz, 1H), 7.39 (s, 2H), 6.88 (d, *J* = 9.2 Hz, 1H); ¹³C{¹H} NMR (151 MHz, DMSO-*d*₆) δ 155.4, 136.0, 133.1, 128.2, 114.7, 110.9, 103.3; IR (KBr) ν 3444, 3336, 3213, 2146, 1632, 1587, 1561, 1476, 1300, 1256, 1121, 1062, 920, 827, 745, 715, 670 cm⁻¹; HRMS (ESI) [M]⁺ *m/z* calcd for C₇H₄N₃O₂S: 194.0024; found: 194.0026. Anal. Calcd for C₇H₅N₃O₂S: C, 43.07; H, 2.58; N, 21.53; S, 16.43. Found: C, 43.08; H, 2.38; N, 21.30; S, 16.33.

4.4.1.2. General procedure for synthesis of thiocyanates through method B¹³

A suspension of NaNO₂ (167.0 mg, 2.2 mmol) in water (1 mL) was added over 10 min to an ice-cooled solution of 2-iodoaniline (2.0 mmol) and H₂SO₄ (6 N, 3 mL). After the addition, the mixture was stirred for an additional hour. Next, a solution of KSCN (274.9 mg, 2.8 mmol) and CuSCN (243.5 g, 2.0 mmol) in water (2 mL) was added at room temperature over a period of 1 h. During the addition the solution turned from yellow to brown. The mixture was stirred overnight and then filtered. The precipitate was washed with CH₂Cl₂ three times. The combined organic extracts were washed with water and dried (Na₂SO₄) and the solvent was removed. The resulting solid residue (adsorbed onto silica) was purified by column chromatography (~10 % AcOEt/pet. ether) and crystallized from DCM/cyclohexane to yield pure product.



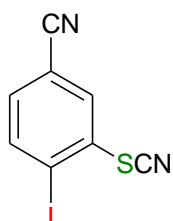
3-Iodo-4-thiocyanatobenzonitrile (3.67). Starting from 4-amino-3-iod-benzonitrile using method B. 180.0 mg (32 % yield) from 488.0 mg of substrate. White crystals: mp 164-165 °C; ¹H NMR (600 MHz, CDCl₃) δ 8.09 (d, *J* = 1.6 Hz, 1H), 7.83 (d, *J* = 8.3 Hz, 1H), 7.76 (dd, *J*₁ = 8.3 Hz, *J*₂ = 1.6 Hz, 1H); ¹³C{¹H} NMR (151 MHz, DMSO-*d*₆) δ 142.6, 138.4, 133.0, 128.0, 116.1, 113.5, 109.0, 94.3; IR (neat) ν 2228, 2154, 1576, 1535, 1446, 1371, 1263, 1192, 1103, 1021, 894, 820, 689 cm⁻¹; HRMS (APCI) [M-H]⁻ *m/z* calcd for C₈H₂IN₂S: 284.8983; found: 284.8988. Anal. Calcd for C₈H₃IN₂S: C, 33.59; H, 1.06; N, 9.79; S, 11.21. Found: C, 33.67; H, 1.18; N, 9.80; S, 11.42.



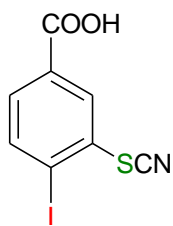
SCN 2-Iodo-4-nitro-1-thiocyanatobenzene (3.69). Starting from 2-iodo-4-nitroaniline using method B. 207.0 mg (34 % yield) from 528.0 mg of substrate. Light yellow crystals: mp 103-104 °C; ^1H NMR (400 MHz, CDCl_3) δ 8.66 (d, $J = 2.3$ Hz, 1H), 8.34 (dd, $J_1 = 8.8$ Hz, $J_2 = 2.4$ Hz, 1H), 7.90 (d, $J = 8.8$ Hz, 1H); $^{13}\text{C}\{^1\text{H}\}$ NMR (101 MHz, CDCl_3) δ 147.3, 140.3, 134.6, 127.8, 124.6, 109.1, 93.4; IR (neat) ν 3090, 2922, 2851, 2165, 1584, 1558, 1502, 1438, 1330, 1274, 1252, 1110, 1017, 954, 898, 864, 820, 730, 682 cm^{-1} ; HRMS (APCI) $[\text{M}]^-$ m/z calcd for $\text{C}_7\text{H}_3\text{IN}_2\text{O}_2\text{S}$: 305.8960; found: 305.8963. Anal. Calcd for $\text{C}_7\text{H}_3\text{IN}_2\text{O}_2\text{S}$: C, 27.47; H, 0.99; N, 9.15; S, 10.48. Found: C, 27.46; H, 1.08; N, 8.87; S, 10.75.

4.4.1.3. General procedure for synthesis of aryl iodides *via* Sandmeyer reaction¹⁴

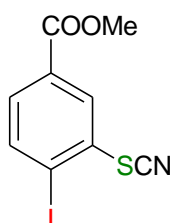
To the appropriate substrate **3.60** or **3.61** (6.0 mmol), H₂SO₄ (15 % in water, 6 mL) was added, and the obtained mixture was cooled to 0 °C in ice bath. A solution of NaNO₂ (1.1 eq, 6.6 mmol, 460.0 mg) in water (2 mL) was added dropwise to the reaction mixture and after that CH₃CN (~10 mL) was added and the mixture stirred at 0 °C for 30 min. Ice cooled solution of KI (1.5 eq, 9 mmol, 1.490 g) in water (2 mL) was added to the reaction mixture at 0 °C and stirred at room temperature overnight. Saturated solution of sodium thiosulfate was added dropwise until the color change from dark to light. Organic layer extracted by EtOAc and washed with water and purified by 10-20% DCM/pet. ether on a silica gel column and crystallized from DCM/cyclohexane to yield pure product.



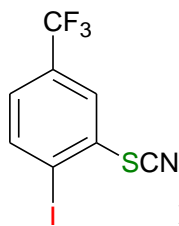
4-Iodo-3-thiocyanatobenzonitrile (3.62). Starting from 4-amino-3-thiocyanatobenzonitrile using method A. 600.0 mg (35 % yield) from 1.05 g of substrate. Yellow crystals: mp 187-188 °C; ¹H NMR (600 MHz, CDCl₃) δ 8.00 (d, *J* = 8.1 Hz, 1H), 7.96 (d, *J* = 1.7 Hz, 1H), 7.33 (dd, *J*₁ = 8.1 Hz, *J*₂ = 1.8 Hz, 1H); ¹³C{¹H} NMR (151 MHz, CDCl₃) δ 141.1, 134.1, 132.4, 130.9, 116.9, 114.5, 109.1, 101.6; IR (neat) ν 3078, 2922, 2228, 2158, 1703, 1524, 1446, 1375, 1278, 1259, 1211, 1006, 872, 827, 745, 674 cm⁻¹; HRMS (APCI) [M-H]⁻ *m/z* calcd for C₈H₂IN₂S: 284.8983; found: 284.8987. Anal. Calcd for C₈H₃IN₂S: C, 33.59; H, 1.06; N, 9.79; S, 11.21. Found: C, 33.62; H, 1.11; N, 9.98.



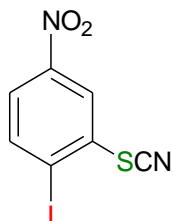
4-Iodo-3-thiocyanatobenzoic acid (3.76). Starting from 4-amino-3-thiocyanatobenzoic acid using method A. 350.0 mg (75 % yield) from 300.0 mg of substrate. White crystals: mp 180-185 °C; ^1H NMR (400 MHz, DMSO- d_6) δ 8.20 (d, $J = 1.7$ Hz, 1H), 8.14 (d, $J = 8.1$ Hz, 1H), 7.68 (dd, $J_1 = 8.1$ Hz, $J_2 = 1.8$ Hz, 1H); $^{13}\text{C}\{^1\text{H}\}$ NMR (101 MHz, DMSO- d_6) δ 165.8, 140.7, 132.6, 131.7, 130.7, 129.5, 111.1, 105.1; IR (neat) ν 1684, 1576, 1550, 1457, 1416, 1375, 1289, 1244, 1211, 1129, 1010, 924, 898, 834, 756, 723 cm^{-1} .



4-Iodo-3-thiocyanatobenzoic acid methyl ester (3.63).¹⁵ To the solution of 4-amino-3-thiocyanatobenzoic acid (1.0 mmol, 305.09 mg) in diethyl ether (20 mL), a solution of CH_2N_2 (3 eq., 3.3 mmol, freshly prepared from 308.0 mg of *N*-methyl-*N*-nitrosourea) in diethyl ether was added at 0 °C, and the reaction mixture was stirred for 30 minutes. The solvent was removed, and the crude product was purified by column chromatography using silica gel 10% EtOAc/pet. ether. White crystals (250 mg, 78 % yield): ^1H NMR (600 MHz, CDCl_3) δ 8.34 (d, $J = 1.9$ Hz, 1H), 7.96 (d, $J = 8.2$ Hz, 1H), 7.70 (dd, $J_1 = 8.2$ Hz, $J_2 = 1.9$ Hz, 1H), 3.95 (s, 3H). mp 88-89 °C; IR (neat) ν 2158, 1710, 1580, 1534, 1449, 1427, 1364, 1289, 1252, 1185, 1114, 1010, 965, 902, 849, 752 cm^{-1} ; HRMS (ESI) $[\text{M}+\text{H}]^+$ m/z calcd for $\text{C}_9\text{H}_7\text{INO}_2\text{S}$: 319.9242; found: 319.9247.



1-Iodo-2-thiocyanato-4-trifluoromethylbenzene (3.81). Starting from 2-thiocyanato-4-trifluoromethylaniline (**3.79**) using method A. 17 % yield. White crystals: mp 132-135 °C; ^1H NMR (600 MHz, CDCl_3) δ 8.16 (s, 1H), 8.13 (d, $J = 8.6$ Hz, 1H), 7.70 (d, $J = 8.3$ Hz, 1H); $^{13}\text{C}\{^1\text{H}\}$ NMR (151 MHz, CDCl_3) δ 156.05, 139.33, 128.22, 128.00, 127.78, 127.57, 124.81, 123.52, 123.50, 123.47, 123.45, 123.01, 122.97, 118.15, 118.13, 118.10, 118.07, 109.15; IR (KBr) ν 1461, 1431, 1401, 1315, 1263, 1185, 1159, 1107, 1084, 1051, 957, 883, 853, 820, 715 cm^{-1} ; HRMS (ESI) $[\text{M}+\text{H}]^+$ m/z calcd for $\text{C}_8\text{H}_3\text{F}_3\text{INS}$: 329.9061; found: 329.9070. Anal. Calcd for $\text{C}_8\text{H}_3\text{F}_3\text{INS}$: C, 29.20; H, 0.92; N, 4.26; S, 9.74. Found: C, 29.35; H, 1.04; N, 4.26; S, 10.19.



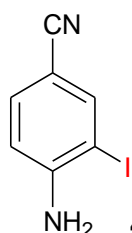
1-Iodo-4-nitro-2-thiocyanatobenzene (3.82). Starting from 4-nitro-2-thiocyanatoaniline (**3.80**) using method A. 30 % yield. Yellow crystals: mp 121-122 °C; ^1H NMR (600 MHz, CDCl_3) δ 8.56 (d, $J = 2.4$ Hz, 1H), 8.08 (d, $J = 8.6$ Hz, 1H), 7.92 (dd, $J_1 = 8.6$ Hz, $J_2 = 2.4$ Hz, 1H); $^{13}\text{C}\{^1\text{H}\}$ NMR (151 MHz, CDCl_3) δ 149.13, 141.35, 134.51, 124.24, 123.17, 108.98, 103.88; IR (KBr) ν 3082, 2922, 1591, 1517, 1438, 1345, 1252, 1058, 1013, 875, 797, 734 cm^{-1} ; HRMS (APCI) $[\text{M}-\text{H}]^-$ m/z calcd for $\text{C}_7\text{H}_2\text{IN}_2\text{O}_2\text{S}$: 304.8882; found: 304.8881. Anal. Calcd for $\text{C}_7\text{H}_3\text{IN}_2\text{O}_2\text{S}$: C, 27.47; H, 0.99; N, 9.15; S, 10.48. Found: C, 27.59; H, 0.91; N, 9.28.

4.4.1.4. General procedure for synthesis of aryl iodides by pyridinium iodochloride¹⁶

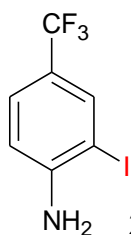
An appropriate aniline (10.0 mmol) and pyridinium iodine monochloride (2.41 g, 10.0 mmol) were dissolved in methanol (80 mL) and stirred at ambient temperature from 2 hours to 24 hours. The progress of the reaction was controlled by TLC analysis. A saturated solution of sodium thiosulfate was added dropwise until the color change from red to yellow. The reaction mixture was concentrated to 2/3 volume, extracted with CH₂Cl₂, dried over Na₂SO₄, and evaporated to dryness. A pale-yellow residue was purified by column chromatography (~10 % AcOEt/pet. ether) and crystallized from pet. ether/CH₂Cl₂ to obtain pure product. Compounds **3.64**,²⁴ **3.65**²⁵ and **3.66**²⁶ are known compounds, and they have been synthesized and identified before through known procedures.

Preparation of pyridinium iodochloride¹⁷

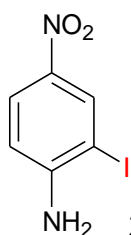
To a solution of pyridine (0.062 mol, 5 mL) in acetic acid, a solution of iodine monochloride (1.0 eq., 0.062 mol, 10.0 g) in acetic acid was added slowly at 0 °C with continuous stirring. The yellow solid was filtered, dried and recrystallized from ethyl alcohol. 19.0 g (63% yield) from 10.0 g of substrate.



4-Amino-3-iodobenzonitrile (3.64).²⁴ Starting from 4-aminobenzonitrile (**3.56**) using method B. 4.525 g (93 % yield) from 3.62 g of substrate. Brown crystals: mp 111-112 °C (lit.²⁴ mp 94-97 °C); ¹H NMR (600 MHz, CDCl₃) δ 7.90 (d, *J* = 1.8 Hz, 1H), 7.39 (dd, *J*₁ = 8.4 Hz, *J*₂ = 1.8 Hz, 1H), 6.70 (d, *J* = 8.4 Hz, 1H), 4.63 (s, 2H); ¹³C{¹H} NMR (151 MHz, CDCl₃) δ 150.6, 142.9, 133.4, 118.4, 113.6, 102.0, 81.9; IR (neat) ν 3455, 3343, 2214, 1613, 1587, 1494, 1405, 1308, 1189, 1182, 1025, 894, 820, 708, 667 cm⁻¹; HRMS (ESI) [M]⁺ *m/z* calcd for C₇H₅IN₂: 243.9497; found: 243.9485. Anal. Calcd for C₇H₅IN₂: C, 34.45; H, 2.07; N, 11.48. Found: C, 34.54; H, 2.13; N, 11.20.



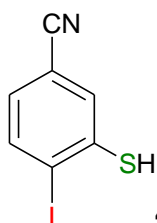
2-Iodo-4-trifluoromethylaniline (3.65).²⁵ Starting from 4-trifluoromethylaniline (**3.58**) using method B. 2.75 g (96 % yield) from 1.611 g of substrate. Light yellow crystals: mp 45-46 °C (lit.²⁵ mp 45-46 °C); ¹H NMR (600 MHz, CDCl₃) δ 7.87 (d, *J* = 1.2 Hz, 1H), 7.37 (dd, *J*₁ = 8.4 Hz, *J*₂ = 1.6 Hz, 1H), 6.74 (d, *J* = 8.4 Hz, 1H), 4.41 (s, 2H); ¹³C{¹H} NMR (151 MHz, CDCl₃) δ 149.7, 136.3, 136.3, 136.3, 136.3, 126.7, 126.7, 126.6, 126.6, 126.3, 124.5, 122.7, 121.9, 121.6, 121.4, 121.2, 120.9, 113.6, 82.2; IR (neat) ν 3406, 3298, 3194, 1625, 1599, 1505, 1408, 1315, 1289, 1140, 1085, 1089, 1025, 894, 820, 764, 723, 667 cm⁻¹; HRMS (ESI) [M-H]⁻ *m/z* calcd for C₇H₄F₃IN: 285.9341; found: 285.9344. Anal. Calcd for C₇H₅F₃IN: C, 29.29; H, 1.76; N, 4.88. Found: C, 29.36; H, 1.78; N, 4.88.



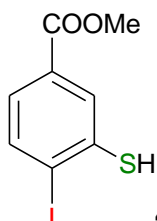
2-Iodo-4-nitroaniline (3.66).²⁶ Starting from 4-nitroaniline (**3.59**) using method B. 1.41 g (53 % yield) from 1.38 g of substrate. Yellow crystals: mp 108-109 °C (lit.²⁶ mp 110-112 °C); ¹H NMR (600 MHz, CDCl₃) δ 8.57 (d, *J* = 2.5 Hz, 1H), 8.06 (dd, *J*₁ = 8.9 Hz, *J*₂ = 2.5 Hz, 1H), 6.70 (d, *J* = 8.9 Hz, 1H), 4.84 (s, 2H); ¹³C{¹H} NMR (151 MHz, CDCl₃) δ 152.4, 139.4, 135.6, 125.8, 112.3, 80.6; IR (neat) ν 3473, 3365, 2109, 1602, 1576, 1487, 1293, 1256, 1151, 1110, 1028, 898, 812, 741, 706, 682 cm⁻¹; HRMS (ESI) [M-H]⁻ *m/z* calcd for C₆H₄IN₂O₂: 262.9317; found: 262.9315.

4.4.1.5. General procedure for synthesis of mercaptans¹⁸

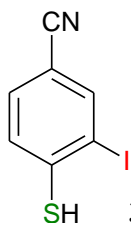
To the mixture of the appropriate thiocyanate (1.0 mmol) in MeOH, NaBH₄ (1.3 eq, 1.3 mmol, 50.0 mg) was added by portions at 0 °C and stirred at room temperature for 30 minutes. The progress of the reaction was monitored by TLC. After completion of the reaction, HCl (1M, 6 mL) was added and the organic phase was separated by EtOAc, dried over sodium sulfate and evaporated to dryness in *vacuo* and was used for the next step without further purification.



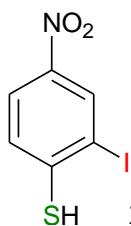
4-Iodo-3-mercaptobenzonitrile (3.41). Starting from 4-Iodo-3-thiocyanatobenzonitrile (**3.62**). White solid; ¹H NMR (600 MHz, CDCl₃) δ 7.90 (d, *J* = 8.2 Hz, 1H), 7.63 (d, *J* = 1.7 Hz, 1H), 7.06 (dd, *J*₁ = 8.2 Hz, *J*₂ = 1.8 Hz, 1H), 4.30 (s, 1H); ¹³C{¹H} NMR (151 MHz, CDCl₃) δ 141.2, 140.6, 130.6, 129.0, 117.7, 113.1, 103.9; HRMS (ESI) [M]⁻ *m/z* calcd for C₇H₃INS: 259.9030; found: 259.9029.



4-Iodo-3-mercaptobenzoic acid methyl ester (3.42). Starting from 4-Iodo-3-thiocyanatobenzoic acid methyl ester (**3.63**). ¹H NMR (600 MHz, CDCl₃) δ 8.02 (d, *J* = 1.9 Hz, 1H), 7.85 (d, *J* = 8.2 Hz, 1H), 7.42 (dd, *J*₁ = 8.2 Hz, *J*₂ = 1.9 Hz, 1H), 4.24 (s, 1H), 3.90 (s, 3H); ¹³C{¹H} NMR (151 MHz, CDCl₃) δ 166.24, 139.98, 139.48, 131.01, 129.09, 127.20, 104.01, 52.56; HRMS (ESI) [M-H]⁻ *m/z* calcd for C₈H₆IO₂S: 292.9133; found: 292.9142.



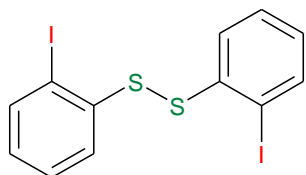
3-Iodo-4-mercaptobenzonitrile (3.43). Starting from **3-Iodo-4-thiocyanatobenzonitrile (3.67)**. HRMS (ESI) $[M-H]^-$ m/z calcd for C_7H_3INS : 259.9030; found: 259.9037.



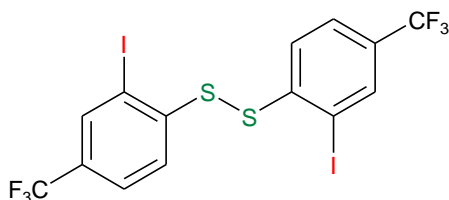
2-Iodo-4-nitrobenzenethiol (3.45). Starting from 2-iodo-4-nitro-1-thiocyanatobenzene (3.69). 1H NMR (600 MHz, $CDCl_3$) δ 8.64 (d, $J = 2.3$ Hz, 1H), 8.15 (dd, $J_1 = 8.8$ Hz, $J_2 = 2.3$ Hz, 1H), 7.52 (d, $J = 8.8$ Hz, 1H); HRMS (ESI) $[M-H]^-$ m/z calcd for $C_6H_3INO_2S$: 279.8929; found: 279.8934.

4.4.1.6. General procedure for synthesis of disulfides^{19,20}

Sodium sulfide ($\text{Na}_2\text{S}\cdot 9\text{H}_2\text{O}$, 5.5 mmol, 1.317 g, 1.1 eq.) and powdered sulfur (170 mg) were dissolved in boiled water (2.0 mL) by heating and stirring and the mixture cooled to 0 °C. In the second flask, to a solution of appropriate amine (1.0 mmol) in THF (5 mL) and AcOH (4 mL) was added (1.1 mmol, 210 mg) of *p*-TsOH \cdot H₂O. Immediately, pale solids were precipitated. As little as possible of AcOH was added to the suspension until the solution turned clear again. The solution was cooled to -10 °C in an ice-salt bath and then *t*-BuONO (2 mmol) was added dropwise to the reaction. The mixture was stirred for 30 min at this temperature and then allowed to warm to room temperature for another 30 min. The clear solution was poured into 100 mL of diethyl ether, and the diazonium tosylate salt was precipitated. After filtration, the product was collected and washed with THF and diethyl ether. Finally, the product was dried in vacuo and 1 eq of this salt was dissolved in water and ethanol and added dropwise at below 5 °C to the first flask. When addition was completed, the mixture allowed to warm up to room temperature and stirred overnight then heated in the water bath to 50 °C. The organic phase was separated, dried over Na_2SO_4 and evaporated to dryness in vacuo and purified by petroleum ether.



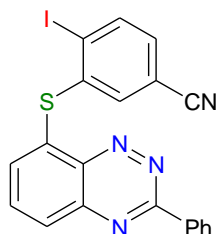
1,1'-Disulfanediybis(2-iodo-3-benzene) (3.75). Colourless solid, ¹H NMR (600 MHz, CDCl_3) δ 7.82 (d, $J = 7.8$ Hz, 1H), 7.52 (d, $J = 8.0$ Hz, 1H), 7.34 (t, $J = 7.6$ Hz, 1H), 6.95 (t, $J = 7.5$ Hz, 1H).



1,1'-Disulfanediybis(2-iodo-4-trifluoromethylbenzene) (3.73). Colourless solid, ¹H NMR (600 MHz, CDCl_3) δ 8.04 (d, $J = 0.9$ Hz, 1H), 7.57 (dd, $J_1 = 8.4$ Hz, $J_2 = 1.3$ Hz, 1H), 7.52 (d, $J = 8.4$ Hz, 1H).

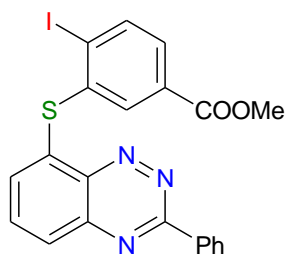
4.4.2. Synthesis of phenylsulfanyl-3-phenylbenzo[1,2,4]triazines²¹

To a stirred solution of crude thiol (1.10 mmol) dissolved in DMSO (4 mL), NaH (60%, 45 mg, 1.10 mmol) was added in one portion. After 15 min 8-fluoro-3-phenylbenzo[*e*][1,2,4] triazine (225.2 mg, 1.00 mmol) was added and the reaction was stirred under Ar at 80 °C for 1 - 5 h (TLC analysis). After cooling, DCM (30 mL) was added, and organic layer was washed well with water (3×25 mL) and brine (25 mL). The combined organic extracts were dried over anhydrous Na₂SO₄, and the solvent was evaporated. The resulting solid residue (adsorbed onto passivated silica) was purified by column chromatography (passivated silica), solvent was evaporated, and the residue was recrystallized from MeCN.

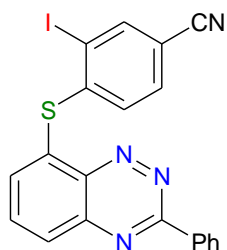


4-Iodo-3-(3-phenylbenzo[1,2,4]triazin-8-ylsulfanyl)benzonitrile (3.46).

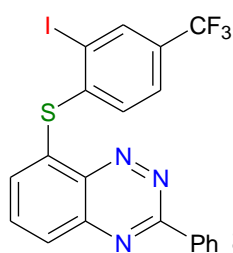
251.0 mg (39 % yield) from 313.6 mg of substrate (8-fluoro-3-phenylbenzo[*e*][1,2,4] triazine). Yellow solid: mp 178-180 °C; ¹H NMR (600 MHz, CDCl₃) δ 8.78 (dd, *J*₁ = 6.5 Hz, *J*₂ = 2.8 Hz, 1H), 8.15 (d, *J* = 8.2 Hz, 1H), 8.01 (d, *J* = 8.5 Hz, 1H), 7.84 (t, *J* = 7.9 Hz, 1H), 7.68 (d, *J* = 1.6 Hz, 1H), 7.65 – 7.55 (m, 2H), 7.31 (dd, *J*₁ = 8.2 Hz, *J*₂ = 1.6 Hz, 1H), 7.25 (s, 1H); ¹³C{¹H} NMR (151 MHz, CDCl₃) δ 160.8, 144.1, 142.5, 141.5, 140.8, 137.5, 136.5, 135.7, 135.2, 132.2, 132.0, 129.3, 129.2, 129.1, 128.2, 113.8; IR (neat) ν 2228, 1550, 1498, 1464, 1379, 1323, 1282, 1215, 1170, 1110, 1073, 1021, 980, 909, 827, 790, 700 cm⁻¹.



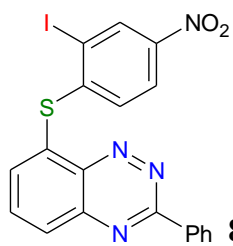
4-Iodo-3-(3-phenylbenzo[1,2,4]triazin-8-ylsulfanyl)benzoic acid methyl ester (3.47). 435.0 mg (61% yield) from 320.2 mg of substrate (8-fluoro-3-phenylbenzo[*e*][1,2,4] triazine). Yellow solid: mp 213-215 °C; ^1H NMR (600 MHz, CDCl_3) δ 8.86 – 8.70 (m, 2H), 8.38 (d, $J = 1.4$ Hz, 1H), 8.17 (d, $J = 8.3$ Hz, 1H), 7.86 (d, $J = 8.4$ Hz, 1H), 7.78 (dd, $J_1 = 8.3$ Hz, $J_2 = 1.5$ Hz, 1H), 7.73 (t, $J = 7.9$ Hz, 1H), 7.60 (d, $J = 3.8$ Hz, 3H), 6.92 (d, $J = 7.4$ Hz, 1H), 3.90 (s, 3H); $^{13}\text{C}\{^1\text{H}\}$ NMR (151 MHz, CDCl_3) δ 165.8, 160.6, 143.8, 142.2, 141.2, 140.2, 137.4, 137.1, 135.6, 135.4, 132.0, 131.8, 131.4, 129.1, 129.0, 126.2, 126.0, 114.4, 52.6; IR (neat) ν 1710, 1576, 1539, 1494, 1427, 1364, 1319, 1271, 1230, 1110, 1013, 976, 834, 793, 756, 700 cm^{-1} ; HRMS (ESI) $[\text{M}+\text{H}]^+$ m/z calcd for $\text{C}_{21}\text{H}_{14}\text{IN}_3\text{O}_2\text{S}$: 499.9930; found: 499.9932. Anal. Calcd for $\text{C}_{21}\text{H}_{14}\text{IN}_3\text{O}_2\text{S}$: C, 50.51; H, 2.83; N, 8.42; S, 6.42. Found: C, 50.42; H, 2.69; N, 8.41; S, 6.43.



3-Iodo-4-(3-phenylbenzo[1,2,4]triazin-8-ylsulfanyl)benzonitrile (3.48). 45.0 mg (55 % yield) from 39.8 mg of substrate (8-fluoro-3-phenylbenzo[*e*][1,2,4] triazine). Yellow solid: mp 219-220 °C; ^1H NMR (400 MHz, CDCl_3) δ 8.82 – 8.72 (m, 2H), 8.19 (d, $J = 1.6$ Hz, 1H), 8.10 (dd, $J_1 = 8.5$ Hz, $J_2 = 1.0$ Hz, 1H), 7.91 (dd, $J_1 = 8.5$ Hz, $J_2 = 7.4$ Hz, 1H), 7.62 – 7.59 (m, 3H), 7.57 (dd, $J_1 = 7.3$ Hz, $J_2 = 1.0$ Hz, 1H), 7.49 (dd, $J_1 = 8.2$ Hz, $J_2 = 1.7$ Hz, 1H), 7.20 (d, $J = 8.2$ Hz, 1H); $^{13}\text{C}\{^1\text{H}\}$ NMR (101 MHz, CDCl_3) δ 160.7, 146.6, 144.5, 142.9, 142.5, 135.9, 135.7, 135.1, 132.2, 132.1, 132.1, 131.6, 129.6, 129.2, 129.1, 116.8, 112.2, 101.3; IR (neat) ν 2225, 1576, 1543, 1509, 1442, 1375, 1323, 1256, 1103, 1047, 1010, 980, 875, 820, 801, 697 cm^{-1} ; HRMS (ESI) $[\text{M}+\text{H}]^+$ m/z calcd for $\text{C}_{20}\text{H}_{11}\text{IN}_4\text{S}$: 466.9827; found: 466.9824. Anal. Calcd for $\text{C}_{20}\text{H}_{11}\text{IN}_4\text{S}$: C, 51.52; H, 2.38; N, 12.02; S, 6.88. Found: C, 51.81; H, 2.58; N, 12.01; S, 6.89.



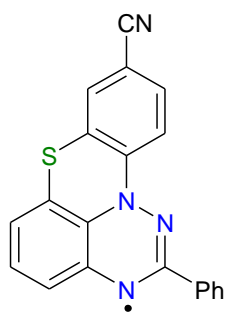
8-(2-Iodo-4-trifluoromethylphenylsulfanyl)-3-phenylbenzo[1,2,4]triazine (3.49). 333.0 mg (62 % yield) from 235.6 mg of substrate (8-fluoro-3-phenylbenzo[*e*][1,2,4] triazine). Yellow solid: mp 165-166 °C; ¹H NMR (600 MHz, CDCl₃) δ 8.79 – 8.75 (m, 2H), 8.23 (d, *J* = 0.9 Hz, 1H), 7.97 (dd, *J*₁ = 8.5 Hz, *J*₂ = 1.1 Hz, 1H), 7.82 (dd, *J*₁ = 8.5 Hz, *J*₂ = 7.4 Hz, 1H), 7.61 – 7.58 (m, 4H), 7.57 (t, *J* = 8.1 Hz, 1H), 7.25 (dd, *J*₁ = 7.4 Hz, *J*₂ = 1.1 Hz, 1H); ¹³C{¹H} NMR (151 MHz, CDCl₃) δ 160.7, 144.1, 143.0, 142.4, 138.1, 137.3, 137.3, 137.3, 137.2, 135.7, 135.3, 134.2, 131.9, 131.8, 131.6, 129.1, 129.1, 129.0, 127.7, 126.2, 126.2, 126.2, 126.1, 123.6, 121.8, 104.7; IR (neat) ν 1591, 1546, 1502, 1371, 1312, 1256, 1160, 1118, 1069, 1010, 980, 883, 827, 740, 697 cm⁻¹; HRMS (ESI) [M+H]⁺ *m/z* calcd for C₂₀H₁₁F₃IN₃S: 509.9751; found: 509.9751. Anal. Calcd for C₂₀H₁₁F₃IN₃S: C, 47.17; H, 2.18; N, 8.25; S, 6.30. Found: C, 47.30; H, 2.42; N, 7.99; S, 6.27.



8-(2-Iodo-4-nitrophenylsulfanyl)-3-phenylbenzo[1,2,4]triazine (3.50). 85.0 mg (54 % yield) from 73.4 mg of substrate (8-fluoro-3-phenylbenzo[*e*][1,2,4] triazine). Yellow solid: mp 204-205 °C; ¹H NMR (600 MHz, CDCl₃) δ 8.83 – 8.69 (m, 3H), 8.15 (dd, *J*₁ = 8.5 Hz, *J*₂ = 1.0 Hz, 1H), 8.02 (dd, *J*₁ = 8.7 Hz, *J*₂ = 2.4 Hz, 1H), 7.95 (dd, *J*₁ = 8.5 Hz, *J*₂ = 7.3 Hz, 1H), 7.72 (dd, *J*₁ = 7.2 Hz, *J*₂ = 1.0 Hz, 1H), 7.64 – 7.55 (m, 3H), 7.11 (d, *J* = 8.7 Hz, 1H); ¹³C{¹H} NMR (101 MHz, CDCl₃) δ 160.7, 149.5, 146.3, 144.6, 142.6, 135.8, 135.2, 135.0, 134.8, 133.5, 132.1, 130.4, 130.3, 129.2, 129.1, 123.6, 99.2; IR (neat) ν 2922, 2855, 1736, 1502, 1442, 1334, 1278, 1248, 1177, 1107, 1013, 976, 797, 738, 697 cm⁻¹; HRMS (ESI) [M+H]⁺ *m/z* calcd for C₁₉H₁₁IN₄O₂S: 486.9739; found: 486.9735. Anal. Calcd for C₁₉H₁₁IN₄O₂S: C, 46.93; H, 2.28; N, 11.52; S, 6.59. Found: C, 46.86; H, 2.42; N, 11.79; S, 6.50.

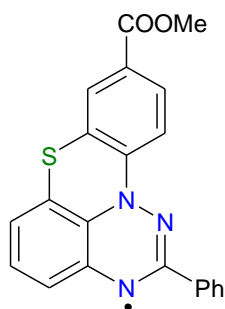
4.4.3. Synthesis of 2-phenyl-3*H*-[1,2,4]triazino[5,6,1-*kl*]phenothiazin-3-yls¹⁵

To a solution of appropriate triazine (0.294 mmol) in 4 mL of dry toluene tris(trimethylsilyl)silane [(CH₃)₃Si]₃SiH (2 eq, 180 μL, 0.588 mmol) was added and stirred at 80 °C under an atmosphere of Ar. Then AIBN (0.6 eq, 0.176 mmol, 28.90 mg) dissolved in dry toluene (2 mL) and was added to the reaction mixture over 4h using a syringe pump. After 4h the reaction mixture was cooled to room temperature and evaporated to dryness. The crude product was separated using a short silica gel column (passivated silica). The radical was washed with warm cyclohexane (3x) and crystalized.



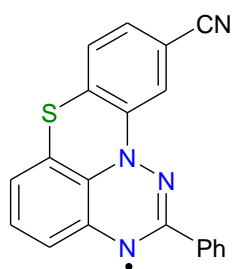
9-Cyano-2-phenyl-3*H*-[1,2,4]triazino[5,6,1-*kl*]phenothiazin-3-yl (3.51).

126.0 mg (82 % yield) from 210.0 mg of substrate. Dark purple: mp 250-253 °C; IR (neat) ν 2221, 1576, 1546, 1461, 1431, 1390, 1323, 1263, 1230 cm⁻¹; UV (CH₂Cl₂) λ_{max} (log ϵ) 248 (3.37), 280 (3.24), 323 (3.25), 404 (2.60), 544 (2.44), 724 (2.09), 786 (2.03) nm; HRMS (ESI) [M+H]⁺ m/z calcd for C₂₀H₁₁N₄S: 340.0783; found: 340.0782. Anal. Calcd for C₂₀H₁₁N₄S: C, 70.78; H, 3.27; N, 16.51; S, 9.45. Found: C, 70.78; H, 3.25; N, 16.50; S, 9.71.



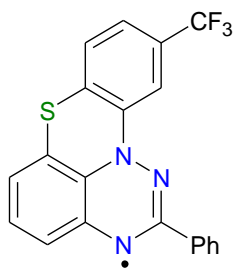
9-Methoxycarbonyl-2-phenyl-3H-[1,2,4]triazino[5,6,1-*kl*]phenothiazin-3-yl (3.52).

158.0 mg (42 % yield) from 200.0 mg of substrate. Dark purple: mp 205-206 °C; IR (neat) ν 1923, 1707, 1587, 1546, 1464, 1423, 1386, 1271, 1248, 1114, 969, 902, 838, 782, 758, 730, 689 cm^{-1} ; UV (CH_2Cl_2) λ_{max} (log ϵ) 248 (4.10), 320 (3.94), 405 (3.23), 541 (3.08), 719 (2.74) nm; HRMS (ESI) $[\text{M}+\text{H}]^+$ m/z calcd for $\text{C}_{21}\text{H}_{14}\text{N}_3\text{O}_2\text{S}$: 373.0898; found: 373.0884. Anal. Calcd for $\text{C}_{21}\text{H}_{14}\text{N}_3\text{O}_2\text{S}$: C, 67.73; H, 3.79; N, 11.28; S, 8.61. Found: C, 67.66; H, 3.85; N, 11.01; S, 8.87.



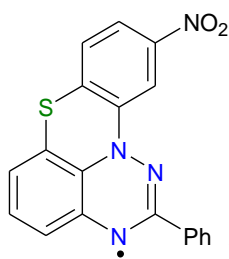
10-Cyano-2-phenyl-3H-[1,2,4]triazino[5,6,1-*kl*]phenothiazin-3-yl (3.53).

30.0 mg (69 % yield) from 60.0 mg of substrate. Dark green: mp 142-143 °C; IR (neat) ν 2225, 1591, 1546, 1468, 1438, 1405, 1375, 1323, 1271, 1170, 1021, 980, 887, 820, 775, 685 cm^{-1} ; UV (CH_2Cl_2) λ_{max} (log ϵ) 264 (4.30), 402 (3.18), 686 (2.42) nm; HRMS (ESI) $[\text{M}+\text{H}]^+$ m/z calcd for $\text{C}_{20}\text{H}_{11}\text{N}_4\text{S}$: 340.0783; found: 340.0774. Anal. Calcd for $\text{C}_{20}\text{H}_{11}\text{N}_4\text{S}$: C, 70.78; H, 3.27; N, 16.51; S, 9.45. Found: C, 70.88; H, 3.56; N, 16.39; S, 9.52.



10-Trifluoromethyl-2-phenyl-3H-[1,2,4]triazino[5,6,1-*k*]phenothiazin-

3-yl (3.54). 110.0 mg (89 % yield) from 150.0 mg of substrate. Dark green: mp 189-190 °C; IR (neat) ν 1599, 1554, 1464, 1431, 1405, 1382, 1319, 1222, 1155, 1103, 1060, 1028, 995, 928, 883, 823, 779, 730, 689 cm^{-1} ; UV (CH_2Cl_2) λ_{max} (log ϵ) 249 (3.07), 254 (3.07), 279 (3.05), 304 (3.03), 396 (2.21), 501 (1.81), 685 (1.81), 741 (1.77) nm; HRMS (ESI) $[\text{M}+\text{H}]^+$ m/z calcd for $\text{C}_{20}\text{H}_{11}\text{F}_3\text{N}_3\text{S}$: 383.0706; found: 383.0709. Anal. Calcd for $\text{C}_{20}\text{H}_{11}\text{F}_3\text{N}_3\text{S}$: C, 62.82; H, 2.90; N, 10.99; S, 8.39. Found: C, 62.70; H, 2.91; N, 10.74; S, 8.72.



10-Nitro-2-phenyl-3H-[1,2,4]triazino[5,6,1-*k*]phenothiazin-3-yl (3.55).

28.0 mg (84 % yield) from 45.0 mg of substrate. Dark green: mp 81-82 °C; IR (neat) ν 1595, 1550, 1490, 1464, 1379, 1334, 1297 cm^{-1} ; UV (CH_2Cl_2) λ_{max} (log ϵ) 255 (4.25), 295 (3.90), 354 (3.47), 614 (3.22), 669 (3.34) nm; HRMS (APCI) $[\text{M}+\text{H}]^+$ m/z calcd for $\text{C}_{19}\text{H}_{11}\text{N}_4\text{O}_2\text{S}$: 359.0603; found: 359.0600. Anal. Calcd for $\text{C}_{19}\text{H}_{11}\text{N}_4\text{O}_2\text{S}$: C, 63.50; H, 3.09; N, 15.59; S, 8.92. Found: C, 63.62; H, 4.23; N, 11.73; S, 9.06.

4.5. References

- (1) Liu, M.; Li, X. L.; Chen, D. C.; Xie, Z.; Cai, X.; Xie, G.; Cao, Y. *Advanced Functional Materials*. **2015**, 25(32), 5190-5198.
- (2) Kaszyński, P.; Constantinides, C. P.; Young Jr, V. G. *Angewandte Chemie International Edition*. **2016**, 55(37), 11149-11152.
- (3) Bachman, G. B.; Welton, D. E.; Jenkins, G. L.; Christian, J. E. *Journal of the American Chemical Society*. **1947**, 69(2), 365-371.
- (4) Van Galen, P. J.; Nissen, P.; Van Wijngaarden, I.; Ijzerman, A. P.; Soudijn, W. *Journal of Medicinal Chemistry*. **1991**, 34(3), 1202-1206.
- (5) Constantinides, C. P.; Obijalska, E.; Kaszynski, P. *Organic Letters*. **2016**, 18(5), 916-919.
- (6) Nagy, J.; Nyitrai, J.; Kolonits, P.; Lempert, K.; Gergely, A.; Párkányi, L.; Kálmán, A. *Journal of the Chemical Society, Perkin Transactions 1*. **1988**, (12), 3267-3274.
- (7) Fell, J. B.; Fischer, J. P.; Baer, B. R.; Blake, J. F.; Bouhana, K.; Briere, D. M.; Marx, M. A. *Journal of Medicinal Chemistry*. **2020**, 63(13), 6679-6693.
- (8) Zhao, K.; Long, G.; Liu, W.; Li, D. S.; Gao, W.; Zhang, Q. *The Journal of Organic Chemistry*. **2019**, 85(1), 291-295.
- (9) Anuradha, V.; Srinivas, P. V.; Aparna, P.; Rao, J. M. *Tetrahedron Letters*. **2006**, 47(28), 4933-4935.
- (10) Jasinski, M.; Szczytko, J.; Pocięcha, D.; Monobe, H.; Kaszynski, P. *Journal of the American Chemical Society*. **2016**, 138(30), 9421-9424.
- (11) Bartos, P., Young Jr, V. G.; Kaszynski, P. *Organic Letters*. **2020**, 22(10), 3835-3840.
- (12) Sawhney, S. N.; & Boykin, D. W. *The Journal of Organic Chemistry*. **1979**, 44(7), 1136-1142. (13) Still, I. W.; Sayeed, V. A. *Synthetic Communications*. **1983**, 13(14), 1181-1192.
- (14) Gong, S.; Chang, Y. L.; Wu, K.; White, R.; Lu, Z. H.; Song, D.; Yang, C. *Chemistry of Materials*. **2014**, 26(3), 1463-1470.

- (15) Bartos, P.; Celeda, M.; Pietrzak, A.; Kaszyński, P. *Organic Chemistry Frontiers*. **2022**, 9(4), 929-938.
- (16) Lalut, J.; Santoni, G.; Karila, D.; Lecoutey, C.; Davis, A.; Nachon, F.; Rochais, C. *European Journal of Medicinal Chemistry*. **2019**, 162, 234-248.
- (17) Khansole, S. V.; Mokle, S. S.; Sayyed, M. A.; Vibhute, Y. B. *Journal of the Chinese Chemical Society*. **2008**, 55(4), 871-874.
- (18) Okamoto, H.; Wu, J.; Morita, Y.; Takenaka, S. *Bulletin of the Chemical Society of Japan*. **2002**, 75(1), 175-179.
- (19) Xing, B.; Ni, C.; Hu, J. *Angewandte Chemie International Edition*. **2018**, 57(31), 9896-9900.
- (20) Allen, C. F. H.; MacKay, D. D. *Organic Syntheses*. **1943**, 2, 580.
- (21) Núñez, A.; Sánchez, A.; Burgos, C.; Alvarez-Builla, J. *Tetrahedron*. **2004**, 60(29), 6217-6224.
- (22) Lang, R. C.; Williams, C. M.; & Garson, M. J. *Organic Preparations and Procedures International*. **2003**, 35(5), 520-524.
- (23) Malik, J. K.; Noolvi, M. N.; Manvi, F. V.; Nanjwade, B. K.; Patel, H. M.; Manjula, S. N.; & Barve, A. *Letters in Drug Design and Discovery*. **2011**, 8(8), 717-724.
- (24) Vaidyanathan, G.; Affleck, D. J.; & Zalutsky, M. R. *Journal of Medicinal Chemistry*. **1994**, 37(21), 3655-3662.
- (25) Drennhaus, T.; Leifert, D.; Lammert, J.; Drennhaus, J. P.; Bergander, K.; Daniliuc, C. G.; & Studer, A. *Journal of the American Chemical Society*. **2023**, 145(15), 8665-8676.
- (26) Wescott, L. D.; & Mattern, D. L. *The Journal of Organic Chemistry*. **2003**, 68(26), 10058-10066.